THE ANATOMICAL BASIS OF SENSORY TUNING IN AUDITORY CORTICAL MICROCIRCUITS

A thesis submitted for the degree of
Doctor of Philosophy of Imperial College London

Alexander Morris

Department of Bioengineering

IMPERIAL COLLEGE LONDON

2016

ABSTRACT

Unlike other sensory cortices, the auditory cortex receives inputs that have undergone extensive processing from the periphery and a number of subcortical nuclei. While sub-cortical auditory nuclei are well described, modelled and understood, the auditory cortex is relatively under-researched. Our understanding of the processing of simple and complex stimuli is incomplete. In addition, cortical connectivity and anatomy is still only sparsely described. This thesis aims to address some of the gaps in our understanding of auditory cortical processing. I first sought to investigate responses to pure tone stimuli (a fundamental building block of complex auditory stimuli) to understand how basic information is represented sub-threshold in auditory cortex. This involved performing *in vivo* whole cell recordings on neurons in mouse AI and quantifying responses to pure tone stimuli. My results demonstrate that AI neurons can exhibit complex frequency response profiles, where there is some indication that certain responses may be restricted to specific electrophysiological cell types.

In order to understand in more detail how cortical responses are formed and also the transformations that occur, we need to understand how thalamic inputs are integrated and subsequent outputs computed. mGRASP is an exciting new technique that enables identification of synaptic contacts between spatially distinct but connected neuronal populations. I employed mGRASP to: 1) test it's efficacy as a tool for assessing connectivity of disparate brain regions and subsequently 2) to measure and describe the spatial arrangement of synaptic inputs from thalamic projection cells onto cortical cells. Bulk viral labeling uncovered a somatocentric distribution of thalamic synapses onto neurons in AI, regardless of cell type and laminar location. *In vivo* whole cell transfection of individual cells was then performed, for the first time, in order to isolate the technique on a single cell level and correlate synaptic distributions with frequency response profiles.

It has been suggested that cortex may play a critical role in the transformation of auditory responses from simple to complex representations. Comodulation-masking release (CMR) is an auditory phenomenon that uses cues of speech perception (a complex auditory stimulus) to allow the segregation of one sound from another (and its subsequent detection). It has been suggested that this high order processing occurs in auditory cortex. To test this I first demonstrated the presence of CMR in auditory cortex. I then applied optogenetics as a functional perturbation to measure the causal relationship between cortex and CMR processing. My results show that signal detection thresholds were lowest in broadband coherently modulated maskers, indicating that a correlate of *across*-channel CMR exists at the level of cortex. Furthermore the presence of noise history significantly improved sensitivity. In order to determine if this mechanism relies on cortical circuitry, AI was silenced during the noise history by activating ChR2-PV+ interneurons. This disruption resulted in increased thresholds, suggesting that circuitry in auditory cortex plays an integral role in detecting salient sounds in complex background noise.

Acknowledgements

I would first of all like to thank my supervisor, Paul Chadderton, for giving me the opportunity to carry out a PhD. He has always been patient and supportive of me throughout my time in his lab. The first PhD student is gifted with foresight and I envisage a long and successful career with many nature publications.

Joe, this section most likely won't do you justice in the role you played in shaping my understanding of auditory neuroscience, nonetheless I will give it a go. Your guidance and our 'debates' were crucial to me getting to this point. I can only hope that I returned the favour by expanding your knowledge regarding genetics. But I fear the traffic is very much one way.

To Luca Annecchino, thank you for helping me identify various errors in my approach using your two-photon rig (and much more) and also drinking our frustration away...late into the night. To Jun Laru, combined with Joe, getting me to code, pushing through with mGRASP and staying late till 5 in the morning working away. To the other members of the Chadderton lab, Matty and Susu for advice about viral injections and patching, Gaelle, Caroline and Alex thank you for all of your support and advice. If you all read through this (which you better) I could've put a hell of a lot more but its late and my brain just aint working plus I'll thank you all in person, except Laru...Seoul is just a bit far. Many thanks to Zoki, Bata, Maja, Jovana, Tamara, Tanja, Angelina and Masha for all you have done, feeding, drinking, laughing and generally providing escapism.

Finally to my Mum, Dad and Christina thank you for your emotional and financial support. My higher education has lasted 7 years and how I'm going to pay that back is still a topic of on-going investigation, bare with me. Ive mentioned drinking a few times here. Just so you know it was always responsible.

Dejana, well looky here you get your own page! This was clearly done of my own volition and also not in expectation of some reward. It was done because, you my Serbian goddess (other readers skip past this page for your own health) have the patience of a saint and giving you your own page is just a small token of my appreciation. Thank you for firstly helping me in the lab but more importantly staying with me throughout the duration of my PhD and supporting me at every step, especially when I was granted 24hr access! I wouldn't have been able to make it this far without you ljubav.

CONTENTS

List of Figures

List of Tables

1 LITERATURE REVIEW

The central goal of sensory neuroscience is to understand how neural networks generate perception from the information gathered from the world around us. In order to achieve this it is necessary to determine the roles that individual neurons perform within those circuits. Over the past 10 years genetic techniques have been developed offering researchers new tools with which to probe neural networks in new and exciting ways. Given that these advancements are highly developed in *mus musculus*, it is necessary to compare and confirm previous work dedicated to identifying the functional properties of auditory neurons in other animal models. Therefore in this thesis, I describe the functional responses of neurons in primary auditory cortex to simple and complex stimuli and attempt to correlate them with underlying anatomical features and circuits. In order to contextualise these focal points, it's necessary to mention auditory scene analysis, how particular transformations are made along the ascending auditory pathway and finally provide a more in depth view of complex stimuli such as CMR.

1.1 GENERAL PRINCIPLES OF SOUND

The ability to understand our environment through our senses appears effortless, yet these processes remain crucial to survival. One such process involves perceiving sound. Sounds are pressure waves that propagate through a medium, most commonly air and given that they are waves, they are comprised of two crucial components that can vary with time: amplitude and frequency. If our brains and ears are in good order, we are able to distinguish a multitude of sounds ranging from falling rain, the rustling of leaves in the wind, the slamming of a door, the rumble of an engine, the click-clack of high heels or speech. But what is it about the physical properties of these sounds that enable us to distinguish them and build a perceptual experience? In order to understand how perception is created it is necessary to first look at how sounds are received.

1.1.1 Auditory scene analysis

Our auditory system has evolved to receive sensory input and build an accurate representation of it. How the auditory system extracts these components from the environment is best explained through the use of an analogy. In this example you have a lake and somewhere along its perimeter you dig two narrow channels and attach in the middle of each channel a handkerchief. As waves enter the channels they cause the handkerchiefs to move and based on their movement you must infer

the number of boats present in the lake, where they are located, which has the largest motor and determine if the wind is blowing (Bregman, 1994). That is in essence the type of crude information gathered from our sensory organs, from which the auditory system must decipher in order to answer these questions.

Fortunately, instead of a handkerchief we have more intricate mechanisms that extract the components of sound from our environment. Sound is channeled through the ear canal by the pinna where it encounters the tympanic membrane, initiating the first stage of transduction. The auditory ossicles transfer the vibrations of the tympanic membrane to the oval window on the cochlea. This step not only acts as a relay point but also an amplifier The cochlea is a hard hollow snail-shell like structure that spirals inwards, comprised of three fluid filled channels. One of these channels is known as the organ of Corti where lined, on its inner wall, are receptors known as hair cells bathed in a potassium rich endolymph fluid. There are inner and outer hair cells, where the former is involved in the transduction of sound into electrical signals and the latter is involved in the mechanical feedback amplification of quiet sounds (Hudspeth, 2008). There is typically one row of inner hair cells and three rows of outer hair cells and they are arranged parallel to the length of the cochlea spreading from the base to the apex of the basilar membrane. The basilar membrane has a non-uniformal structure as it varies in width and stiffness, where it is widest and most flexible at the apex of the cochlea, and narrower and stiffer at the basal end (Bacon et al., 2004). Based on this structure, the maximal displacement of basilar membrane is dependent on the frequency of a sound.

These factors contribute to the unique properties of the cochlea that enable it to act as a mechanical frequency analyser. The apical ends of the hair cells, as the name suggests, are stereo-cilia that are in contact with the tectoral membrane and at the basal end are synapses with cochlear nerve fibers (Takasaka & Smith, 1971). If the stapes (the auditory ossicle in contact with the oval window) transferred a low frequency vibration to the fluid in the cochlea, it would result in the vibration of the basilar membrane located at the apex of the cochlea, causing the microcilia on hair cells to push up against the tectoral membrane thus depolarizing them (Narayan et al., 1998). This results in frequency dependent displacement of microcillia on hair cells, with high frequencies effecting cells located at the base of the cochlea and low frequencies at the apex. Therefore this spatial arrangement of frequency-tuned hair cells along the basilar membrane generates a place code, otherwise known as cochleotopy or tonotopy.

Therefore if we unwound the cochlea and recorded from the cochlear nerve fibres,

we would be able to produce a cochleogram. If we take the example of a recording of the spoken word “shoe” (Figure 1.1 A) we would expect to reproduce the same pattern of frequency and amplitude changes over time in a cochleogram. Given that different sounds are comprised of different frequencies and amplitude changes over time, the cochlea will faithfully represent them in a neural pattern of firing. So it would be somewhat romantic to imagine that the auditory system provided the brain with a detailed pattern of neural excitation that reflected a spectrogram. However, like love, this neglects a fundamental feature of sounds in our environment, they’re messy. The ‘shoe’ spectrogram is produced in isolation with no contaminating noise. In reality a spectrogram recording of “shoe” in our environment would pick up overlapping sounds (Figure 1.1 B), making it almost impossible to distinguish the contributing components. The cochlea represents the most basic breakdown of the auditory environment; therefore the auditory system must employ complex mechanisms in order to overcome this inherent problem.

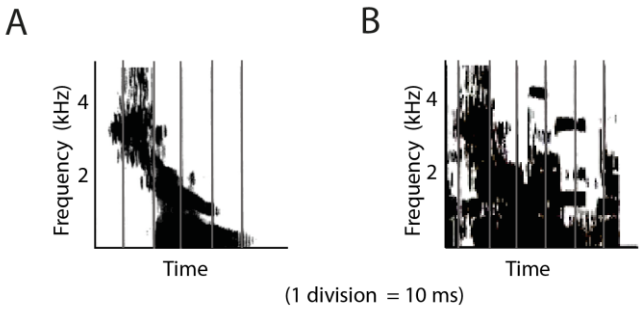

Figure 1.1

Spectrogram of spoken words: **A** Spectrogram of the word “shoe” **B** Spectrogram of the word “shoe” in the presence of other sounds. (taken from Bregma, Auditory scene analysis pg 7-8)

1.2 TECHNIQUES FOR PROBING THE AUDITORY SYSTEM

In the auditory system, like other sensory modalities, psychophysical studies generate interesting questions and functional and anatomical studies attempt to explain them. However there is great variability in their approach, where each technique serves a specific purpose; ranging from a macro- perspective, to identifying its individual components in circuits. The current bottleneck lies in our ability to identify the relationship between structure and function. In this section I describe common techniques applied to the auditory system, the type of functional information that can be gathered and the advent of new methodologies that can help further our understanding of stimulus representations and how they’re formed.

1.2.1 Electrophysiological

In neuroscience the most commonly asked questions are; what aspects of a stimulus do neurons encode and is this information reliably encoded over time? How do populations of neurons work in concert to represent information and how does this neural activity eventually correlate with behaviour? At present there are multiple ways of investigating some of these questions, where they fall in to either of two categories; invasive or non-invasive. Noninvasive methods include electroencephalogram (EEG), Magnetoencephalography (MEG), diffuse optical tomography (DOT), functional magnetic resonance imaging (fMRI) and diffusion tensor imaging (DTI). These techniques offer the great advantage of being able to probe large-scale neural activity in humans and animal models without the need for surgery. These techniques however forego high spatial resolution in favour of increased temporal resolution and vice versa, this results in data that is often less informative than invasive techniques, as the activity that is measured is very indirect. Invasive techniques include; LFP, multi-electrode recordings, intracellular recordings, calcium imaging and viral techniques. These techniques allow for finer scale probing of neural circuits, acquiring functional data at faster timescales.

1.2.1.1 Local field potential (LFP) recordings

The local field potential (LFP) can be used, with relative ease, to identify synaptic responses across populations, where in the auditory system it is often used to map tonotopic organisation in auditory nuclei (Kayser et al., 2007), or identify correlates of mismatched negativity in animal models (Nelken & Ulanovsky, 2007). LFP recordings involve using a low impedance microelectrode to record the aggregated electric potential in extracellular space with respect to a reference electrode. These electrical fields are produced by any excitable membrane, whether it's of somatic, dendritic or of axonal origin. As a result the overall field is composed of fast (action potential) and slow components (synaptic activity). The LFP waveform is thus dependent on multiple current sources, which must be temporally synchronized and spatially dense in order to have a significant impact on its amplitude and frequency. Synaptic activity, appears to meet this criteria best and hence impacts the LFP significantly (Logothetis & Wandell, 2004; Niedermeyer & da Silva, 2005). Na^+ action potentials, calcium spikes, gap junctions, ephaptic effects and neuronal architecture also have an impact but to a lesser degree, where their contribution to the subtleties in waveform dynamics is still widely debated (Kamondi et al., 1998; d. N. Lorente, 1947; Niedermeyer & da Silva, 2005; Ozen et al., 2010; Ylinen et al., 1995). Overall, the spatial origin of current sources is difficult to determine and as a result the contribution of individual neurons cannot be established.

1.2.1.2 Extracellular multiunit recordings

Unlike LFP recordings that measure a compound signal from a relatively large area of the brain, Microwire multielectrodes and silicon-based microelectrodes record spiking activity on a local level. By placing multiple electrodes close to neuron it is possible to isolate single unit activity due to variations in spike timing and waveforms (M. Sutter & Schreiner, 1995; M. A. Wilson & McNaughton, 1993). This process is otherwise known as spike sorting. This method has clear advantages, as it enables a user to perform long-term electrophysiological recordings of a population of neurons, which can be ideal for identifying correlates of plasticity and learning. However there are, as always, drawbacks. Sampling bias is an inherent issue with this technique, as neurons with high spontaneous firing rates are better represented than neurons with low spontaneous firing rates. Furthermore contamination of neighbouring spike activity will inevitably affect the recorded spike shape making it harder to definitively isolate single units.

1.2.1.3 Intracellular recordings

To overcome these issues it is necessary to physically isolate individual cells and record their responses *in vivo*. One such method utilizes sharp microelectrodes, where individual neurons are essentially ‘speared’ by micropipettes creating a very small pore (50-200 nm diameter). This results in minimal exchange between the intracellular fluid and the electrolytes in the pipette where electrical events generated by the neurons membrane can then be recorded (Eccles et al., 1967). The most obvious drawbacks; recordings suffer from high access resistance, are typically less stable than the patch-clamp technique (discussed later) and isolating small structures such as dendrites or even small inhibitory neurons can prove to be an extremely difficult task.

The patch-clamp technique, developed by Bert Sakmann and Erwin Neher (Hamill et al., 1981; Neher & Sakmann, 1992; Sakmann & Neher, 1984), is a more versatile technique than sharp electrode recordings. The pipette typically has a larger pore (0.5 – 2 μm), where a positive pressure is applied to prevent blockage. When there is an increase in resistance, the pressure is released and contact is made with a portion of a single cell. In this mode, while attached to a neuron’s membrane (seal), it is possible to perform a cell-attached recording. The advantage of cell-attached recordings is that they minimize structural damage to a neuron whilst also enabling the recording of unambiguous single-cell spike activity, due to high resistance of the seal (>1GΩ). Upon the application of suction, it is possible to rupture the portion of membrane covering the pore of the pipette and therefore gain intracellular electrical

access. Depending on the size of the pore is it possible to obtain low resistances between the pipette and neuron (access resistance<40MΩ), enabling reliable manipulation of currents and voltages. This mode not only reveals the neural output, in terms of spike activity, but it also illuminates the subthreshold activity generated by the recorded neurons pre-synaptic partners. This therefore offers a unique insight into how neurons generate spike output and how individual neurons contribute to overall network responses (Ferster & Jagadeesh, 1992; Margrie et al., 2002). Given that under whole-cell patch clamp conditions a cell is essentially dialysed with the contents of the intracellular solution, it is possible to manipulate and trace neuronal circuits through the addition of a synthetic dye, protein or even genes. A recent advance has involved delivering genes to individual cells, in order to identify pre-synaptic partners. By combining a functional and biophysical characterization with neuroanatomical information of presynaptic partners it is possible to understand one of the central goals in neuroscience, which is how neural circuits shape an individual cells response (Rancz et al., 2011). Although the whole-cell technique is far from 'high throughput' it remains the gold standard for probing neural circuits.

1.2.1.4 Imaging neural activity

The imaging of neural activity is relatively non-invasive. The most commonly used indicator for imaging neural activity is calcium. Calcium is the universal secondary messenger involved in synaptic transmission. Originally this imaging technique involved the use of synthetic calcium indicators (OGB) that fluoresce when they encounter calcium. Therefore action potentials can be imaged *in vivo* at the single cell level as they trigger changes in cytoplasmic free calcium (Fetcho et al., 1998; Stosiek et al., 2003). However synthetic indicators are difficult to target to specific cell classes and subcellular compartments. This resulted in a shift to the least invasive option, a genetically encoded calcium indicator (GCaMP). Recent GCaMP variants have comparable kinetics and sensitivity to OGB, however its main advantages are that it is far less invasive, it has a minimal cytotoxic effect and can be targeted to subcellular locations (Grutzendler et al., 2002; L. Tian et al., 2009). In the auditory system, when combined with two-photon imaging it is possible to acquire detailed spatial and temporal cellular responses to tonal stimuli (Bandyopadhyay et al., 2010; Chen et al., 2011; Issa et al., 2014). Intrinsic fluorescence imaging is also commonly used in the auditory system, especially when determining tonotopic maps (Versnel et al., 2002), however the low spatial and temporal resolution limits its function to an ancillary role.

1.2.2 Relating structure to function

Classical cell staining techniques (horseradish peroxidase and biocytin) and gross viral labeling methods (AAV, Rabies and Lentiviral) can be used to elucidate detailed neuronal morphologies, allowing end users to classify cell classes and infer basic principles regarding the origin of their inputs. However this coarse structural perspective of circuits cannot inform us of its underlying neuronal activity. By combining electrophysiology with certain genetic tools it can enable researchers to more directly test the relationship that exists between structure and function. The eventual goal is to identify and manipulate functional sub-cellular compartments, specific neuronal types and entire circuits, in order to determine how they contribute to the functional underpinnings of individual neurons, the dynamics of a circuit and the resulting behaviour of an organism (Scanziani & Häusser, 2009).

1.2.2.1 Optogenetics

Optogenetics, a significant advancement from the stimulation electrode, is a powerful tool now widely used for the mapping of functional circuits. It involves the transfection of targeted neurons with light activated ion channels such as channelrhodopsin (ChR2), archaerhodopsin (Arch), light-gated ionotropic glutamate receptors or halorhodopsin (NpHR) (Boyden et al., 2005; X. Li et al., 2005; Szobota et al., 2007). These neurons can then be stimulated or suppressed on a millisecond timescale, therefore allowing researchers to perturb neural circuits with extraordinary temporal precision whilst monitoring neural activity and behaviour. Currently in the auditory system this technique has been used to understand the unique roles of certain cell classes in the structuring of receptive field properties (A. K. Moore & Wehr, 2013). When combining this technique with calcium imaging it enables users to record from a large population of neurons and directly assess functional impact of altering circuit dynamics. The eventual goal is to improve this technique by restricting neuronal manipulation so that it becomes more acute. This can be achieved in two ways; firstly, advancing protein engineering so that it becomes possible to synthesize channels that are more ion selective (ie between Na^+ and K^+), and secondly restrict the control of light-gated channels to dendritic compartments (Scanziani & Häusser, 2009). However currently the most acute way of probing circuits involves performing whole cell recordings while simultaneously controlling the activity of neural populations that may contribute to specific stimulus representations.

1.2.2.2 mGRASP

Even with all the advances in identifying neuronal circuits and manipulating them, mapping their synaptic connectivity has proved a cumbersome task, where it is either

time consuming or inaccurate (Bock et al., 2011; Mishchenko et al., 2010; Sotelo, 2003). However recently the GFP reconstitution across synaptic partners (GRASP) technique has offered a unique breakthrough, where the location of synapses can be detected at high resolution, accurately and quickly (Feinberg et al., 2008). The GRASP technique was initially developed in *C.elegans*, where GFP is split into two nonfluorescent portions (GFP1-10 and GFP11), with each portion tethered to the membranes of two separate neuronal populations (pre-synaptic and postsynaptic). Only when two neurons are close enough in a synaptic cleft, is it possible for the portions to reconstitute and form GFP and therefore fluoresce. Due to species dependent variations in synaptic architecture, this technique had to be modified in order for it to be successfully applied in the mammalian brain (Zhai & Bellen, 2004).

Two different genetic constructs must be made, one for the presynaptic source (pre-mGRASP) and the other for the postsynaptic source (post-mGRASP). Both constructs contain one portion of the split GFP, an N-terminal signal peptide, a transmembrane domain, an extracellular domain, an intracellular domain and a fluorescent protein for neuronal visualisation. For pre-mGRASP, the nematode β-integrin is used as the signal peptide, where it is subsequently fused to the 16 residue GFP11. This section is then linked via a spacer to the extracellular and transmembrane domain of human CD-42 (Feinberg et al., 2008). So far for the most part it is almost structurally identical to the nematode GRASP, however the intracellular domain is significantly altered through the inclusion of rat neurexin-1β containing a PDZ-binding motif.

This binding motif is necessary for the trafficking through the endoplasmic reticulum and golgi, to synaptic clefts (Fairless et al., 2008). Finally to visualise neuronal processes monomeric (m)Cerulean are included in the construct. For post-mGRASP, a modified mouse neuroligin-1 are used to provide a frame, where certain residues are removed in order to prevent binding to endogenous neurexin and hence avoid nonspecific synaptogensis (Dean & Dresbach, 2006). The GFP1-10 portion is included however the signal peptide, transmembrane and extracellular domain residues are not altered from mouse neuroligin-1. To visualise post-mGRASP infected cells, dimeric (d)Tomato is included in the construct, where it is attached to the cytosolic end of post-mGRASP. These constructs are then packaged into the rAAV virus, allowing for precise gene delivery to small populations of neurons. The success of this method does rely on the two neuronal populations being relatively spatially distinct, otherwise infection of both viruses will occur. By using Cre-recombinase dependent viral vectors it is possible to isolate expression in a cell type specific manner. This overcomes the inherent issues previously described, allowing

for mapping of local synaptic connectivity within neuronal populations (Kim et al., 2012). Overall these two recent advancements will enable us to break down cortical neuronal classes that are responsible for shaping functional representations of stimuli and also how they might contribute to the integrative mechanisms that dictate how a neuron responds.

1.3 THE ASCENDING AUDITORY PATHWAY

In order to fully appreciate how perception is developed it is necessary to break down the components of a stimulus and observe how they are encoded and transformed in the auditory system. The auditory system is comprised of a number of nuclei that essentially act as processing stations (Figure 1.2), however our understanding of the exact processing strategies employed at each nucleus varies, as at each step along the ascending auditory pathway neuronal diversity and innervation patterns become more complex.

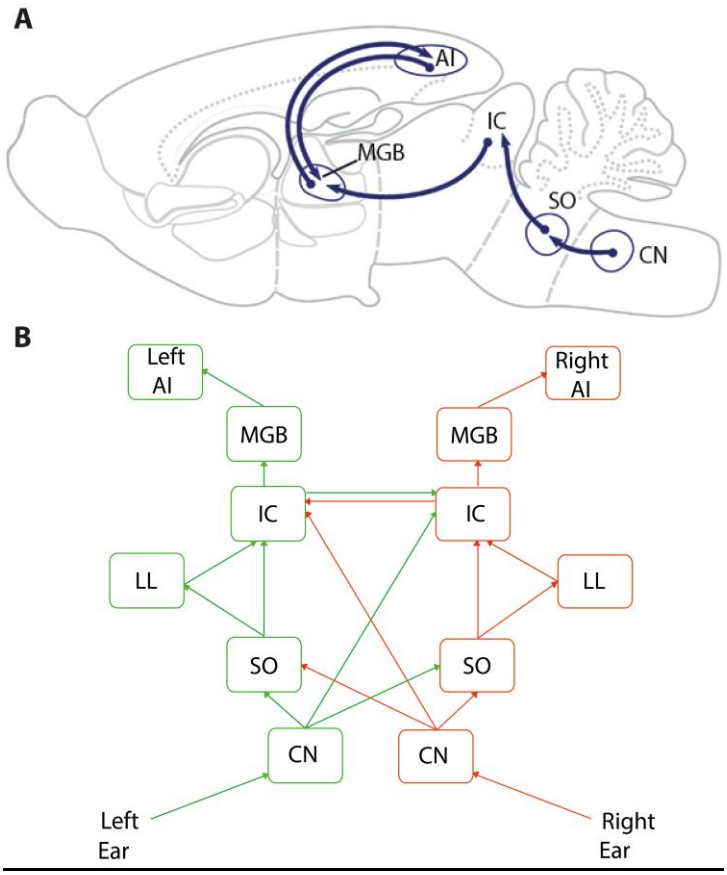

Figure 1.2

Ascending auditory pathway A Ascending auditory pathway in rodents (adapted from Mueller et al 2012) **B** Monaural and binaural flow of auditory information from left and right ears through the ascending auditory

pathway. CN-cochlear nucleus, SO-superior olive, LL-lateral lemniscus, IC-inferior colliculus, MGB-medial geniculate body, AI-primary auditory cortex.

1.3.1 Cochlear nerve

The cochlear nerve is responsible for relaying frequency driven depolarization of hair cells to the cochlear nuclear complex. It is comprised of type I and II spiral ganglion neurons and that innervate the inner and outer hair cells respectively (Nadol et al., 1990; Spoendlin, 1972). Tracer studies using horse radish peroxidase identified that a majority of cochlear nerve fibres are type I where they associate in a one-to-one fashion with inner hair cells (Liberman, 1982). Due to this one-to-one connection individual fibres are very frequency selective. Electrophysiological recordings from individual fibres confirm this, as responses to pure tones evoked very narrow frequency response areas. Furthermore by tracing the fibre, these threshold responses or characteristic frequencies (CF) corresponded to the location of a hair cell along the cochleotopic map (Russell et al., 1986). However this form of 'place code' isn't the only transmission in the auditory nerve used to discriminate frequency. A temporal code is also transmitted which relies on phase locking. In this instance neurons will fire in time with the peaks of sinusoidal stimuli. However this high fidelity phase locking is limited to frequencies below 4 kHz across most species (Crawford & Fettiplace, 1980; Galambos & Davis, 1943; Pfeiffer & Molnar, 1970), with Owls exhibiting the highest limit of about 9 kHz (Sullivan & Konishi, 1984). This indicates that at low frequencies both place and temporal code is employed whereas for high frequencies the place code is preferred. Type II spiral ganglion neurons appear to perform a mechanical role correcting the position of the tectorial membrane, where knockout studies in mice lead to an increase of 40-60 dB in hearing thresholds, suggesting a possible role in amplification (Liberman et al., 2002).

1.3.2 Cochlear nuclear complex

The cochlear nuclear complex is the first stage in the abstraction process. It is located between the medulla and pons, where distinct cell classes are involved in encoding different aspects of sound. The cochlear nuclear complex is comprised of roughly five neuronal classes. Each auditory nerve fiber maintains the tonotopic spatial arrangement with other neighboring fibers as they synapse in the cochlear nucleus. Low frequency information lies in the ventro-lateral plain and high frequency information in the dorso-medial plain (Sando, 1965). However each ipsilateral fibre that enters the nuclear complex bifurcates, essentially creating a 'sheet' of neurons with the same CF as the fibre. This results in an isofrequency domain (Sando, 1965). The ascending branch terminates in the anterior ventral portion (AVCN) and a descending branch in posterior ventral (PVCN) and dorsal cochlear nucleus (DCN) (D. LORENTE, 1949). The AVCN is comprised of several neuronal types. Bushy

cells make up the majority in this division where they receive input from type I spiral ganglion neurons, where the synapses formed are one the largest in the central nervous system (15-30 μm), known as the endbulb of Held (Ryugo & Fekete, 1982). The large amount of neurotransmitter released at these synapses evokes postsynaptic firing of the bushy cells ensuring that frequency information is retained.

The PVCN, is composed most prominently of octopus cells (Brawer et al., 1974; Osen, 1969). These neurons receive multiple inputs from both type I and type II spiral ganglion fibres resulting in broader frequency tuning. Interestingly they only respond to the onset of broadband stimuli with some of the highest temporal precision observed (Golding et al., 1999). Dotted throughout both divisions are multipolar cells, which have slightly broader tuning than bushy cells (Brawer et al., 1974; Osen, 1969; P. H. Smith & Rhode, 1989). These neurons appear to adapt their firing rate depending on the strength of auditory input and not the frequency (Ferragamo et al., 1998). The DCN is a laminated structure comprised of fusiform cells and stellate neurons (Osen, 1969). DCN neurons not only receive input from descending spiral ganglion axons but also from other brain regions, where recent work has suggested that the DCN could play a prominent role in the binaural processing of sound (Davis, 2005). In conclusion all neuronal classes in the cochlear nucleus receive the same input, yet interestingly their output represents a different feature of the sound. This represents the first indication that morphology and unique synaptic arrangements play a critical role in the processing of sound in the ascending auditory pathway.

1.3.3 Superior olivary complex

The superior olivary complex is predominantly responsible for extracting cues of localization.. It is comprised of three major nuclei; the lateral superior olivary nucleus (LSO), the medial superior olivary nucleus (MSO) and the medial nucleus of the trapezoid body (MNTB), where the cells located in these nuclei have some of the most complex functional responses and anatomical structures along the ascending auditory pathway. It receives the vast majority of its input from the AVCN via the ventral acoustic stria and trapezoid body. The MSO is widely regarded as the stage that horizontal sound localization is first encoded (Masterton et al., 1975). Multipolar cells receive bilateral input from low frequency spherical bushy cells located in the left and right AVCN, thus allowing for convergent binaural processing of auditory stimuli. These neurons encode the horizontal location of low frequency sounds as they are diffracted and not reflected resulting in a time difference between when a sound is detected in the left ear and when it detected in the right ear. These differences in time and hence phase are known as, interaural time differences (ITD).

This represents one of two methods employed to determined sound source location. The MNTB is comprised of larger multipolar cells that receive input from contralateral globular bushy cells of the dorso-medial part of AVCN (Jean- Baptiste & Morest, 1975), this results in a majority of input coming from high frequency representations. Axons from MNTB innervate the third olivary nucleus the LSO. The LSO is also comprised of bushy cells, albeit smaller than MSO, where they receive input from ipsilateral input from AVCN and contralateral inhibitory (glycine) input MNTB. This results in LSO receiving more high frequency representations. The LSO can also encode horizontal localization but via a different method (Erulkar, 1972). Given that high frequencies are reflected from the head, there exists an intensity difference between the left and right ear, otherwise known as interaural level difference (ILD) (Boudreau & Tsuchitani, 1969). The LSO and MSO therefore form crude maps of space in the horizontal plane. These ILDs and ITDs are then transferred upstream to the inferior colliculus, however some LSO bushy cells send bilateral projections upstream to the lateral lemniscus.

1.3.4 Inferior colliculus

The inferior colliculus (IC) is the main auditory processing station in the midbrain, where it receives convergent input from the feature extracting brainstem-processing stations. One of its tasks involves integrating ILD and ITD information and sending it to the superior colliculus for reflex orientation to a sound source. Neurons involved in this startle reflex appear exhibit GABAergic control where they appear to receive dopaminergic input (Nobre et al., 2003). The largest body in the IC is the central nucleus (CNIC) followed by the dorsal cortex (DCIC) and external cortex (ECIC). The CNIC is composed of multipolar fusiform cells with their dendrites orientated obliquely where it receives most of its input from the lateral lemniscus and minor connections from commissure of Probst. A peculiar gradient is maintained whereby low frequency representation comes from the ipsilateral ear however high frequency representation comes from the contralateral ear. Neurons in the IC not only preserve the information from the sensory epithelia (tonotopy) but have also shown tuning to sound intensity, duration, the rate of amplitude and frequency changes (modulation rate), direction of change in sound frequency (frequency sweep direction) (Fuzessery & Hall, 1996; Rees & Møller, 1983; Sivaramakrishnan et al., 2004). It is really here in the IC, that we see some more complicated computational mechanisms arising and as a result they exhibit complex tuning curves, reflecting the convergent input they receive where complexity in this regard refers to an array of tuning curve shapes such as to I, O, V, U and multipeaked.

1.3.5 Medial geniculate body

The medial geniculate body (MGB) is the major thalamic nucleus in the auditory pathway. It is comprised of three divisions; the dorsal (MGBd), ventral (MGBv) and medial (MGBm). The ventral division is composed of bitufted neurons where they receive input from the brachium of the IC, therefore maintaining the ordered tonotopic arrangement seen in subthalamic nuclei. MGBv mostly innervates layer IV of cortex via the lemniscal pathway imparting this smooth tonotopic organisation (J. A. Winer, 1984). It is known to be involved in frequency and level integration (Bartlett & Smith, 1999; Miller et al., 2001). MGBd is a more complex structure, with 10 known subdivisions, no clear tonotopic gradient and 8 neuronal types (J. A. Winer, 1984). It receives input from the peripheral portion of IC and MGBv. It appears to have a multimodal role, modulating cortex. MGBm doesn't appear to have a clear auditory role, as it receives sparse input from the lateral lemniscus and the superior olivary complex.

1.3.6 Auditory cortex

There is a basic anatomical and physiological understanding of the neurons in cortex but how they relate to the type of stimulus representations they encode is poorly understood. Therefore I split this section into 1) the types of neurons found in cortex and their physiology and 2) a general holistic view of what functional tasks primary auditory cortex might be performing.

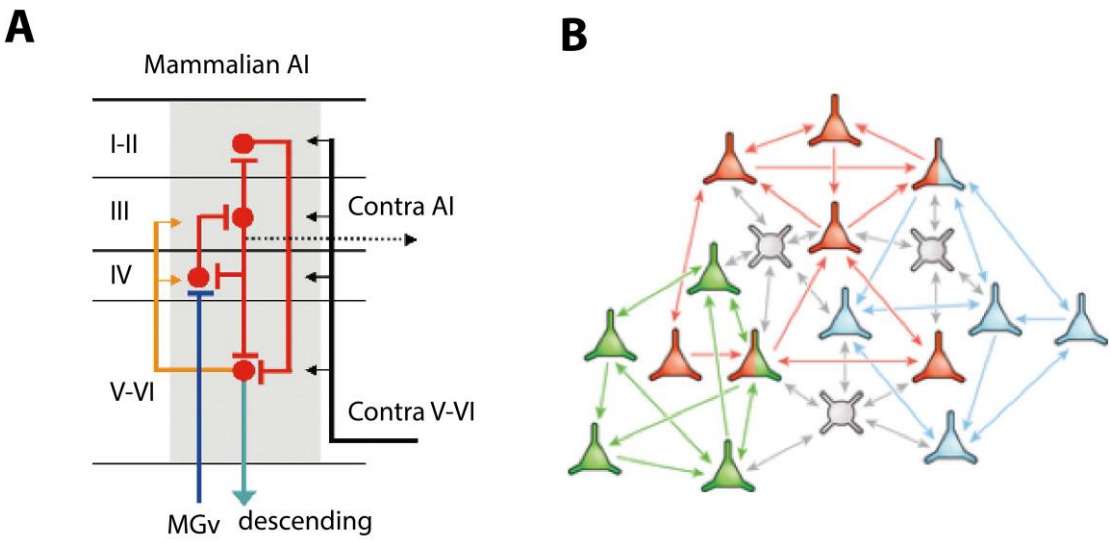

Figure 1.3

Cortical circuits. A Schematic of a canonical corticl cicruit, describing the likely flow of information. **B** Proposed fine circuitry, with cortical circuit formed from overlapping subnetworks.

A. Wang, Y., Brzozowska-Prechtl, A., & Karten, H. J. (2010). Laminar and columnar auditory cortex in avian brain. Proceedings of the National Academy of Sciences, 107(28), 12676-12681.
B. Harris, K. D., & Mrsic-Flogel, T. D. (2013). Cortical connectivity and sensory coding. Nature, 503(7474), 51-58.

1.3.6.1 Structure and anatomy of primary auditory cortex

In all mammals the auditory cortex is located in the temporal lobe. The primary auditory cortex (AI) is the major recipient of innervation from auditory thalamus, and it represents the first stage of higher order cortical processing of sound. The standard model for auditory cortex is the cat, where cytoachitecture and physiology in each field has been described in much detail. Broadly speaking, auditory cortex is comprised of six layers, with a 'canonical' flow of information throughout the microcircuit; thalamic input recipient layer IV, sends projections to layer II/III which in turn drives the output layers V and VI.

1.3.6.2 Layer I

The molecular layer, or more commonly layer I, is comprised of very few neurons and predominantly neuropil. In the rat, roughly 90% of the neurons located in this layer are GABAergic (J. Winer & Larue, 1989). These neurons most likely play a role in inhibiting distal dendritic arbors emanating from layers II-V. Some of these neurons have surprisingly unique morphologies, with dendritic branches running parallel to the surface of the pia for vast distances (J. Winer & Larue, 1989; J. A. Winer, 1984). Excitatory and thalamic axons from auditory and other brain regions terminate in this layer, although the functional role of this layer still remains unclear it has been suggested that it could play a role in critical feed-forward and feedback processes (Matsubara & Phillips, 1988).

1.3.6.3 Layer II/III

The external granular layer or Layer II has multiple morphological cell classes that can be broadly distinguished as either pyramidal or nonpyramidal, where these neurons typically synapse onto other interlaminar layer I-III neurons. Layer II is mainly comprised of medium sized nonpyramidal neurons located closer to the pia and large pyramidal cells located at the border of layer III. One of the nonpyramidal neurons that appear unique to layer II, is the extraverted multipolar cell. It has large dendritic arbors that span a large area in the lateral domain, and it is often used to identify this somewhat difficult layer (Code & Winer, 1985). The external pyramidal cell layer (layer III) has the most diverse group of morphological cell classes in AI. Of the nonpyramidal cell class, spinous stellate cells have been reported where they appear to exhibit their influence within layer III. Interestingly small granule cells and multiple neurogliaform are also reported (Meyer et al., 1984). Small pyramidal cells appear to be located deep in layer III, with their apical dendrites barely reaching layer II. Large pyramidal cells however, appear to extend their dendritic arbors to layer I.

Layer II/III neurons have been shown to exhibit narrow frequency responses areas (FRA) and have lower threshold responses to tones in comparison to deeper layers (except layer IV) (Wallace & Palmer, 2008). However two-photon calcium imaging revealed that the tuning of local spines could be highly heterogeneous most likely explaining the diverse response properties of individual neurons (Bandyopadhyay et al., 2010; Castro & Kandler, 2010; Chen et al., 2011; Rothschild et al., 2010). Furthermore, multi-unit studies also identified that neurons in Layer II/III exhibited sparse and spatially confined responses under both spontaneous and evoked conditions (i.e. tonal responses are encoded by few neurons)(Sakata & Harris, 2009). This highlights that even though layer II/III has relatively narrow tuning curves in comparison to other cortical layers, responses are still highly heterogeneous.

1.3.6.4 Layer IV

The relatively thin internal granule cell layer is almost entirely comprised of pyramidal cells. The dominant pyramidal cell classes are either tufted or multipolar, with smooth aspinous dendrites. It receives predominant input from thalamic projections, however it also receives corticocoritcal, intrinsic and commissural input. Large pyramidal cells have multipolar dendrites that innervate large areas whereas the smaller pyramidal neurons, usually located in the superficial internal granular layer, have more restricted dendritic arbors that are tufted. This apparent morphological dichotomy suggests that they might represent different spatial domains in layer IV. Layer IV axons appear to project to infragranular and supragranular layers (J. A. Winer, 1984). Superficially located nonpyramidal cells in this layer appear to project intrinsically whereas deeper cells project to distant corticocortical targets (Games & Winer, 1988). Superficial neurons in Layer IV exhibit the narrowest frequency tuning in cortex (Wallace & Palmer, 2008), whereas deeper Layer IV neurons have broader frequency tuning similar to Layer V.

1.3.6.5 Layer V

Unlike layer IV, the internal pyramidal cell layer contains a wide variety of morphologically distinct pyramidal and nonpyramidal cell classes. Its projections include, the medial geniculate body, nonprimary auditory fields, brain stem targets, the inferior colliculus and the contralateral AI. In turn it receives a significant number of corticocortical and commissural axonal innervation, predominantly stemming form layer II/III. It comprised of roughly one quarter of the total cortical thickness, where neurons are glutamate, aspartate and GABA immunoreactive. The pyramidal neurons located in this layer are known for their large size and dendritic complexity (thick and thin tufted), where their apical dendrites typically extend to layer I and II/III.

Amongst the nonpyramidal cell classes there are large and small multipolar cells, with oval somata and poorly branched dendrites. Their targets however remain unknown. Whole cell recordings in the somatosensory cortex suggest that thick and thin tufted pyramidal neurons exhibited stereotyped physiological responses (Hattox & Nelson, 2007), given that they represent cortical output it would suggest that these nonoverlapping populations provide unique readouts to their targets. Layer V neurons typically exhibit broader frequency tuning than superficial layers and higher threshold responses (Wallace & Palmer, 2008). They have also been shown, unlike layer II/III, that under evoked conditions they respond with densely distributed activity (ie tonal responses are encoded by changes in the firing rates of large numbers of neurons) (Sakata & Harris, 2009).

1.3.6.6 Layer VI

The deepest layer in cortex, sometimes called the multiform layer or spindle cell layer (Brodmann, 1909; Campbell, 1905). This layer is known to contain the most diverse neuronal population in AI, where currently nine distinct morphological cell classes have been identified. While there is a sharp border between it and the white matter its upper boundary is usually determined by decreasing pyramidal cell size and sparsity. Nonpyramidal cell classes mainly innervate subcortical nuclei where their role, unlike infragranular layers, appears to be excitatory (Prieto et al., 1994; Prieto & Winer, 1999). Probably the most identifiable feature of layer VI, that is also unique to AI, is the giant multipolar cell. Its dendritic arbors can span 600 μm, suggesting that it could encode vast isofrequency or aural representations (Merzenich et al., 1975; Middlebrooks et al., 1980). The pyramidal cell morphologies appear somewhat unorthodox, calling into question whether they are truly pyramidal cells. The small pyramidal cells have simple dendritic arbors and less polarized branching, where the apical dendrite is also titled obliquely with respect to the surface of the pia. Some larger pyramidal cells are classified as inverted, where interestingly it has been suggested that they are GABAergic (Prieto et al., 1994). Population recordings identified that Layer VI neurons, like Layer V, also had broader frequency tuning than superficial layers and higher threshold responses (Wallace & Palmer, 2008). A recent study in primary visual cortex, identified that neurons that send cortico-cortical projections had broader stimulus selectivity as they were predominantly innervated by deep layer VI neurons. On the other hand, cortico-thalamic-projecting cells had narrow stimulus selectivity and received long-range input (Vélez-Fort et al., 2014). This is an interesting discovery, which could suggest that a similar functional microcircuit exists in auditory cortex.

1.3.7 Primary auditory cortex and the development of perception

Unlike subcortical nuclei, our understanding of how primary auditory cortex contributes to the perception of sound remains a topic of ongoing research and debate. Although a crude method, lesion studies have been highly informative. AI appears to be involved in frequency processing and pitch perception (Heffner & Heffner, 1986; Tramo et al., 2002). Furthermore patients with permanent temporal lobe damage, that encompassed AI, had impaired spatial localization (Clarke et al., 2000; Zatorre & Penhune, 2001). Recently reversible impairment studies using $GABA_A$ receptor agonist muscimol in behaving ferrets confirmed these deficits in sound localisation; however, interestingly over time there was a recovery of performance most likely as a result of plasticity (A. L. Smith et al., 2004). However lesion studies and other cortical silencing techniques typically damage axons *en passant* and any other connections that are shared with the lesion site, making it harder to definitively identify contributions of specific fields. Based on fMRI and single unit studies it has been suggested that a hierarchical processing stream exists for extracting 'what' and 'where' components of sound (Rauschecker & Tian, 2000). These two components are segregated in primary areas and emanate outwards to parabelt regions via dorsal and ventral pathways for further specialisation (Bizley & Cohen, 2013; Kaas & Hackett, 2000). Interestingly unlike other sensory cortices, the interconnectivity of core areas underlies this process, suggesting that they may have an influence on one another (Kaas & Hackett, 2000).

1.3.7.1 Tonotopy in cortex

As previously mentioned the cochlea encodes frequency, in a relatively linear manner, where it imparts this organisation onto other nuclei in the ascending auditory pathway. This tonotopic organisation is widely identified as the most prominent feature in AI. Multiple attempts have been made to establish whether other responses occur in AI along the isofrequency contours or parallel to the tonotopic organisation. Other than frequency tuning, investigators attempted to construct other maps based on a neurons level response function, threshold, dynamic range, tuning curve shape, binaural interaction and frequency modulation however they showed no clear topographic order (Schreiner & Winer, 2007). Furthermore unlike in VI, our knowledge of receptive field organisation across cortical depth in AI remains unclear (Linden & Schreiner, 2003).

1.3.7.2 Emergent properties of AI

Out of all the sensory modalities the visual system is the most extensively explored where researchers constantly compare and contrast visual and auditory systems in

the hope of finding a common pattern in sensory processing. However there are some fundamental differences between VI and AI that may suggest that it is not an ideal model for comparison. Neurons in VI encode line orientation and binocular disparity, an ability imparted on them by converging thalamic input and the structure of VI cortical circuitry (Hirsch & Martinez, 2006). In contrast in the auditory system frequency selectivity, level sensitivity, duration, pitch and binaural coding are already encoded in subcortical processing stations. This led some authors to suggest that the equivalent of VI in the auditory system is actually IC (Nelken et al., 2003). It is most likely due to fact that inputs into cortex are already highly processed, that it has proved difficult to ascertain its precise functional contribution. Even the most elemental aspects of sound such as frequency and location, can evoke highly variable responses in AI (Read et al., 2001). So far there doesn't appear to be a particular stimulus that allows for receptive field discrimination in the same way as orientation bars and bar patches do for VI neurons (King & Nelken, 2009).

1.3.7.3 Complex stimuli

Most studies that attempt to identify spatial maps in AI are based on pure tones, as it represents the most basic component of sound. However pure tones rarely exists in the natural world, whereas broadband sounds do. Therefore an alternative approach for assessing frequency-tuning profiles of neurons, used by some researchers, are spectrotemporal receptive fields (STRFs). Frequency tuning is derived this way by taking into account across frequency interactions that occur in broadband stimuli and determining which ones are weighted more heavily, reflecting the type of processing undertaken by auditory neurons. Several authors report complex receptive fields where they attributed this effect to the detection of edges in frequency or time (Christopher deCharms et al., 1998) and other studies reported simple receptive fields, with strong excitatory regions at the neurons best frequency flanked by inhibitory side bands, like in pure tone receptive fields (Fritz et al., 2005). This led some investigators to believe that STRFs in AI are indeed equivalent to orientation and direction selectivity in VI neurons. However these receptive fields were not predictive of responses to more complex, naturalist sounds (Bar-Yosef & Nelken, 2007; Machens et al., 2004). As AI could be considered a higher order-processing centre when compared to V1, in order to understand its true function it may be necessary to adopt more complex naturalistic stimuli. Studies that used species-specific vocalisation revealed that AI neurons exhibited a broad range of responses to the stimulus (Kozlov & Gentner, 2014; Wollberg & Newman, 1972). However how these responses correlate with stimulus identity remains unclear (Chechik et al., 2006).

1.3.7.4 Auditory objects

One proposal is that neurons in AI contribute to behaviourally relevant spectrotemporal patterns, or 'auditory objects' (Nelken et al., 2003). Such a process most likely relies on combination sensitivity and feature selectivity (Suga, 1989). These processes are heavily reliant on the temporal structure of competing sounds, that is if they becomes blurred in time, they will be perceived as one object (Micheyl et al., 2005). It has been suggested that auditory cortex is critical to object formation as it is only at this stage of the auditory pathway that we see a match between neural responses and a listener's ability to distinguish objects (Bizley & Cohen, 2013). Some evidence does suggest that AI neurons ability to lock to the temporal structure of stimuli could play a role in object formation. They are known to have slower responses than subcortical nuclei, with most unable to lock to stimuli above ~ 20Hz (Joris et al., 2004), whereas they show a remarkable sensitivity to stimuli below this rate, where these slow modulation rates are more reflective of natural sounds, such as speech (Chi et al., 2005). However in order to understand how object formation is achieved in the auditory system, as has been done in the visual system, it is necessary to identify if and which neural ensembles are responsible at the level of auditory cortex (Bizley & Cohen, 2013).

1.3.7.5 AI and plasticity

The temporal characteristics of sound effect neuronal responses at all levels of the ascending pathway, but its effect is most prominent in cortex. AI neurons display incredible frequency dependent adaptive plasticity at low rates of repetition. This effect is otherwise known as stimulus specific adaption (Ulanovsky et al., 2003). Multiple studies confirm the remarkable plasticity of AI, where neuronal responses can change rapidly over short timescales (Fritz et al., 2005). It has been suggested that this could serve a purpose in improving performance during perceptual learning (Polley et al., 2006; Schnupp et al., 2006). This dynamic model of AI is in contrast with VI, which doesn't appear to display plasticity on the same timescale, at least in the post-developmental brain. This could be related to a greater influence that AI has on subcortical processing, where it sends considerable feedback connections to earlier subcortical stations, a feature somewhat unique to auditory cortices (King et al., 2007; Suga, 2008).

In conclusion we have a general appreciation for the type of neural responses expected, and a coarse anatomical perspective of the macro structure at the level of auditory cortex. Our knowledge of function and how it is achieved isn't as detailed

and defined as other nuclei in the ascending auditory pathway. Therefore if we are ever to understand how perception is built it is necessary to identify cortical circuits via perturbation, and perform functional and anatomical characterizations of their components.

1. 4 COMPLEX NEURAL MECHANISMS FOR DETECTING PERCEPTUAL FEATURES

A model for how the auditory system processes more complex, broadband naturalistic sounds is co-modulated masking release (CMR). Psychophysical studies identify that the auditory system is unlikely to be just processing spectral information in separate channels, but instead suggest that there are across frequency computations taking place. Some of these computations are likely to be occurring in auditory cortex.

1.4.1 Auditory filters and masking

As previously mentioned, the cochlea is essentially made up of a bank of auditory filters, where they have been shown to act as a row of non-linear, level dependent overlapping band-pass filters (Baumgarte, 1997). Our ability to discriminate different frequencies, otherwise known as frequency resolution, is dependent on the bandwidth of the filters. Over the past 70 years the bandwidth and overall shape of auditory filters has been widely debated where a multitude of different physical and pyschoacoustical measurements have been used to investigate them (Dubno & Dirks, 1989; Glasberg & Moore, 1990; B. C. Moore & Glasberg, 1983). If two sounds are far enough apart in frequency that they fall into different auditory filters, they can be discriminated and detected with relative ease. However if the sounds fall into the same auditory filter, the auditory system encounters a problem known as ‘masking’.

Auditory masking is in effect, the reduction in detectability (threshold) of a sound due to the presence of two or more sounds within the same auditory filter. The mechanism through which masking occurs was initially explained by the ‘power spectrum model’. This model is based on three assumptions 1) sound is filtered by an overlapping bank of auditory filters 2) threshold is determined by the filter with the largest signal to masking noise ratio and 3) the temporal characteristics of a signal are ignored (Verhey et al., 2003). Under this model only noise that falls within an auditory filter of interest can contribute to the masking of a sound, other auditory filters that filter frequencies outside of that region do not contribute (Figure 1.4 B). The importance of auditory filter bandwidths is best represented in individuals with sensorineural hearing loss (SNHL). Due to deficient hair cell function, the bandwidth

of auditory filters in effected individuals is subsequently broader resulting in increased masking.

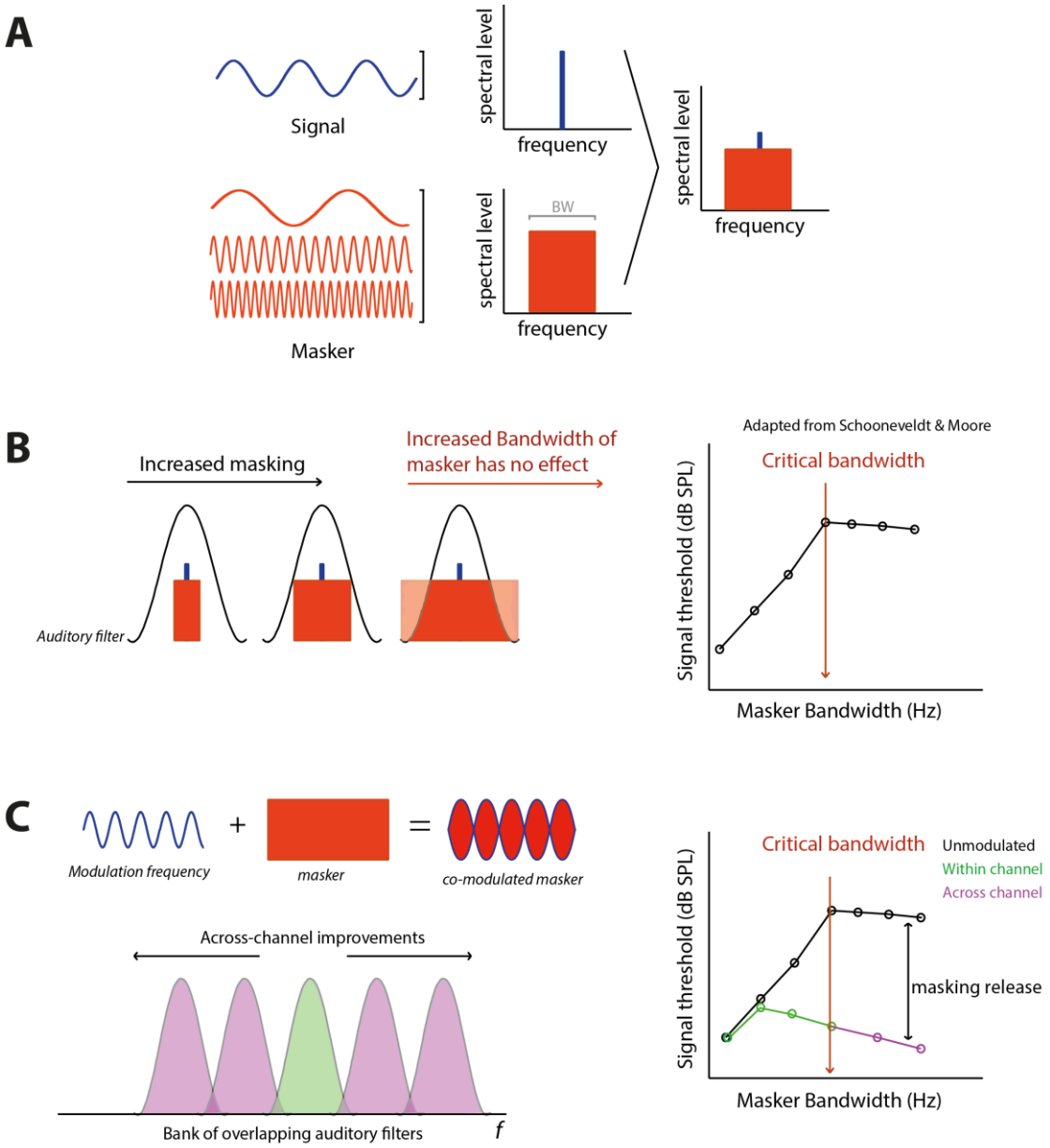

Figure 1.4

Comodulation masking release: **A** Schematic of a masked signal. The masker contains multiple frequencies, depending on how widely distributed the frequencies are it is classified as either broadband or narrowband. **B** The addition of extra noise energy, increases the effect of signal masking up until the critical bandwidth ie the bandwidth of the auditory filter. Any additonal masker energy does not increase detection threshold further **C** By modulating the noise energy the effect of masking is diminished, resulting in improved signal detection thresholds. This can be attributed to within channel and across channel effects.

1 figure adapted from Schooneveldt & Moore (1989). Comodulation masking release for various monaural and binaural combinations of the signal, on-frequency, and flanking bands. J Acoust Soc Am. 85(1):262-272

1.4.2 CMR

However the power spectrum model relies on negating the effect of the temporal characteristic of presented stimuli. This is an interesting assumption as broadband stimuli or white noise without any amplitude modulation rarely occur in nature. Studies identified that if you amplitude modulate the additional sound energy

masking a signal, thresholds in fact decrease (Hall et al., 1984). This effect was termed ‘co-modulation masking release’ (CMR) (Figure 1.4 C). There are two types of proposed CMR that violate the power spectrum model. The first is known as within-channel CMR which suggests that the temporal structure of a masker can greatly influence the reduction of signal thresholds. The second model of CMR is referred to as across channel and it violates the power spectrum in two ways; firstly it proposes that auditory filters that lie outside of the embedded signal do not remain idle but contribute in some way and secondly the temporal properties of a sound, as in within channel CMR, contribute to the reduction in signal detection thresholds. These discoveries led to multiple physiological and psychophysical studies that have attempted to determine the physiological underpinning of both types of CMR.

1.4.3 Different masker types

There are two types of masker employed in CMR experiments. The first masker type involves one co-modulated band-pass noise masker centered on the signal frequency. It was this masker type that originally identified that by modulating the additional noise energy it was possible to reduce signal detection thresholds (Hall et al., 1984; Verhey et al., 1999). The second type of masker type is comprised of multiple narrowband maskers, one centered on the signal and the others spaced above and below it, otherwise known as flanking bands (Schooneveldt & Moore, 1987). Schooneveldt and Morre 1987 proposed three different flanking band setups to assess their impact on CMR. The first utilizes two independent narrow band conditions, one masker is centered on the signal and the other is centered away (DV). The second condition instead of being centered away the flanking bands are centered either side of the on frequency masker (CM). The final condition is the on frequency masker alone (RF). They discovered that thresholds were lower in the CM condition compared to DV and RF. However interestingly they also discovered that the DV condition reduced thresholds compared to the RF condition. It is in this case that the power spectrum model cannot explain the reduction in thresholds beyond the bandwidth of the auditory filter (Schooneveldt & Moore, 1987). These different responses have been attributed to ‘within channel’ and ‘across channel’ effects of CMR. There is still some debate as to whether across channel CMR does exist, as it is predication is dependent on the shape of an auditory filter. By altering the shapes of auditory filters from rectangular to gamma tone filters it is possible to predict CMR without accounting for an across channel process (Verhey et al., 1999). However other studies have observed CMR as a result of including flanking bands at spectral distance of 3 octaves from the on frequency flanking band, where this result can only be accounted for by an across channel process (Cohen, 1991). In conclusion these studies identified that the effect of a masker can be reduced mostly by increasing its

bandwidth, amplitude modulating the noise, modulating this noise at a low frequency, and finally modulating the noise synchronously.

1.4.4 Underlying neural mechanisms

Multiple models have been proposed that attempt to explain CMR, such as the 'dip-listening model' which suggests that the temporal minima of a masker is utilised to enhance detection of the signal (Buus, 1985) or 'the equalization cancellation model' (EC) where the output produced at off-frequency filters is subtracted from the auditory filter where the signal is centered, thus reducing the masking effect (Buus, 1985; Durlach, 1963). The precise neural networks that are involved in CMR are not currently known, however there are a handful of physiological studies that have identified correlates of CMR in the auditory pathway and proposed mechanisms. Some research has indicated that narrowband units are influenced by wideband inhibition from onset units (Figure 1.5), and that this inhibition plays a role in CMR (Pressnitzer et al., 2001). There is some data that suggests that this proposal could be accounted for via the interaction of subtypes of stellate cells in the CN. Onset units (D-type stellate cells) in the CN usually have precise spike timing locked to the onset of sound but little or not sustained responses. They typically have broad frequency response areas that lack an indication of inhibitory side bands (Jiang et al., 1996; Rhode & Greenberg, 1994). However there is one subtype of stellate cell, T-type, which exhibits an initial regular burst in response to onset that decays and becomes more irregular and displays inhibitory side-bands (Blackburn & Sachs, 1990). It has been proposed that this response occurs as a result of axonal innervation from D-type cells traversing VCN and providing inhibitory input onto T-type stellates cells (Arnott et al., 2004; Ferragamo et al., 1998; Pressnitzer et al., 2001). These cell types most likely account for within channel CMR in the CN however recent work has suggested that correlates of CMR might exist at higher order processing stations along the ascending auditory pathway. Extracellular studies performed in the cat under band-widening conditions identified that phase locking plays an important role in signal detection at the single cell level. The authors observed that a vast majority of neurons phase locked to the stimulus in the absence of an embedded signal, where interestingly upon its addition their ability to phase lock was diminished. It was this suppression of phase locking that was presented as the mechanism for the reduction of threshold (Nelken et al., 1999). Alternatively other authors have suggested that a higher order processing strategy, such as object formation (previously mentioned) could be responsible for this effect (Grose & Hall III, 1993; McFadden & Wright, 1992). The exact mechanism through which a masker and a signal can be separated to form separate perceptual objects is

not currently known. Regardless both phase locking suppression and object formation most likely involves complex neural inhibition, forward suppression and adaptation mechanisms (M. Calford & Semple, 1995; Ulanovsky et al., 2004; Wehr & Zador, 2005).

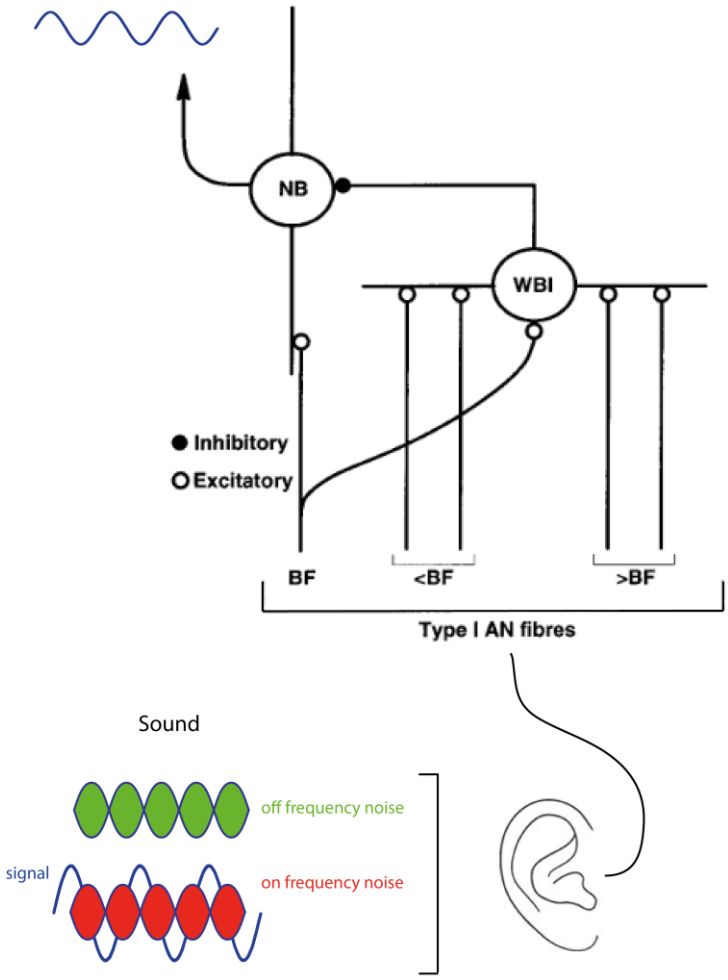

Figure 1.5

Proposed inhibitory circuit contributing to CMR in the CN. Type I auditory nerve fibres provide the wide band inhibitor (WBI) with broad frequency input, whereas the narrowband unit receives a very narrow range of frequency input.

Adapted from, Pressnitzer, D., Meddis, R., Delahaye, R., & Winter, I. M. (2001). Physiological correlates of comodulation masking release in the mammalian ventral cochlear nucleus. The Journal of Neuroscience, 21(16), 6377-6386.

1.5 AIMS OF THIS STUDY

1.5.1 Outline of thesis

In this study, *in vivo* whole cell patch clamp recordings were performed on neurons in the primary auditory cortex, enabling both synaptic and spiking activity to be monitored. Sensory evoked activity in AI was recorded from the left hemisphere of anaesthetized mice. This thesis is divided into three experimental chapters, with each one followed by a separate discussion section:

The first results chapter deals with characterizing the response properties of AI neurons to pure tones. This was carried out in order to determine if response properties with regard to pure tones observed in other animal models also exist in the mouse. Electrophysiological characterization was also performed in order to correlate patterns of responses with identifiable cell classes.

The second results chapter addresses the role of synapse location on synaptic integration. This question was restricted to thalamocortical synapses in AI. The novel mGRASP technique was tested as a means to establish thalamocortical synaptic distribution patterns in AI. Whole cell transfection recordings were then made in order to identify any correlates between synaptic distribution and functional responses.

The third results chapter deals with identifying whether neural correlates of across channel CMR exist at the level of primary auditory cortex. Four different masker conditions were employed to truly make this assessment. Given that correlates of CMR have been shown to exist in different auditory nuclei, it was necessary to determine if any observation at the level of cortex occurred as a result of passive inheritance. By utilising optogenetic techniques cortex can be manipulated in order to identify if its circuitry plays an active role.

The thesis concludes with a general discussion of results and with a primary focus on the potential avenues for future work.

2 MATERIALS AND METHODS

2.1 SURGICAL PROCEDURES

All experiments were carried out in accordance with the U.K. Home Office Animals (Scientific Procedures) Act (1986).

2.1.1 Non-recovery

Both male and female young adult CBA/CA (28-42 day old) mice (Charles River Laboratories or Harlan) were anaesthetized with a mixture of Midazolam (5 mg kg-1) Medetomidin (0.5 mg kg-1) and Fentanyl citrate (0.05 mg kg-1) via intraperitoneal injection, where the depth of anaesthesia was assessed via pedal reflex. Throughout all experiments a rectal probe was inserted to monitor and maintain the animal at 37 ± 0.5°C through the use of a homothermic blanket (FHC, USA). The depth of anaesthesia was tested every 10 minutes using a pinch to the hindlimb. When animals were areflexive, a sagittal cut was made through the skin to expose the cranium and haemostatic clips were used to secure the skin. A light-weight head plate was fixed to the surface of the skull using Histoacrylamide (Braun Corporation, USA). The head plate was then fixed and positioned using an articulated arm (Thor labs, UK). Connective tissue was removed covering the left ecto-sylvian plate and a dental drill (Osada, Japan) was used to make a small craniotomy (1 mm x 1 mm) in order expose the left hemisphere of auditory cortex (2.54 mm caudal of Bregma and 4.2 mm lateral of the midline). The dura was pierced using a fine needle (30 G, Harvard Apparatus, UK), and removed with dural forceps (Inox forceps: tip size = 0.05 x 0.01 mm; Fine Science Tools, Germany). Artificial cerebrospinal fluid (aCSF) was applied every few minutes to the exposed area of cortex in order to keep the area moist.

2.1.2 Recovery

For recovery surgeries, the same method as above was used with minor additions. Prior to the initiation of any surgical implementation a non-steroidal anti-inflammatory drug (Carprofen; 5 mg/kg) was provided via intra-peritoneal administration in order to provide post-operative analgesia and aid recovery. Post-experimentation, the cranial window was covered with aCSF – agarose and then kept in place with a silicone-based elastomer (Kwik-Cast; World Precision Instruments, USA), in order to prevent

damage. Acrylic dental cement (Kemdent, UK) and a layer of nail varnish were applied to reinforce the window. The mice were then injected intraperitonealy with a mixture of Naloxon (5 mg kg-1) Flumazenil (0.5 mg kg-1) and Atipamezol (0.05 mg kg-1), in order to counteract the effect of the anaesthesia. The animals were then transferred to a heated incubation chamber (~ 36°C) where they were given sufficient time to recover. Analgesia was maintained using Buprenorphine (0.8 mg/kg) jelly for 1-7 days.

2.1.2.1 Optogenetic viral injection

Aseptic procedures and post-operative care was maintained as previously mentioned. Six week old PV-cre (B6;129P2-Pvalbtm1(cre)Arbr, Jax stock no. 8069) mice were anaesthetized and held using ear bars on a stereotaxic mount (Angle 2, Leica). A small craniotomy was made with a dental drill ~1.9mm lateral from midline and ~2.7mm caudal to bregma. Mice were then injected with ChR2/AAV (pAAV-EF1a-double floxed-hChR2(H134R)-EYFP-WPRE-HGHpA, www.addgene.org). A thin glass pipette holding the virus was positioned in auditory cortex and the viral titre (0.5µl) was then slowly injected over a period of 20 minutes. The pipette was then slowly retracted and the craniotomy sealed with Kwik-Cast and an additional layer of acrylic dental cement was placed over the top forming a hard seal. Mice were then sutured and recovered as previously mentioned.

2.1.2.2 mGRASP

The same injection protocol and recovery procedure was maintained however. Wild type mice were anaesthetized and held using ear bars on a stereotaxic mount. A small craniotomy was made above auditory cortex (~ 4 mm lateral from midline and ~2.7 mm caudal to bregma) and second craniotomy above medial geniculate body (~1.9 mm lateral from midline and ~ 3.5 mm caudal to bregma). Auditory cortex was injected with post-mGRASP (*post*; paavCAG-post-mGRASP-2A-dTomato; Addgene, cat. no. 34912) and the medial geniculate body with pre-mGRASP (*pre*; paavCAG-pre-mGRASP-mCerulean; Addgene, cat. no. 34910). Each thin glass pipette holding the corresponding virus was positioned and the viral titre (0.3µl) for the pre-virus and 50 nl of the post virus was slowly injected over a period of 5 minutes. The pipettes were then slowly retracted and each craniotomy sealed with Kwik-Cast and acrylic dental cement. Mice were then sutured and recovered as previously mentioned.

2.2 STIMULUS PRESENTATION

Auditory stimuli were generated and calibrated using Matlab and stored as files to be used later, all signal levels were calibrated (5-100kHz flat spectrum ±1.5dB SPL). The following stimuli were saved in their structures as a single file and presented during neural recordings. All sound files were also presented using Matlab to interface with RPvdsEX (Tucker Davis Technologies; TDT, USA), which ran on an RZ6 (TDT) driving a free-field speaker (ES1, TDT).

2.2.1 Pure tone stimuli

During recordings, mice were situated in the center of a sound-attenuating anechoic chamber (Industrial Acoustic Company, UK), and stimuli were presented from 1 calibrated speaker, positioned at a distance of 5 cm from the right ear (contralateral). To determine the frequency response area (FRA) of a recorded neuron an array of 117 tones were presented in a pseudo-random order, each lasting 100ms. The array consisted of thirteen logarithmically spaced frequencies (1/3 octave steps) spanning 3–48 kHz, and nine tone intensities (10–90 dB SPL at 10 dB steps) with a 1 second inter-stimulus interval.

2.2.2 CMR stimuli and laser stimulation

Stimuli were sinusoidally amplitude-modulated (SAM) tone maskers presented in the presence of a pure tone signal. Three bandwidth configurations were used: two broadband conditions (IM and CM) and a narrowband condition. The signal frequency was selected as the characteristic frequency (as determined from a neurons FRA). In the narrowband condition this involved a 10Hz SAM at CF. The broadband conditions consisted of an on-frequency band (10Hz SAM at CF), a low off-frequency band (3 x 0.125 octave spaced 10Hz SAM pure tones centered at 0.5 octaves below CF) and a high off-frequency band (3 x 0.125 octave spaced 10Hz SAM pure tones centered at 0.5 octaves above CF). These off-frequency bands were designed so that the additional sound energy lies outside of the mouse auditory filter centered at CF. The phase of the envelope of the on-frequency band remained identical for all conditions. For the IM condition the envelope of the off-frequency bands was selected at random between 0-180° whereas the off-frequency bands in the CM condition had identical envelope phases with the on frequency band. The masker portion for all three conditions lasted 500ms with a pre-cursor of 400ms positioned 100ms before. A short-CM condition was also included where it is almost

identical to the Long-CM condition except it lacked a pre-cursor. Long conditions were preceded and followed by 500 ms of silence and the short condition was preceded by 1000 ms and followed by 500ms of silence (inter-stimulus interval of 2 s). The embedded pure tone signal was comprised of three 50ms SAM tone pips (10Hz modulator) positioned in the 3-5th troughs of the masker. In total there were 8 different signal conditions were used for each masker condition, a noise alone (i.e. no signal) condition and seven SNR conditions (-10 to 20dB SNR in 5 dB steps). For mice expressing ChR2 exclusively in PV cells, an optical fibre attached to laser (473nm; SLOC, China), was positioned ~1mm from the cortical surface. The laser was controlled via TTL signals generated by a digital processor (RZ6, TDT). The laser power was calibrated to have an effective fibre tip power of 5 mW, which is more than sufficient for *in vivo* stimulation (Cardin et al., 2010). I conducted preparatory controls using multi-site electrodes at different depths and observed no observable difference in optogenetic perturbation across depth. Finally in addition the same control was performed using a patch electrode, recording from deep layers and again there was no observable difference in optogenetic perturbation. Successful PV-ChR2 transfection was determined based on PV+ YFP+ co expression. Previous immunohistochemistry experiments confirmed that 96.7% of ChR2-mCherry neurons expressed PV (Cardin et al., 2009). Furthermore during optogenetic stimulation I observed significant cortical silencing that was also in line with PV+ neuronal activation (time course), therefore I can assume that there was minimal contamination in other cell types.

2.3 ELECTROPHYSIOLOGY

2.3.1 Internal solution

Table 2.1 Internal solution

Compound	Concentration (mM)
K-gluconate	135
KCL	7
HEPES	10
Phosphocreatine	10
Mg-ATP	2
Na2-ATP	2
Na2-GTP	0.5

Internal solution was adjusted to pH 7.28 with KOH, and had an osmolality in the range of 280-290 mOsm.

2.3.2 *In vivo* patch clamp recordings

Low-resistance patch pipettes (4-7 MΩ) (Sakmann & Neher, 1983; Pei *et al.*, 1991) were used to achieve whole-cell recordings *in vivo*. Pipettes were made from filamentous borosilicate glass capillaries (inner diameter: 0.86 mm, outer diameter: 1.5 mm; Harvard Apparatus, UK), using a Narishige PC10 vertical puller (Narishige, Japan). Pipette tips were initially calibrated using a scanning electron microscope, where tips had to be smooth and targeted resistances typically correlated with a size was 0.5-1 µm (Figure 2.1).

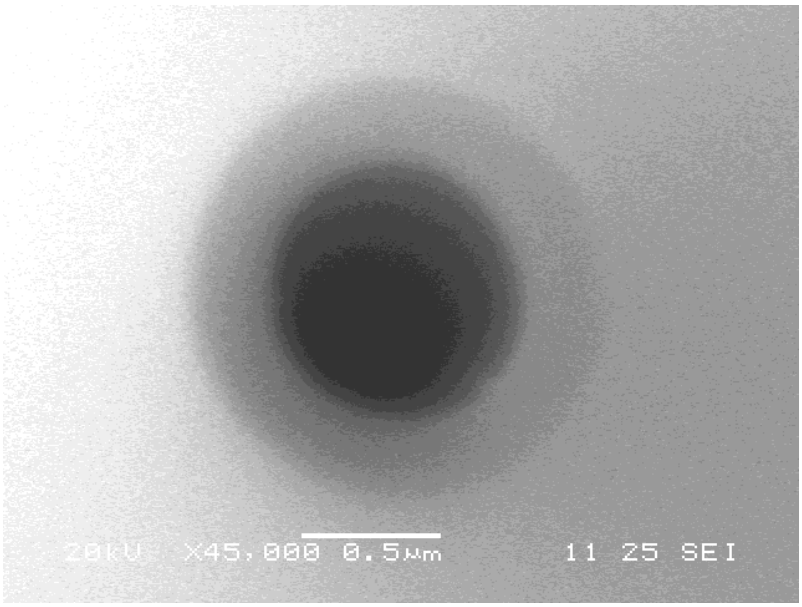

Figure 2.1

SEM image of Pipette tip. Gold-coated pipette tip imaged using SEM. The observed pipette had a resistance of 7 MΩ.

Cells were 'hunted' *in vivo* in voltage-clamp mode using a Multiclamp 700A amplifier (Axon Instruments, USA), controlled via Multiclamp Commander software (Margrie *et al.*, 2002). A positive pressure of ~200 mbar was applied across the pipette in order to prevent blockage. Using a square voltage step (+10 mV, 10 ms steps at 100 Hz), evoked current was monitored, as it acts as an indicator of resistance, where an increased resistance most often indicated a cell membrane in close proximity. Pipettes were rapidly advanced through the brain to a depth of interest. In order to increase sensitivity the positive pressure was reduced to ~30 mbar and the pipette advanced in 1.8 µm steps. When a cell membrane is deemed to be near, a 'three step rule' is applied and pressure was rapidly released. This rapid release would often lead to adherence of a cell to the tip of the pipette, where a strong seal was

identified by a large increase in resistance ~1-10 GΩ. However in the eventually of a poor seal, mild negative pressure was applied to facilitate seal formation. Following successful seal formation, commonly referred to as a cell-attached configuration, the electrode capacitance was cancelled semi-automatically (Multiclamp Commander Software; Axon Instruments, USA) prior to gaining electrical access to the cell. Rapid suction was applied in order to break the cell membrane and establish the whole-cell configuration. Upon gaining whole-cell access, the amplifier was switched to current-clamp mode followed by subsequent bridge-balancing. The angle of approach was always 45 degrees and assuming a flat cortical surface, cortical depth can be estimated.

2.4 IMAGING

2.4.1 Tissue processing and imaging of labelled synapses

For gross viral labelling, brains were analyzed 14 d after recording. Deeply anaesthetized mice were transcardially perfused with cold PBS (0.1 M) followed by fixation with cooled 4% paraformaldehyde (wt/wt) in PBS (0.1 M) and stored at 4 °C for 1 hour. Brains were then washed in PB (0.1 M) and mounted in agarose to provide support. Coronal brain sections (50–70 μm) were cut using a vibrating microtome (VT1000 S) and rinsed in PB in order to remove PBS whose crystallisation can cause autofluoresence. Fluorescence images were acquired on a Leica SP5 laser-scanning confocal microscope. Multi-tile scanned images were performed on a x40 oil objective with a variable zoom (x 2-10) depending on the size of the cell of interest. The power of each laser and the breadth of the PMTs were adjusted accordingly in order to avoid photobleaching and image saturation.

Table 2.2 PMT and Laser settings

Fluorophores	Excitation (nm)	Emission (nm)
mCerulean (presynaptic)	405	441-485
mGRASP	488	496-554
dTomato (postsynaptic)	561	559-639

2.4.2 Plasmid amplification and *In vivo* whole cell transfection

A small sample of pCAG-post-mGRASP-2A-dTomato was kindly provided by Dr Kim laboratory (KIST, Korea). In order to amplify the sample, plasmids were transformed and grown in *Escherichia coli* Stbl3 (Invitrogen) cells to avoid recombination. The cells were lysed and plasmid extracted and purified using an endotoxin-free Gigaprep kit (Qiagen) with the final titre (10mg) aliquoted and suspended in ultrapure H_2O (Qiagen). Correct plasmid sequences were digested and verified by subsequent DNA sequencing. Plasmid aliquots (10 µl) were firstly diluted in H_2O and added to a concentrated standard intracellular solution (~600 mmol/kg). This yielded a final plasmid concentration of ~50–350 ng μl^{-1} and internal solution osmolality of 280 mmol/kg. *In vivo* whole cell transfection is achieved via passive diffusion of plasmid from the internal solution to the cytosolic space of a cell (Rancz et al., 2011). After electrophysiological recordings have been performed the patch pipette was slowly withdrawn (~2 µm s^{-1}) whilst simultaneously monitoring the seal test pulse in voltage-clamp mode to determine access resistance. Typically once the pipette is far enough from the cell, the nanotube that represents the connection between the two eventually pulls an outside-out patch of membrane, a criterion that is considered important but not crucial to cell survival. A successful outside-out patch was confirmed by applying a brief negative pressure pulse in order to break the seal where no indication of action currents indicated that it was successful.

2.5 DATA ACQUISITION AND ANALYSIS

2.5.1 Electrophysiology

Data were low-pass filtered at 3 - 10 kHz and acquired at 25 kHz via an ITC- 18 interface (Instrutech, USA) using Axograph X software (Axon Instruments, USA). Data were analysed offline using Axograph X and Matlab. The junction potential difference between the internal and extracellular solutions was not measured and corrected for. Resting membrane potential (Vm) was measured immediately after formation of the whole-cell configuration (‘break-in’).

2.5.2 Pure tone responses and intrinsic properties

Upon successful break-in, intrinsic properties were determined (input resistance, membrane time constant, rheobase) using 400 ms step current injections ranging

from –200 pA to 200 pA (25 or 50 pA current steps). This ensured sufficient amplitude to induce saturating firing rates in order to determine spike half-width, rheobase and inter-spike intervals. Events were rejected if access resistance exceeded 70MΩ. These intrinsic properties were measured using Axograph X (Mac). Tone evoked responses were analyzed using Matlab. A mean baseline is taken prior to the presentation of the tone and PSP amplitudes greater than 0.5 mV were calculated at stated time windows. Peak times were determined as the time taken from the initiation of a time window to the peak amplitude. Frequency responses arrays were then smoothed using a pyramidal 3 x 3 window. Characteristic frequency was taken as the frequency yielding a defined response at the lowest signal level. Best frequency was taken as the frequency yielding the largest response.

2.5.3 CMR analysis

The mean membrane potential across all repeats (x10) was determined using Matlab. The noise alone condition was then subtracted from each of seven SNR conditions in order to isolate signal responses (1.2 -1.45 s). The peak amplitude and time of the signal-evoked response was calculated in this time window. For cortical inactivation experiments the preceding laser stimulation did not influence subsequent signal-evoked responses, as there was no significant difference between the CM-short and CM-short opto condition.

2.5.4 mGRASP analysis

The three channels (red, blue and green) were separated and using imageJ or Fiji. A tiled image encompassing postsynaptic neurons (red channel) was stitched into a *z*-stack image and exported in .tiff format. Postsynaptic morphologies were reconstructed using Neutube (www.neutube.com). I developed a custom Matlab code in order to identify axonal density, neuronal area and puncta. A 1x1 µm grid was set in order to define the overlap of all three channels, and a rolling ball radius of 0.25 µm was applied to the green channel in order to quantify the number of synapses. This automated procedure was verified by manually inspecting stack images in Fiji or imageJ to confirm the correct detection of puncta.

2.5.5 Statistics

Datasets were deemed to be significantly different if $p < 0.05$, unless stated otherwise. Results are presented as mean ± SEM. Normal distributions were

determined by plotting a histogram and applying a Gaussian fit. For identifying statistical differences in parametric datasets student *t*-test or ANOVA were used. In order to determine if changes in the independent variables significantly affect dependent variables, a one way Multivariate Analysis of Variance (MANOVA) was used. When identifying significant associations between datasets a quantile-quantile (Q-Q) plot was used. If the data was normally distributed a Pearson's correlation coefficient was used to determine the strength of the relationship. Conversely if the data was non-parametric a Spearman Rank correlation was used. All data are presented as mean ± SEM unless otherwise stated.

3 SYSTEMATIC CHARACTERISATION OF NEURAL RESPONSES IN PRIMARY AUDITORY CORTEX

3.1 INTRODUCTION

One of the most fundamental tasks that the brain performs regarding the perception of sound is the segregation and integration of spectral and temporal information. Neurons tuned to specific frequencies transmit stimulus information along the ascending auditory pathway, from the cochlea to auditory cortex (Kaas et al., 1999). Frequency tuning in auditory cortical areas has been characterised in many different species including cat, rat, monkey and ferret (Bartlett et al., 2011; Gaese & Ostwald, 2001; M. L. Sutter, 2000). Advances in the genetic manipulation of neurons have enabled researchers to probe and elucidate the functioning of individual cells and circuits, furthering our understanding of how neurons encode stimuli in the brain. This powerful new tool however has been largely restricted to the mouse (*Mus Musculus*), resulting in a shift to using the mouse as a critical model for auditory research. As a result our understanding of how frequency information is transmitted through the auditory system must be re-examined/quantified and compared to other species to determine how analogous it is. Work has already begun with the systematic quantification/comparison between cortical fields in the mouse using extracellular techniques. This approach has already identified systematic differences in auditory cortical fields in the mouse (Joachimsthaler et al., 2014; Linden & Schreiner, 2003), however, remarkably little is known about subthreshold properties.

Beyond encoding the frequency components of a sound, the auditory system must also unravel its temporal properties. Previous studies have shown that temporal resolution is degraded, to varying degrees, at the level of auditory cortex when compared to peripheral sub-stations along the ascending pathway (Creutzfeldt et al., 1980; Evans & Whitfield, 1964; Merzenich et al., 1975; Whitfield & Evans, 1965). This effect is characterised by a reduction in on-going phasic responses, such as peaks and troughs of the signal, driven by this loss of temporal precision. While there is loss in high fidelity temporal coding, it is replaced by strong responses to the initiation of a sound (onset) and its termination (offset) (Volkov & Galazjuk, 1991). How this mechanism emerges and fits into an overall coding strategy at the level of cortex remains a mystery. Most work, has suggested that at the level of cortex, somewhat unsurprisingly, that the offset response simply encodes the termination of a sound allowing the auditory system to

potentially group objects not only based on their initiation but their cessation (Brand et al., 2000; N. Xu et al., 2014). Early studies failed to report the existence of offset responses, likely due to the suppressive effects of certain anaesthesia (barbiturates), however recent reports of significant offset responses were performed, either in awake or ketamine/halothane anaesthetised preparations (Moshitch et al., 2006; Volkov & Galazjuk, 1991). The physiological observation of offsets responses was initially attributed to post-inhibitory rebound firing (M. Calford & Webster, 1981; He et al., 1997; Heil et al., 1992; Volkov & Galazjuk, 1991), however, recent work has described a non-overlapping synaptic mechanism driving responses to sound onsets separate to that of offsets (Scholl et al., 2010). Furthermore a few studies confirm that onset and offset tuning is distinct at both sub and suprathreshold levels with highly variable frequency response profiles (Moshitch et al., 2006; Scholl et al., 2010). The potential functional significance of the offset response warrants further investigate into its mechanistic evolution through the auditory system and its potential impact on behaviour.

Another aspect that remains poorly understood is the relationship between auditory processing properties of neuronal classes across cortical layer. Until recently depth dependent changes in the breadth of frequency tuning was attributed to non-preferential input onto cells in thalamo-recipient layers. More specifically this effect resulted in Layer IV neurons exhibiting narrower tuning than Layer V and Layer II/III. A recent study has identified that there is a non-uniformal distribution of intrinsic burst firing (IB) pyramidal cell class across depth (Nowak et al., 2003). In addition, other studies in the rat have identified that different pyramidal cell classes in layer V respond to frequency presentation differently, with intrinsic burst-like (IB) cells exhibiting broad frequency tuning and regular spiking (RS) cells showing narrow frequency tuning (Sun et al., 2013). This observation combined with the fact that they have distinct long-range targets, could suggest that neuronal classes play different roles in the transfer of auditory information (Gao & Zheng, 2004; Le Bé et al., 2007; Schubert et al., 2001). Given that depth dependent changes in the breadth of frequency tuning were determined via extracellular recordings it is difficult to ascertain whether separate classes of cells contribute more to this effect. Therefore in this chapter I performed intracellular recordings in order to acquire intrinsic membrane properties to classify cell classes and group functional responses accordingly, in an attempt to further our understanding of the processing of pure tones in AI of the mouse.

3.2 RESULTS

3.2.1 Quantification of onset and offset responses to pure tones in AI

Whole cell recordings were performed in primary auditory cortex of the anaesthetised mouse (Figure 3.1 A). Upon achieving a successful seal and break in, neurons were presented with an array of 13 frequencies at 9 levels in a pseudo-random order. Post-synaptic potentials were recorded (Figure 3.1 B) and mapped to their corresponding pure tone, allowing for the construction of a neurons frequency response area (FRA) (Figure 3.1 C). Each trace in the example cell represents a repeat (grey line) with its average response indicated (black line) for each stimulus pairing. The number of repeats was set to maximise cell viability for further experimentation. Onset responses were classified as post-synaptic potentials that occur throughout the duration of the stimulus (100ms) and offset responses are classified as post-synaptic potentials from the point of its cessation, lasting 100 ms beyond.

3.2.2 Onset responses are more sensitive to sound level than offset responses.

The sensitivity of neurons was compared to perceptual sound detection thresholds in the mouse (Koay et al., 2002). Cells were first categorised by their frequency tuning properties where the frequency evoking responses at the lowest sound level (the Threshold) was deemed that cells Characteristic Frequency (CF). Cells were grouped according to their CF (3-48kHz at 1/3 octave bins) and the mean threshold calculated. Demonstrating the mean sensitivity of cells tuned at those frequencies. This was then compared to behavioural responses in the same species (Figure 3.2A). The data confirms previously reported audiogram trends, where thresholds decrease significantly (ANOVA, $F=1.4$, $p<0.05$) up to ~20kHz (Figure 3.2 B). This trend was reflected in offset responses where there was also a significant decrease (ANOVA, $F=2.1$, $p<0.05$), however interestingly thresholds were on average 5.3 dB higher than onset responses (Figure 3.2 C).

3.2.3 Comparison of frequency tuning between onset and offset responses.

Previous studies failed to acknowledge the existence of offset responses (Heil, 1997; D. Phillips et al., 1994; M. Sutter & Schreiner, 1995; M. L. Sutter & Schreiner, 1991). It was only until recently that awake or non-barbiturate anaesthetised experiments highlighted that responses to offsets are actually quite common (Moshitch et al., 2006; Volkov & Galazjuk, 1991). Until now this effect has not been observed in the mouse. In addition

these previous reports identified responses to sound onset and offset using extracellular recordings, as a result no subthreshold information has been provided. Therefore, using whole cell recordings I measured postsynaptic potentials at sound onset and offset in the mouse under nonbarbiturate -anaesthesia. Of the 201 cells recorded 7% had pure onset responses (n=14), 2% had pure offset responses (n=5) and with the vast majority, 91% responding to both sound onset and offset (n=182). These data confirm the presence of offset responses in mouse AI; I next examined frequency tuning properties in more detail. One way of characterising auditory neurons is to determine the breadth of frequency information it receives. This is most commonly referred to as bandwidth, where neurons with small bandwidths are considered more frequency selective than those with broader bandwidths. Two bandwidth measures were selected, one at 10dB (BW10) above the each neurons threshold and the other at 40dB (BW40, Figure 3.2B). Onset responses at 10dB were narrower (1.16±0.4 oct) on average than 40dB (1.9±0.05 oct) (Figure 3.3 C). This trend was also reflected in offset responses where 10dB bandwidths were narrower (1.3±0.05 oct) than 40dB (2.1±0.04 oct) (Figure 3.2D). Interestingly offset bandwidths at 10db and 40dB were broader than onset bandwidths (ANOVA, 10dB, $F=3.4$ $p<0.05$. ANOVA, 40dB $F=3.8$ $p<0.05$). These results indicate two things: firstly, that most neurons recorded exhibited V-shaped tuning in both onset and offset responses. Secondly, subthreshold offset responses have larger bandwidths.

The frequency response area of a neuron is typically determined using extracellular recordings. Previous studies in the rat identified that suprathreshold tuning curves underestimate the breadth of inputs onto cortical neurons, where subthreshold tuning curves are shown to expand significantly beyond them (de Ribaupierre et al., 1972; Kaur et al., 2004; Volkov & Galazjuk, 1991; Wehr & Zador, 2005). I, therefore, confirmed this observation in the mouse (n=48). Onset subthreshold tuning at 10dB was on average 0.7±0.2 octaves wider than suprathreshold tuning (two-sided sign test, $p<<0.01$). Onset subthreshold tuning at 40dB was on average 1.3±0.3 octaves wider than suprathreshold tuning (two-sided sign test, $p<<0.01$) (Figure 3.4 A). Offset subthreshold tuning at 10dB was on average 1.3±0.3 octaves wider than suprathreshold tuning (two-sided sign test, $p<<0.01$). Offset subthreshold tuning at 40dB was on average 1.3±0.5 octaves wider than suprathreshold tuning (two-sided sign test, $p<<0.01$) (Figure 3.4 B). This data reaffirms previous findings, which show that subthreshold frequency tuning widths are larger than suprathreshold tuning widths. I then examined suprathreshold differences in onset and offset bandwidth to see if this subthreshold dichotomy is also observed in their suprathreshold activity. Suprathreshold onset bandwidth at both BW10 (0.63±0.4 oct) and BW40 (0.68±0.04 oct) were slightly

larger than their offset counter parts at BW10 (0.61±0.4 oct) and BW40 (0.64±0.03 oct), however they were not significantly different (Figure 3.5 A). This result directly contradicts the subthreshold trend, as there was no significant difference in bandwidth between onset and offset responses. I quantified spike latencies and the total number of spikes at onset and offset. There was no significant difference between total number of spikes elicited during onset and offset. Interestingly spikes generated during offset had slower (37.4±16.5 ms) latencies than onset (31.8±17.4 ms) on average. However again the result falls short of significance, suggesting that the sample size (n=48) is too small or that the overall bandwidth is the same (unpaired t-test, $p = 0.2$). Therefore at this point no firm conclusions regarding onset and offset suprathreshold bandwidth can be made

3.2.4 Onset responses have shorter peak latencies than offset responses

Spikes are generated based on three key parameters; EPSP peak amplitude, time course and distance to threshold (Jack et al., 1975; Rall et al., 1967). Therefore given that there is no significant difference between onset and offset suprathreshold bandwidths, one would assume that onset and offset EPSP dynamics are similar. However, a recent study demonstrated offset responses, in the awake cat, have longer decay times and lower peak amplitudes than onset responses (Qin et al., 2007). I therefore quantified tone evoked EPSPs across the FRA, in terms of peak amplitude (mV) and peak latency (ms) for onset and offset responses (n=182) (Figure 3.6 A). Interestingly the mean peak amplitude of onset responses (6.51±0.2 mV) were larger than offset responses (4.4±0.4 mV), however the difference was no statistically significant (Figure 3.6 B). On the other hand, peak latencies were significantly different (unpaired t-test, $p<<0.01$), as onset tone evoked EPSP's were on average faster (23.3±1 ms) than offsets (45.6±1.6 ms) (unpaired t-test, $p<<0.01$) (Figure 3.6 B). This would indicate that based on the magnitude of input both onset and offset responses are just as likely to reach threshold and evoke a spike.

3.2.5 Frequency tuning of both Onset and Offset responses is complex

The most common way of characterising frequency response is by identifying a neurons BF, the frequency which elicits the largest EPSP and its CF, the frequency that evokes the threshold response. A recent study in the rat found that onset and offset BF tuning were usually located at different frequencies in a given cell (Qin et al., 2007). In this data set receptive field processing also appears complex, where in a given cell BF and

CF weren't always the same in both onset and offset responses (Figure 3.7A). In onset responses, on average 60% of neurons (n=120) had BFs that were different from their CFs, where 40% (n=81) showed identical BF and CF tuning (Figure 3.7 B). This trend was reflected in the offset tuning where 52% of cells had BFs that differed from their CF, and 48% having BF tuning identical to CF. This shows that for both onset and offset responses the shape/structure of FRAs isn't always symmetrical and more likely complex. I then compared BF and CF tuning between onset and offsets to see if frequency tuning represented in each response matched. BF tuning between onset and offset differed, with 60% (n=109) of cells showing identical tuning and 40% (n=73) with mismatched tuning, however the distribution was not statistically significant (Figure 3.7 D). CF in contrast varied significantly between onset and offset (ANOVA, $F=0.38$, $p<0.05$) with 30% (n=55) of cells with identical tuning and 70% (n=127) with a wide range of different frequencies.

3.2.6 Subthreshold tuning correlates with suprathreshold tuning in onsets

In order to confirm whether this complexity correlates with suprathreshold tuning, onset and offset frequency tuning was compared for suprathreshold and subthreshold responses (Figure 3.8 A). This data suggests a strong linear correlation for both onset BF (Pearson's correlation coefficient, $r = 0.83$, $p<<0.01$) and CF (Pearson's correlation coefficient, $r = 0.76$, $p<<0.01$) tuning at sub and suprathreshold (Figure 3.8 B&D). This trend is less evident in offsets, where CF sub and suprathreshold tuning show a weaker correlation (Pearson's correlation coefficient, $r = 0.3$, $p=0.03$) with no significant correlation between BF subthreshold and suprathreshold tuning (Figure 3.8 C&E). This result would suggest that BF and CF tuning in onset correlate best with suprathreshold tuning. Subthreshold BF offset doesn't correlate with suprathreshold BF whereas CF tuning at sub and suprathreshold does correlate. This result does in part confirm previous extracellular observations whereby onset tuning differs from offset however CF appears to be the measure that best represents the difference in tuning.

3.2.7 Onset FRAs are more compact than Offset FRAs

Both awake and anaesthetised studies in cats and monkeys have revealed a large variety of shapes in frequency response areas (Abeles & Goldstein, 1972; Christopher deCharms et al., 1998; Moshitch et al., 2006; Pelleg-Toiba & Wollberg, 1989). This apparent heterogeneity in FRA shapes most likely explains the difference between BF and CF tuning in individual cells. However a quantitative analysis of these shapes has

never been performed in the mouse. Moshitch et al performed extracellular recordings on anaesthetised cats and compared FRA shapes in AI using a parameter called 'compactness'. This parameter involves measuring the area bounded by a tuning curve and comparing it to its perimeter. Units with high compactness are typically V-shaped FRAs, whereas units with low compactness were either diffuse FRAs with many weak responses distributed over a broad frequency range, or were very sharply tuned units (Figure 3.9 A&B). I therefore applied this analysis to the FRA structures of this neuronal population (n=182) in order to extract more information beyond the standard bandwidth measure. On average onset FRAs were more compact (3.3±0.01) than offset FRAs (2.9±0.01). The low compactness seen in offset responses are due to diffuse/complex FRAs with many weak responses distributed over a broad frequency range (unpaired t-test, $p = 0.05$) (Figure 3.9 C).

3.2.8 FRAs become more diffuse with depth

It is often reported that different layers in cortex show varying levels of complexity. These depth dependent changes in complexity were attributed to non-preferential input onto cells in thalamo-recipient layers. More specifically this effect resulted in Layer IV neurons exhibiting more compact tuning than Layer V and Layer II/III (Joachimsthaler et al., 2014; Linden & Schreiner, 2003; Rothschild et al., 2010). I compared for the first time onset and offset FRA shapes across depth to confirm if this trend is present in the mouse. Indeed, onset FRAs decreased in compactness with depth (unpaired t-test, $p < 0.05$), whereas offset FRA shapes appeared uniformal across depth (Figure 3.9 D). This trend in onsets appears to agree with the commonly held belief that FRA complexity increases with depth, with the exception of Layer IV. I therefore investigated in greater detail the FRA shapes responsible for this significant trend. I concluded that 92% of cells at the 600µm bin were very narrowly tuned FRAs, resulting in a low compactness value comparable to diffuse FRAs (Figure 3.9 B, left). Offset FRAs were instead extremely diffuse with 2% of all FRAs exhibiting narrow tuning (Figure 3.9 B, right). These results confirm that complexity does increase with depth.

3.2.9 Intrinsic membrane characterisation of IB and RS cells

Recent work in the rat identified distinct frequency responses between intrinsic burst-like (IB) pyramidal cells and regular spiking (RS) cells. This result could suggest that neuronal classes play different roles in the transfer of auditory information (Gao & Zheng, 2004; Le Bé et al., 2007; Schubert et al., 2001). Given the nature of extracellular

recordings it is difficult to determine which particular cell class is responsible for depth dependent changes in frequency tuning. I recorded intrinsic membrane properties of individual cells and correlated them with frequency response profiles, in an attempt to; firstly, confirm that pyramidal cell classes can exhibit different frequency tuning in the mouse and secondly assess whether certain patterns of onset/offset responses can be attributed to a specific cell class. Membrane properties and dynamics of recorded cells were determined by presenting a series of current steps, ranging from -200pA to 200pA (Figure 3.10 A-C). In order to qualify for analysis, recordings must have low access resistance (n=54) (28.4 ± 3.3 MΩ) and spike shape stability. Responses were then placed in two electrophysiological classes; intrinsic bursters (IB) and regular spikers (RS) based on two qualities; 1st inter-spike intervals and spike half-widths. Intrinsic bursters are defined as having shorter 1st inter-spike intervals, higher frequency average inter-spike intervals and smaller spike half-widths than regular spiking pyramidal cells (ANOVA $p < 0.05$). Another discerning criteria that is usually determined via morphological recovery, is soma size. IB cells are known to have larger soma than RS cells (Nowak et al., 2003). Input resistance (Ri) has been previously used as a marker for cell size, where neurons with large input resistances tended to be smaller than those with larger input resistances (Dégenètais et al., 2002). Based on these criteria three types of neuronal cell class were established in this dataset, Regular spiking (RS), Intrinsic Burst (IB) and Fast-spiking (FS) (Figure 3.10 A-C). Based on these two distinct classes six other electrophysiological properties were compared (Fig 3.10 D); Spike height, Input resistance, membrane time constant, rheobase, 1st spike interval and halfwidth. Of these measures tau (ANOVA p = 0.04) and Ri (ANOVA p = 0.04) also showed significant differences between the two populations. RS cells have higher input resistance than IB cells (39.71± 9.5 MΩ), longer membrane time constants (3.41± 0.09 ms), longer 1st spike intervals (14.36± 0.77 ms) and larger spike half-widths (0.49 ± 0.08 ms). Therefore I can successfully distinguish between RS and IB cells based on 3 parameters; input resistance, 1st ISI and spike-halfwidth (ANOVA, p <0.05).

3.2.10 IB cells have more diffuse FRA tuning than RS cells

Input resistance showed the most significant difference therefore it was selected as the measure through which to compare IB and RS cells to frequency tuning. Given that cell class has been previously correlated with the breadth of frequency tuning, I selected compactness as the best measure to quantify the difference between IB (n=4) and RS cells (n=11). I firstly confirmed that onset frequency tuning thresholds show a strong negative correlation with a neurons resting membrane potential (r=-0.5, p<0.05, Figure

3.11 A). Interestingly the effect was not reflected in offset responses. I then compared the compactness of onset and offset FRAs between IB and RS cells. There appeared to be an overall mild positive linear correlation ($r = 0.3$, $p = 0.15$), between input resistance and compactness (Figure 3.10 B left) in onset responses. IB cells on average had more diffuse FRAs ($3.3x10^{-2}±3.5x10^{-3}$), than RS cells ($3.8x10^{-2}±1x10^{-3}$), however the difference between the two populations, given the small sample size was not significant (unpaired t-test, $p = 0.12$). Offsets were then compared (Figure 3.11 B, right), where IB cells on average had more compact FRAs ($3.4x10^{-2}± 4x10^{-3}$), than RS cells ($3 x10^{-2}±3.6x10^{-3}$). This is interesting as the result suggests that indeed IB cells had broader, more diffuse FRAs than RS cells at onset, however for offset responses the trend is reversed. However both results fall short of significance therefore no conclusive remarks can be made. Given that the peak latency of EPSPs varied between onset and offset, could neuronal class be responsible for this observed trend? Interestingly for onset responses IB cells exhibited slower peak latencies (66 ± 4 ms) on average than RS cells (43.5 ± 8.5 ms) (Figure 3.11 C, left). This trend was also observed in the offset responses where IB cells exhibited slower peak latencies (82 ± 23 ms) on average than RS cells (77.5 ± 13 ms) (Figure 3.11 C, right). However these results, again due to the sample size, fall short of significance.

3.3 DISCUSSION

This chapter has focused on performing a systematic quantification of frequency tuning in AI of the mouse, allowing for comparison and confirmation of previous observations in other species under anaesthetised or awake conditions. Remarkably little was known about subthreshold properties and their relationship with frequency tuning, therefore, these data provide valuable insight into subthreshold auditory processing. I also applied this analysis to an under researched phenomenon attributed to the detection of sound duration at the level of cortex, the offset response. Under anaesthesia, the mouse auditory cortex is as rich as awake preparations, with neurons exhibiting a broad range of subthreshold FRA bandwidths and frequency tuning. Interestingly onset and offset CF frequency tuning was highly heterogeneous in the same unit, suggestive of an important functional role in the processing of auditory stimuli.

3.3.1 Onset responses had lower thresholds than offset

This data identifies 24kHz to be the frequency that elicits the lowest response threshold in the anaesthetised mouse, where threshold was on average 21 dB SPL. Single-unit studies in both anaesthetised mice (Linden & Schreiner, 2003), cats (Imaizumi et al., 2004; Schreiner & Cynader, 1984), ferrets (Bizley et al., 2005), rats (Pandya et al., 2008; Polley et al., 2007) and awake monkeys (Recanzone et al., 2000; Scott et al., 2011) showed slightly lower thresholds (0-10 dB SPL on average). This is an interesting discovery as anaesthesia has only been shown to impact threshold levels, by roughly 10 dB SPL (Linden & Schreiner, 2003) when compared to awake preparations in the mouse (Koay et al., 2002). Given that the data I have presented is subthreshold, I would have expected lower threshold levels than those presented by extracellular recording and higher than awake preparations. I cannot rule out the possibility that the type of anaesthetic used in my preparation could effect threshold levels more than that reported in the literature, where all anaesthetised preparations mentioned are either Ketamine/xyalzine or inhalable halogenated ether. Interestingly it doesn't appear to affect the overall shape of the audiogram where my data confirms a similar optimal hearing range of 15-25kHz (Koay et al., 2002; Linden & Schreiner, 2003). For the first time onset and offset responses were compared where two clear differences can be identified. Firstly, onset thresholds are on average 10 dB SPL lower than offsets and secondly the trend across frequency, although significant in both cases, is less prominent in offsets. The significance of this effect is unclear, however both

responses play a role in sound processing and perception as they contribute when tones are soft.

3.3.2 Onset and Offset bandwidths

One way of characterising auditory neurons is based on their bandwidths. We can infer two key pieces of data from the bandwidth; Firstly, larger bandwidths indicate input from a broad range of frequencies and secondly the ratio between bandwidth at 10 dB above threshold (BW10) and 40 dB above threshold (BW40) can allow for discrimination between I and U, V and O of FRA shapes i.e. its response across the frequency spectrum. I report subthreshold BW10 and BW40 (1-3 octaves) similar or larger than other studies using multi-unit recordings in AI of the anaesthetised cat (M. Kimura & Eggermont, 1999; Moshitch et al., 2006; Noreña & Eggermont, 2002; Schreiner & Sutter, 1992), rat (Pandya et al., 2008; Polley et al., 2007), ferret (Bizley et al., 2005), bat (Hoffmann et al., 2008) and the mouse (Joachimsthaler et al., 2014). This result would suggest that the anaesthetic, although it may increase threshold, it does not appear to have a suppressive effect on the processing of auditory stimuli at the level of cortex. It also confirms that the breadth of subthreshold tuning curves expand significantly beyond those of suprathreshold tuning curves (de Ribaupierre et al., 1972; Kaur et al., 2004; Volkov & Galazjuk, 1991; Wehr & Zador, 2005). In this regard offset tuning had a broader bandwidth at both BW10 and BW40 than onset responses. This is an interesting discovery as it suggests that sound offset represent a broader frequency range than the frequency range that initiated the response in the first place.

I then compared onset and offset subthreshold bandwidths to their suprathreshold counterparts, in order to determine how comparable they are. As expected, subthreshold bandwidths in both onset and offset were significantly larger that their suprathreshold tuning curves (Figure 3.4) (M. B. Calford et al., 1983; Eggermont, 1996). Interestingly although the subthreshold bandwidths in my dataset are similar or larger than those previously reported, the suprathreshold bandwidths were on average smaller (1 octave). This can most likely be accounted for by the fact that a smaller frequency range was used to acquire this data (4 octaves) than in previous studies (5-6 octaves) and the sample size (n=48) of spike data is significantly smaller than that obtained by extracellular recordings. Therefore if a larger frequency range was used I would expect both subthreshold and suprathreshold bandwidths to expand further. Further recordings must be done to confirm with confidence the bandwidths of suprathreshold onset and offset

responses.

3.3.3 Suprathreshold bandwidths

Although suprathreshold bandwidths between offset and onset responses appear to be the same there could be a translational difference between their subthreshold responses and spike activity. In other words, even though suprathreshold bandwidths are the same there could be a difference in the rate code and latency. Therefore spike latencies and the total number of spikes at onset and offset were quantified. The spike data implies that there is no significant difference between the total number of spikes at onset and offset. Regarding spike latency, onset responses appeared to exhibit shorter latencies than offset responses however the result was not significant. Therefore it is possible that there is no suprathreshold difference in bandwidth between onset and offset responses in the mouse. However given that spikes are generated based on EPSP peak amplitude and time course (Jack et al., 1975; Rall et al., 1967), we would expect to observe the same trend in subthreshold responses. Interestingly the mean peak amplitude of onset responses were larger than offset responses and onset peak latencies were faster than offsets (Figure 3.8 B). This result confirms previous extracellular observations in the anaesthetised cat (Qin et al., 2007). This would suggest that offset responses are less likely to elicit a spike than onset responses. However the suprathreshold data indicates that there is no difference, therefore this could suggest that although offset EPSPs are smaller, the baseline membrane potential is sufficiently elevated to still reach threshold. The elevated baseline membrane potential and subsequent offset PSP dynamics could be explained by membrane biophysical properties. The PSP caused by offset inputs appear to have smaller amplitudes and slower peak latencies, this could be explained in part by a decrease in input resistance caused by the onset inputs thus reducing the cells ability to store charge, which in effect attenuates the offset driving force. Interestingly the baseline membrane could also be sufficiently elevated making it easier for the incoming offset input to elevate the cells membrane potential to threshold. This would result in a false equivalence between onset inputs and offset inputs having dissimilar driving forces, as both produce similar spike output. Another factor to consider is that although subthreshold offset bandwidths are broader their responses are weakly distributed across frequency, which should result in narrower suprathreshold tuning. In order to confirm this hypothesis more suprathreshold data must be acquired

3.3.4 Frequency response areas are complex

As mentioned previously bandwidth can be used to infer the shape of a neurons FRA. The data presented earlier in this chapter identified that bandwidths at 10dB above threshold are on average smaller than the bandwidths at 40dB for both onset and offset responses. This result strongly suggests that subthreshold bandwidths are not I-shaped. V-shaped tuning curves at the level of cortex are reported in abundance, with previous work in the mouse (Joachimsthaler et al., 2014; Linden & Schreiner, 2003) and other species (Bizley et al., 2005; Hoffmann et al., 2008; M. Kimura & Eggermont, 1999; Moshitch et al., 2006; Noreña & Eggermont, 2002; Pandya et al., 2008; Polley et al., 2007; Schreiner & Sutter, 1992) reporting their presence. There was no significant difference between onset and offset responses in this regard, as they had similar ratios between BW10 and BW40. However other studies also confirm the presence of more complex structures such as, multi-peaked and circular FRAs (Abeles & Goldstein, 1972; Christopher deCharms et al., 1998; Moshitch et al., 2006; Pelleg-Toiba & Wollberg, 1989). It has been suggested that a single tone can evoke a large population response (Schreiner, 1998), most likely due to a variety of FRA shapes that likely overlap in non-identical populations (D. P. Phillips, 1995). I therefore employed a similar method to Moshitch et al, in order to go beyond the basic bandwidth ratio measure and identify how compact subthreshold FRAs are for the first time in Mouse AI. Surprisingly, offset responses were relatively more diffuse. Diffuse FRAs most likely occur as result of responses that were evoked across a broader range of frequencies, thresholds were lower and finally the perimeter of offset FRAs was larger as a result of multiple lobes. However, finely tuned FRAs could also be classified as diffuse based on this measure, as the perimeter is significantly larger than the bounded area. Interestingly, these types of diffuse FRA were found to be almost exclusive to onset responses.

3.3.5 FRA shapes are depth dependent

Depth dependent changes in complexity have been widely observed in auditory cortex (Joachimsthaler et al., 2014; Linden & Schreiner, 2003; Rothschild et al., 2010). However the exact role it plays in at the network level and its potential impact on behaviour remains elusive (De Martino et al., 2015; Linden & Schreiner, 2003). Recent work has shown that layer 2/3 neurons receptive fields are modulated by behaviour and cortical state, suggestive of context dependent processing of auditory input (De Martino et al., 2015; Petersen & Crochet, 2013).

Therefore it is necessary to identify different processing strategies employed across depth and eventually identify the cell types that may be responsible. For the first time onset and offset FRA shapes were compared across depth in the mouse, where depth dependent changes occurred in onset response FRAs but not offset responses. Finely tuned FRAs, were preferentially located at recording depths of 600µm. Given that the suggested depth of these whole cell recordings can be extremely unreliable, as they are based solely on the coordinates of the manipulator, it is difficult to suggest which layer contributes to this effect. However, previously mentioned studies identified the thalamo-recipient layer IV as having more narrowly tuned FRAs with complexity increasing as you follow the canonical cortical circuit. Therefore it is likely that cells recorded at depths of 600µm correspond to Layer IV. In order to confirm this hypothesis it is necessary to perform a histological recovery of recorded neurons, and more accurately measure their cortical depth. Once this is performed it may be possible to answer how and why the cortex is organised in such a specific way and determine its relevance to behavioural output.

3.3.6 Diffuse shapes are more likely to have divergent BF CF tuning

The most common way of characterising frequency response is by identifying a neurons BF and CF. In this data set receptive field processing also appears complex, where in a given cell BF and CF weren't always the same in both onset and offset responses (Figure 3.7 A). A majority of both onset and offset responses had different CF and BF tuning. The phenomenon remains controversial as it has been reported in other species (Kaas, 2011; South & Weinberger, 1995) but not the mouse (Joachimsthaler et al., 2014). This apparent mismatch, could be attributed to the observed complexity in FRA shapes. If FRAs in AI commonly have multiple peaks, as has been suggested by the compactness measure and seen in other studies (Abeles & Goldstein, 1972; Christopher deCharms et al., 1998; Moshitch et al., 2006; Pelleg-Toiba & Wollberg, 1989), then it would be expected that CF will differ from BF in the FRA. Given that both CF and BF elicit spike activity in onsets responses (Figure 3.8) we can assume that they encode relevant stimulus information. However in offset response the picture is less clear. Offset subthreshold CF did significantly correlate with suprathreshold CF, albeit to a lesser extent than onset responses, but offset subthreshold BF did not correlate with suprathreshold BF. As a majority of cells had CF tuned to a higher frequency than BF in both onset and offset responses, one possibility that could explain this effect relates to the mouse audiogram (Figure 3.2).

We have previously observed that threshold responses are lower between 15-25 kHz in onset and offset responses. Given that neurons in AI receive a variety of intracortical inputs resulting in more complex FRAs, it therefore wouldn't be unreasonable to suggest that a consequence of this yields an interesting integrative process. In effect, regardless of subthreshold BF tuning, a neuron at the level of cortex is likely to receive intracortical input from cells tuned close to 20 kHz, resulting in shift in its CF to higher frequencies. The exact functional relevance of this apparent asymmetry is unknown.

3.3.7 Onset and offset tuning are different

For the first time in the mouse AI, I compared the subthreshold tuning of onset and offset responses. My findings are in accordance with previous extracellular studies in the rat and monkey (Qin et al., 2007; B. Tian & Rauschecker, 2003), which described inconsistent tuning between onset and offset responses. Roughly 1/3 of neurons exhibited identical BF and CF tuning, with roughly 2/3 of neurons with inconsistent tuning. Given that both tuning paradigms evoke spiking this apparent diversity between tuning of onset and offset responses suggests a functional role. It has been proposed that they act as 'dynamic filters' for natural sounds, whereby the stimulus duration impacts a neurons filtering properties (Qin et al., 2007).

3.3.8 Cell class and frequency tuning are likely correlated

Recent work firstly identified that there is a non-uniformal distribution of cell class across depth (Nowak et al., 2003) and secondly, these cell classes displayed distinct frequency responses. These results could suggest that neuronal classes play different roles in the transfer of auditory information (Gao & Zheng, 2004; Le Bé et al., 2007; Schubert et al., 2001). Given that a non-overlapping synaptic mechanism drives responses to sound onsets separate to that of offsets (Scholl et al., 2010), it could be possible that the functional dichotomy of certain cell classes extends beyond onset frequency tuning. For the first time in the mouse I employed the whole cell technique to carry out two tasks: Identify cell classes and compare their onset and offset responses. Using current steps as the sole means through which cell class is identified can lead to ambiguous results, however based on the criteria previously set out in this chapter (Figure 3.10) I was able to successfully identify 3 separate cell classes. Assuming that cell size can be determined from input resistance, my data would suggest that cell size is positively correlated with compactness and negatively correlated with peak latency, where IB cells on average had more diffuse onset FRAs

and longer peak latencies than RS cells. These trends were not reflected in the offset responses. This is an interesting discovery, as it firstly could agree with a previous observation in the rat between IB and RS cells (Sun et al., 2013), but more importantly restricts this effect to onset responses, suggesting synaptic inputs responsible for the offset responses are not class dependent. IB neurons have been shown to innervate higher order thalamic nuclei whereas RS cells mainly project intracortically and to the contralateral cortex (J. A. Winer, 2005). The spectrally and temporally broad responses of IB cells combined with its intrinsic burst like nature, most likely ensures the robust transfer of rich stimulus information to higher order cortices, which MGBd is known to innervate (Sun et al., 2013; J. A. Winer, 2005). The functional relevance of this circuitry could revolve around fine tuning where it has been previously suggested that this route contributes to the refinement of motor commands (S. M. Sherman, 2007). RS cells and their ipsi and contralateral projections, on the other hand are more likely to be involved in inducing plasticity (Suga & Ma, 2003).

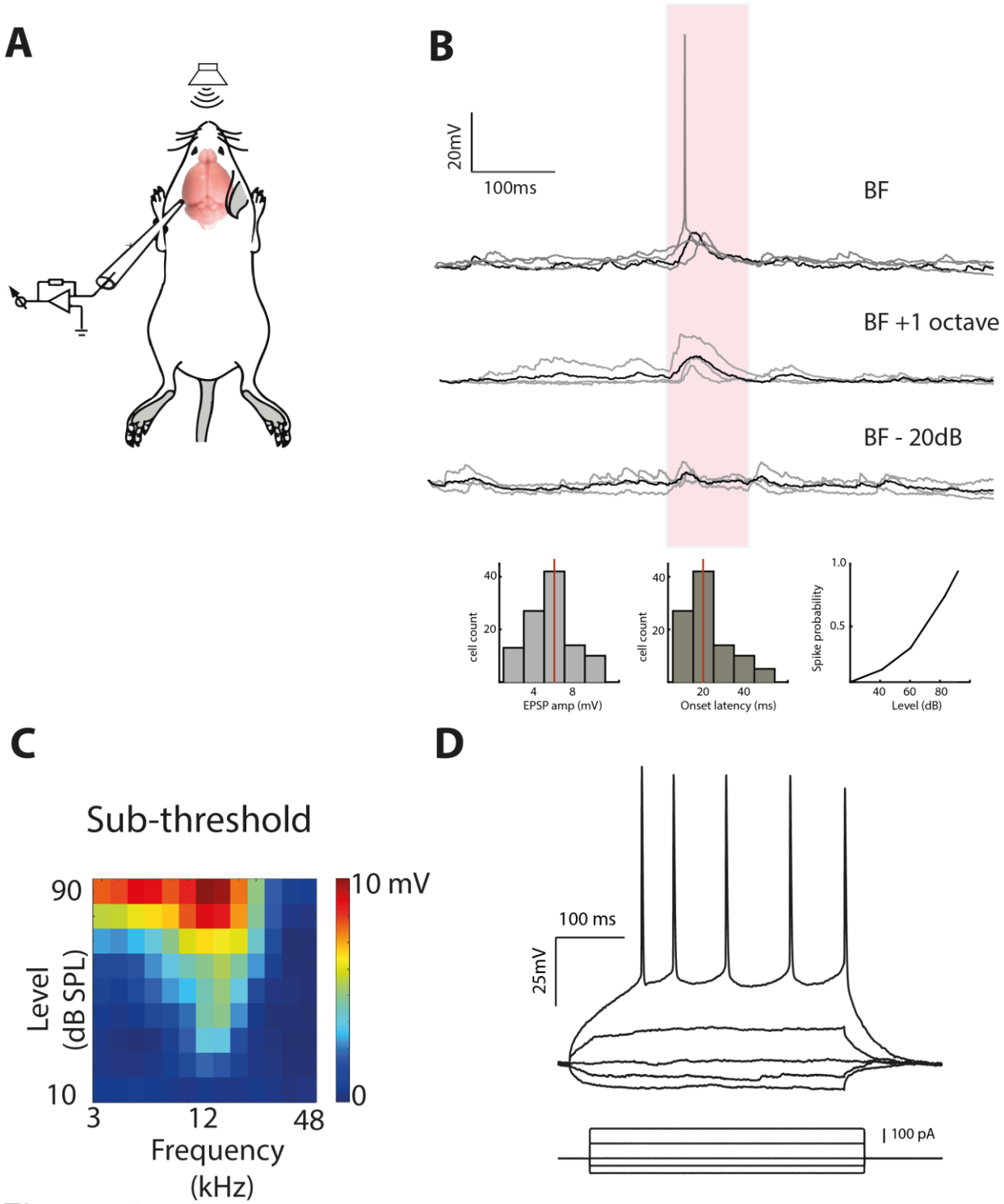

Figure 3.1

Example data acquired via whole cell Recordings: A Experimental setup. Whole cell recordings are perfomed on the the left hemisphere of mouse primary auditory cortex (AI) **B** Tone evoked responses under three different stimulus conditions. Large EPSP's reflect a neurons tuning to a specific frequency at a given level, where the black line is the mean membrane potential. Bottom left, histogram of EPSP amplitude bound by the FRA, red line indicating the mean EPSP amplitude. Middle, EPSP timing with mean onset latency indicated by the red line. Right, probability to spike dependent on tone level **C** Membrane potential is plotted for 117 stimulus conditions yielding a frequency response area (FRA). **D** Pyramidal cell response to hyperpolarising and depolarising current steps.

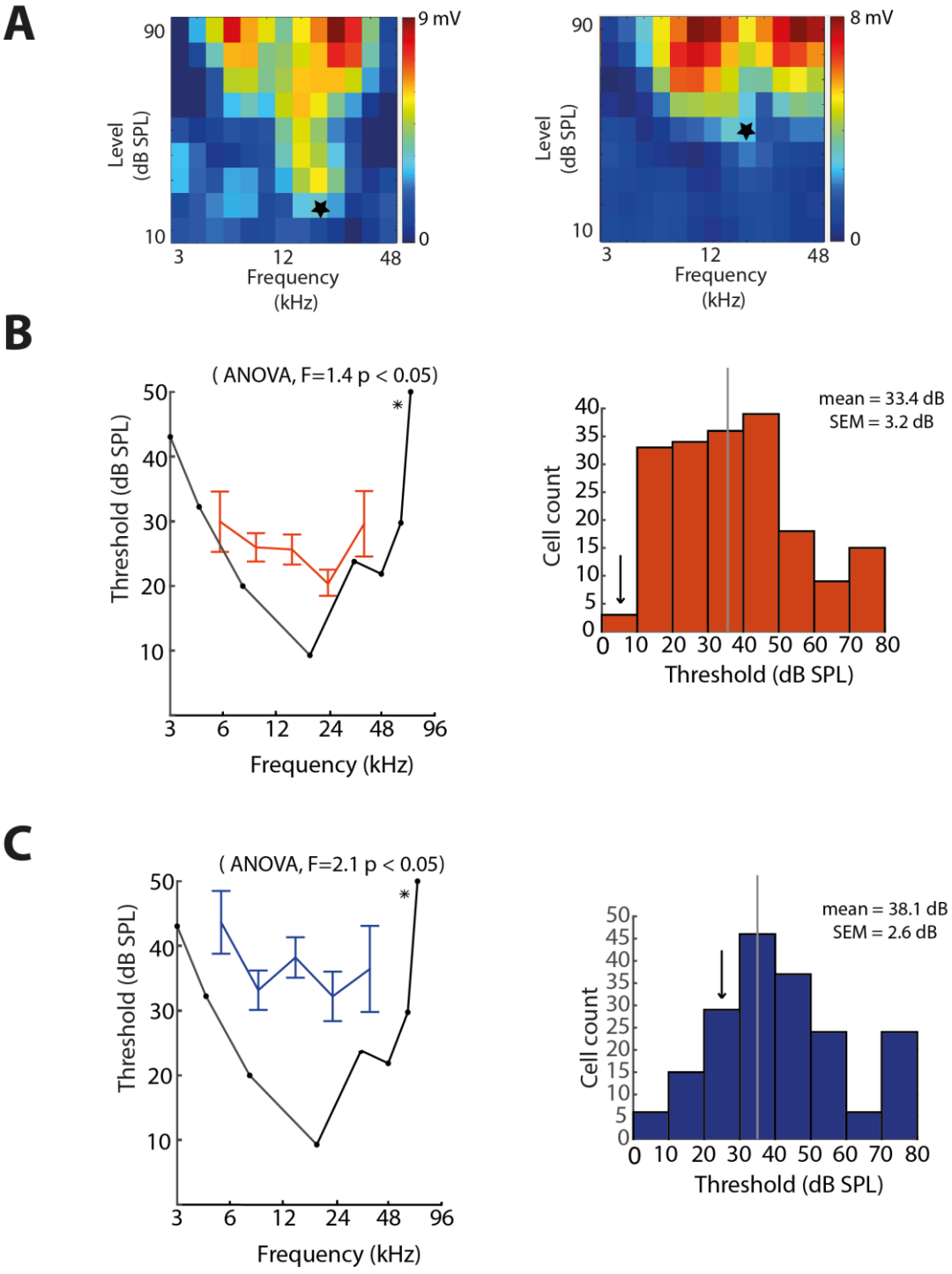

Figure 3.2

Onset and Offset frequency tuning thresholds reflect behavioural output * A Example FRA, for onset (left) and offset (right), where threshold is identified (star) **B** *left,* Comparison of mean threshold responses across frequencies and a mouse audiogram (Heffner et al, 2002*) at onset . Thresholds decreased with increasing CF (red), reflecting a similar trend observed in the audiogram (black) *Right,* Histogram of threshold levels across the neuronal population. **C** *Left,* Comparison of mean threshold responses across frequencies and a mouse audiogram (Heffner et al, 2002) at offset. Thresholds decreased with increasing CF (blue), reflecting a similar trend observed in the audiogram (black) *Left,* Histogram of threshold levels across the neuronal population. Grey lines indicate the mean and arrows the example cells shown in A.

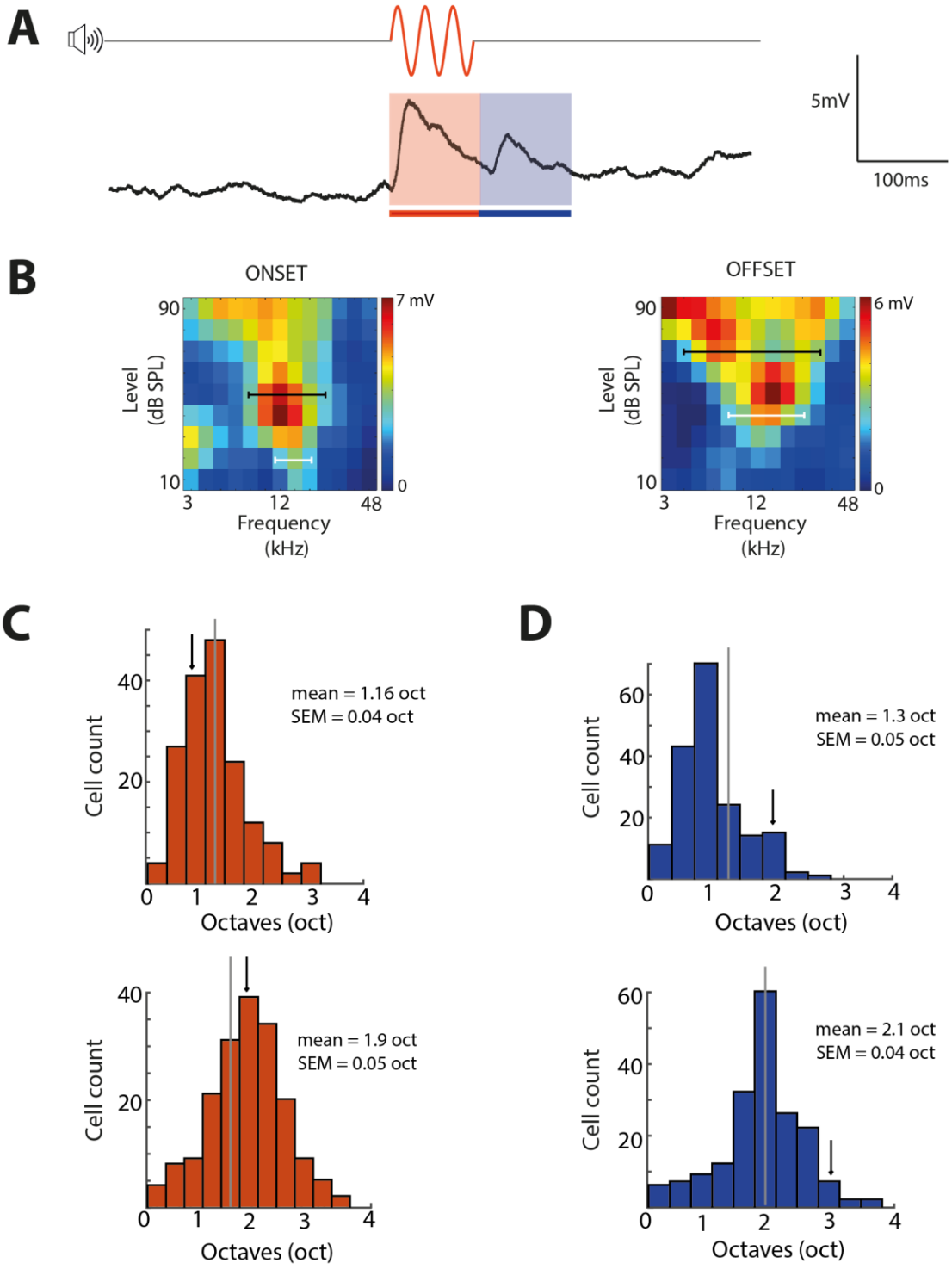

Figure 3.3

Frequency tuning widths are narrower in onset responses compared to offset responses A Example subthreshold membrane trace, showing onset (100 ms red) and offset (blue 100ms) responses. **B** Representative FRAs for onset and offset, where bandwidths at 10dB (white) and 40dB (black) above threshold are identified **C** Histogram of onset bandwidths (n=182) at 10dB (top) and 40dB (bottom) **D** Histogram of offset bandwidths at 10dB (top) and 40dB (bottom), where the grey line represents the mean bandwidth. Black arrows indicate example cells.

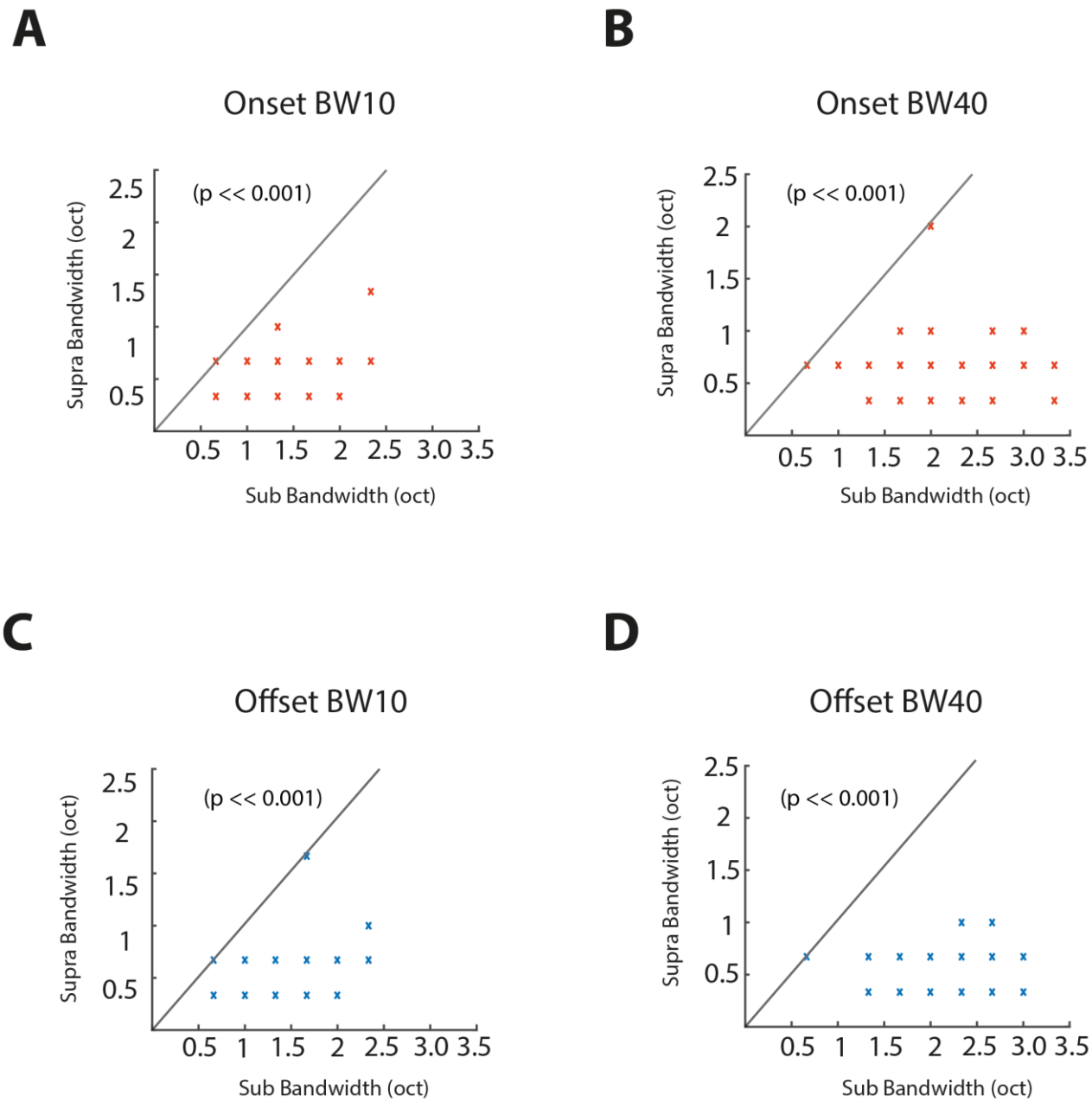

Figure 3.4

Supra- and subthreshold tuning for onset and offset responses. (A two sided sign test was performed for this analysis). **A** Comparison of onset bandwidth at 10dB, subthreshold onset bandwidths are on average larger ($p << 0.001$) than the suprathreshold. **B** Comparison of onset bandwidth at 40dB, subthreshold onset bandwidths are on average larger ($p << 0.001$) than the suprathreshold. **C** comparison of offset bandwidth at 10dB, subthreshold offset bandwidths are on average larger ($p << 0.001$) than the suprathreshold. **D** Comparison of offset bandwidth at 40dB, subthreshold offset bandwidths are on average larger ($p << 0.001$) than suprathreshold bandwidths.

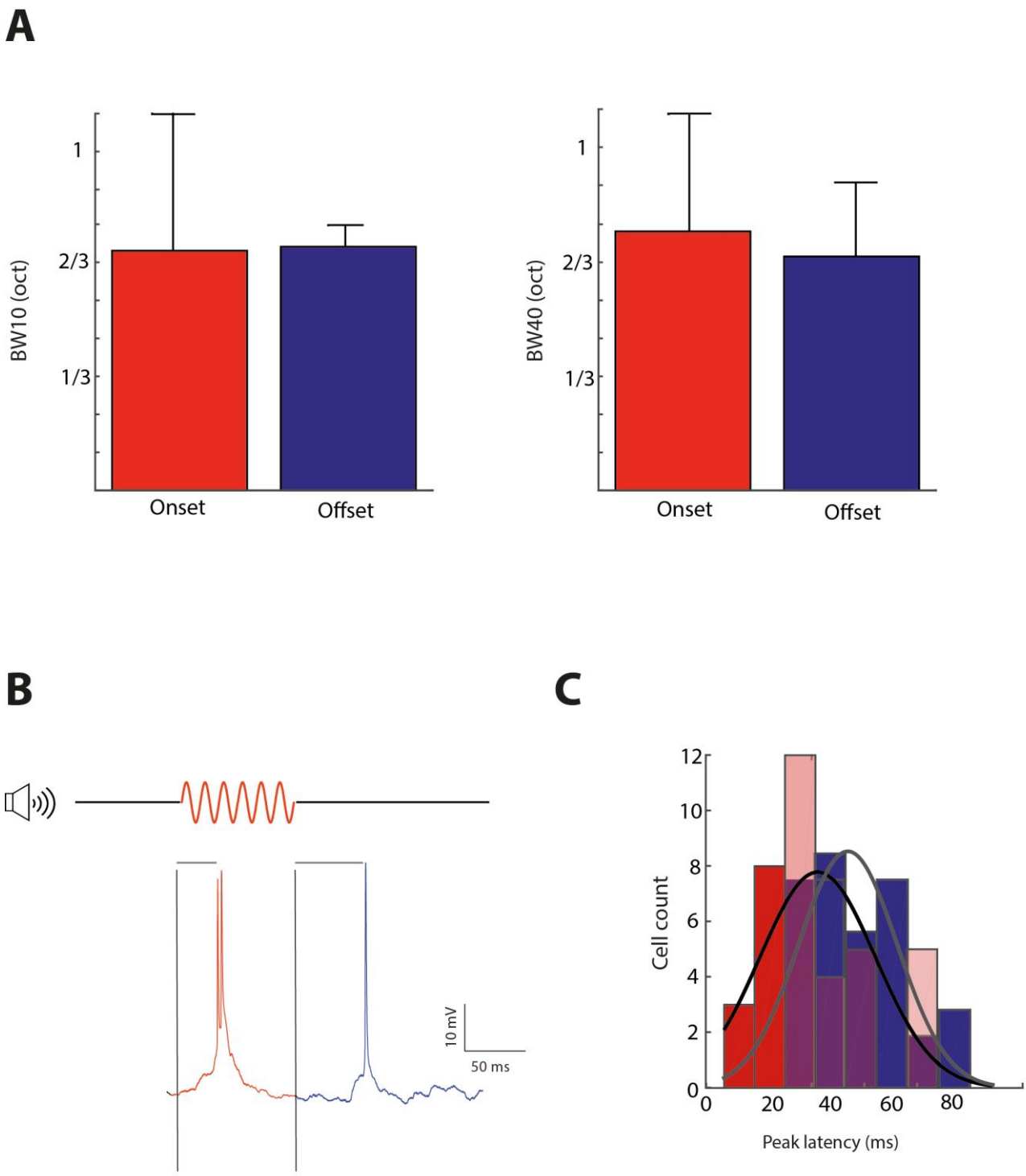

Figure 3.5

Onset and offset suprathreshold bandwidths are similar. A (left) Suprathreshold onset bandwidth at 10dB above threshold for onset and offset responses. (Right) Suprathreshold onset bandwidth at 40dB above threshold for onset and offset responses. **B** Example trace for calculating onset (red) and offset (blue) peak latency (grey line) **C** Histogram of suprathreshold onset and offset peak latencies, with distribution fits for onset (black) and offset (grey) responses. No results were significant

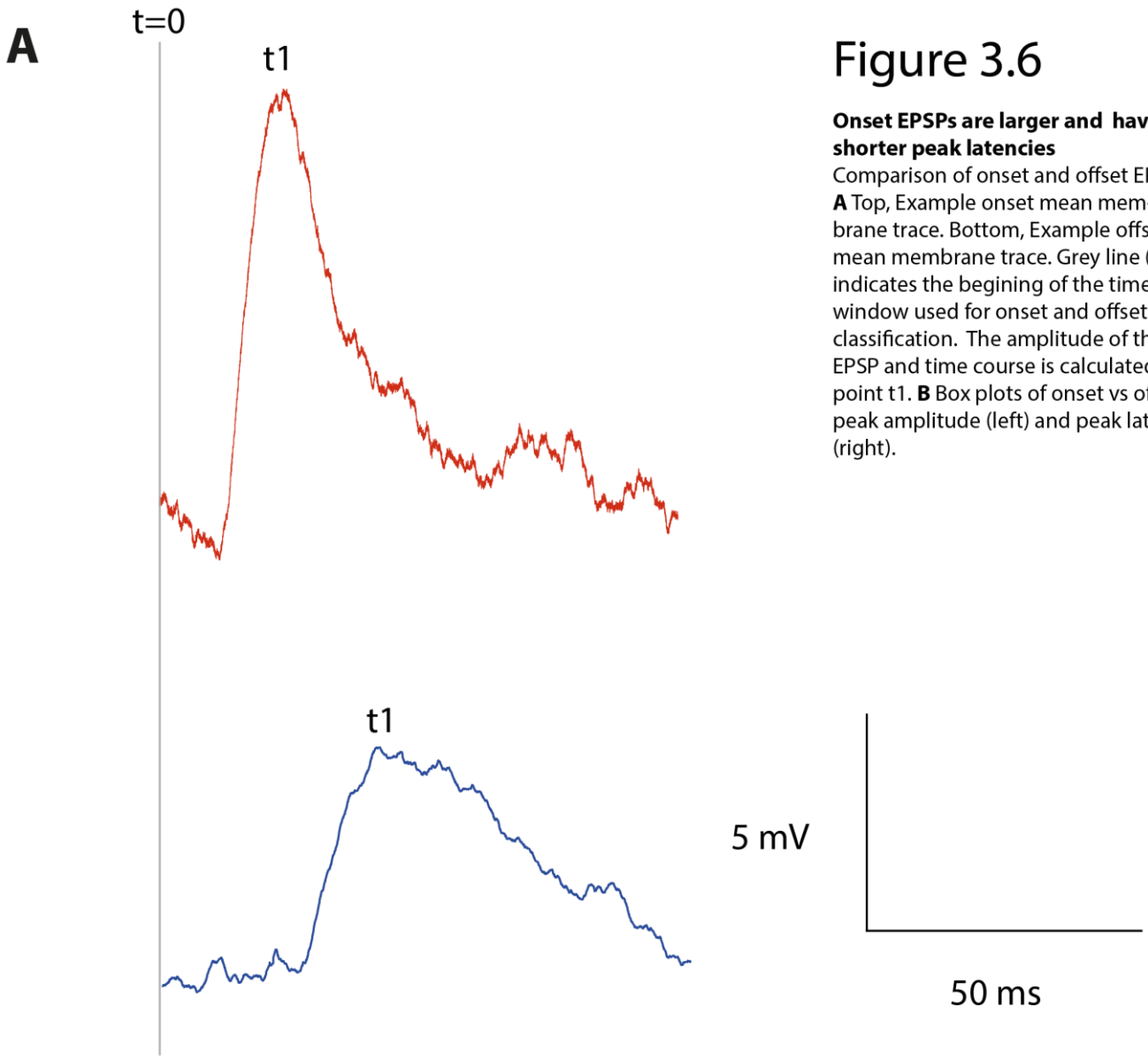

Figure 3.6

Onset EPSPs are larger and have shorter peak latencies
Comparison of onset and offset EPSPs **A** Top, Example onset mean membrane trace. Bottom, Example offset mean membrane trace. Grey line (t=0) indicates the begining of the time window used for onset and offset classification. The amplitude of the EPSP and time course is calculated at point t1. **B** Box plots of onset vs offset peak amplitude (left) and peak latency (right).

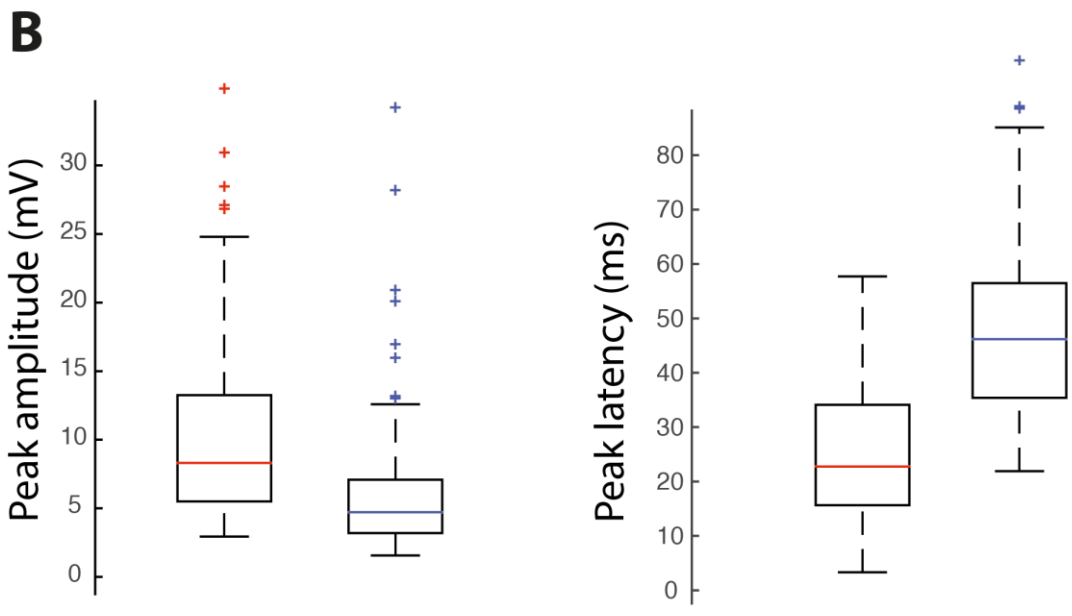

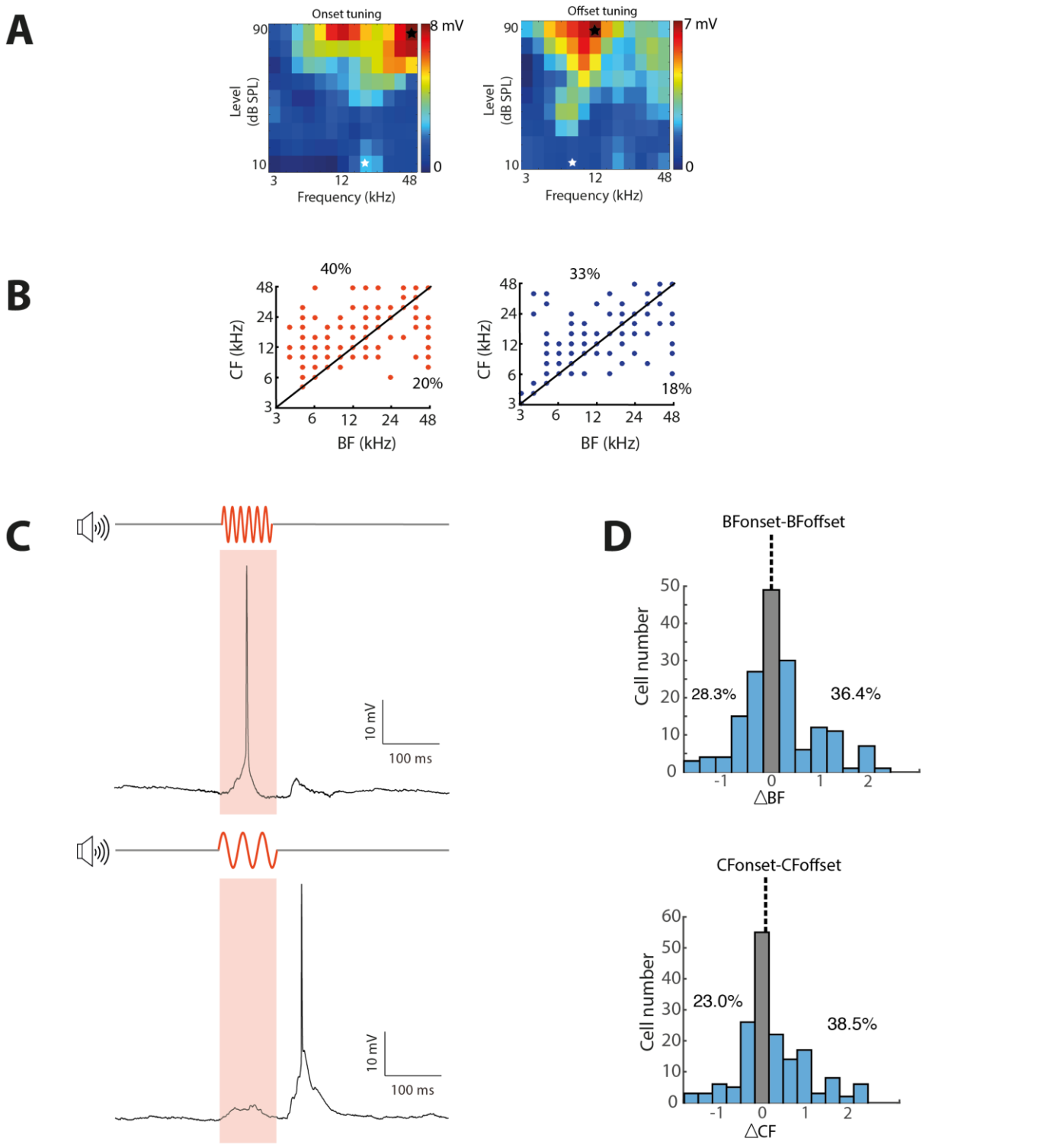

Figure 3.7

Onset versus offset frequency receptive field processing is complex A Onset FRA (left) and offset FRA (right), where BF (black star) and CF (white star) are indicated has having different tuning. Comparison between BF and CF tuning in onset responses (left) and comparison between BF and CF tuning in offset responses, where a majority of cells had BFs at a lower frequency than their CF counterpart. **B** Comparison of Onset tuning with offset tuning, where offset was on average tuned to slightly higher frequencies than onset. **C** Example traces of onset and offset responses at two different frequencies. In this example a higher frequency (top) evokes a spike but not in the offset response. At the lower frequency (bottom) the opposite effect is observed. **D** Histogram comparing onset BF and offset BF (top) and onset CF with offset CF (bottom).

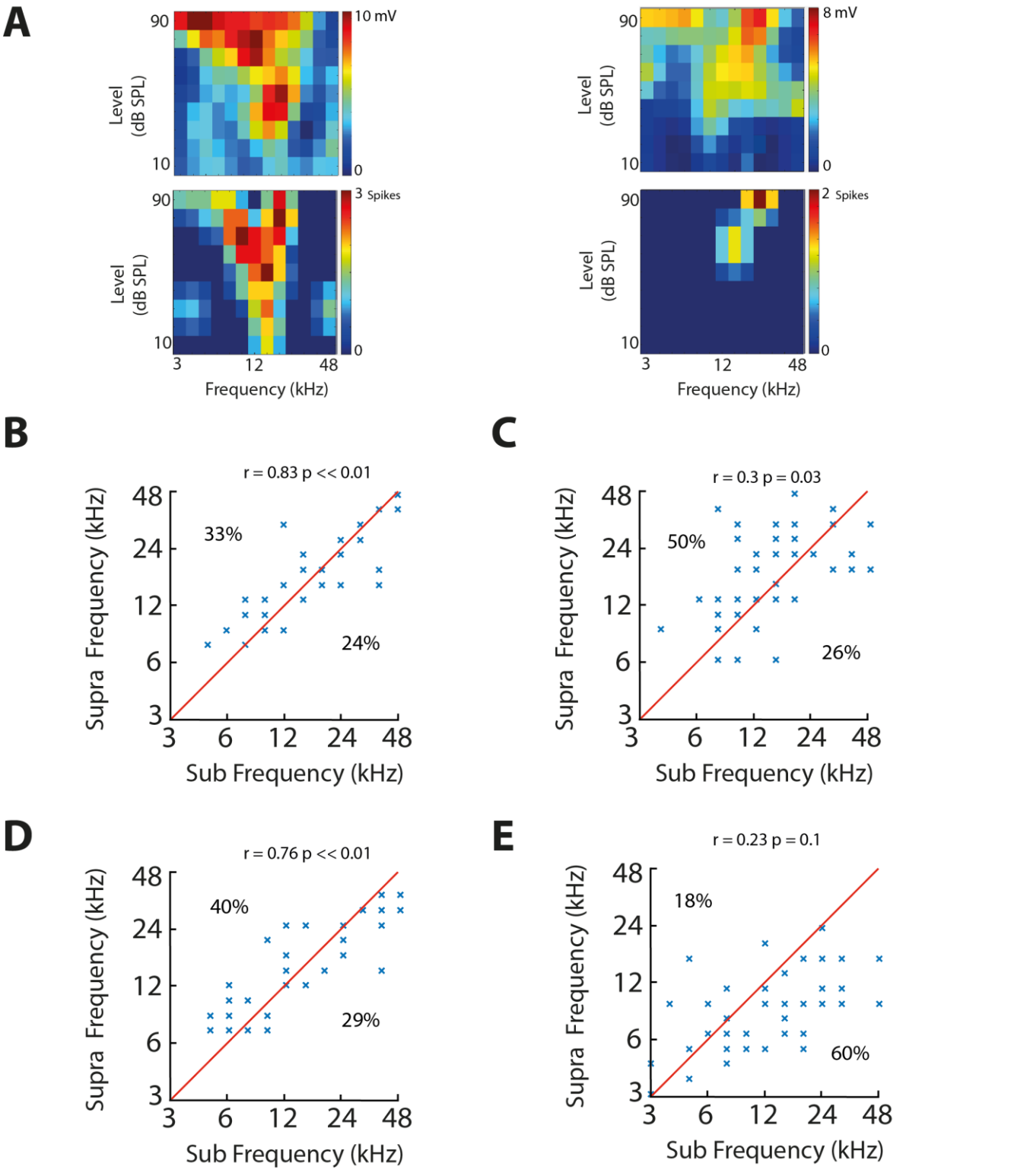

Figure 3.8

Supra- and subthreshold tuning is strongly correlated in onset responses. (Pearson's correlation coefficient was used for this analysis) **A** Top panel, typical subthreshold tuning curves for onset (*right*) and offset (*left*). Bottom panel, typical suprathreshold tuning curves for the same cell at onset (*right*) and offset (*left*). **B** Comparison of Onset CF tuning, where there was a strong significant positive linear correlation. **C** Comparison of Offset CF tuning, where there was a mild positive linear correlation. **D** Comparison of Onset BF tuning, where there was a strong significant positive linear correlation **E** Comparison of Offset BF tuning, where there was a weak positive linear correlation that did no meet significance.

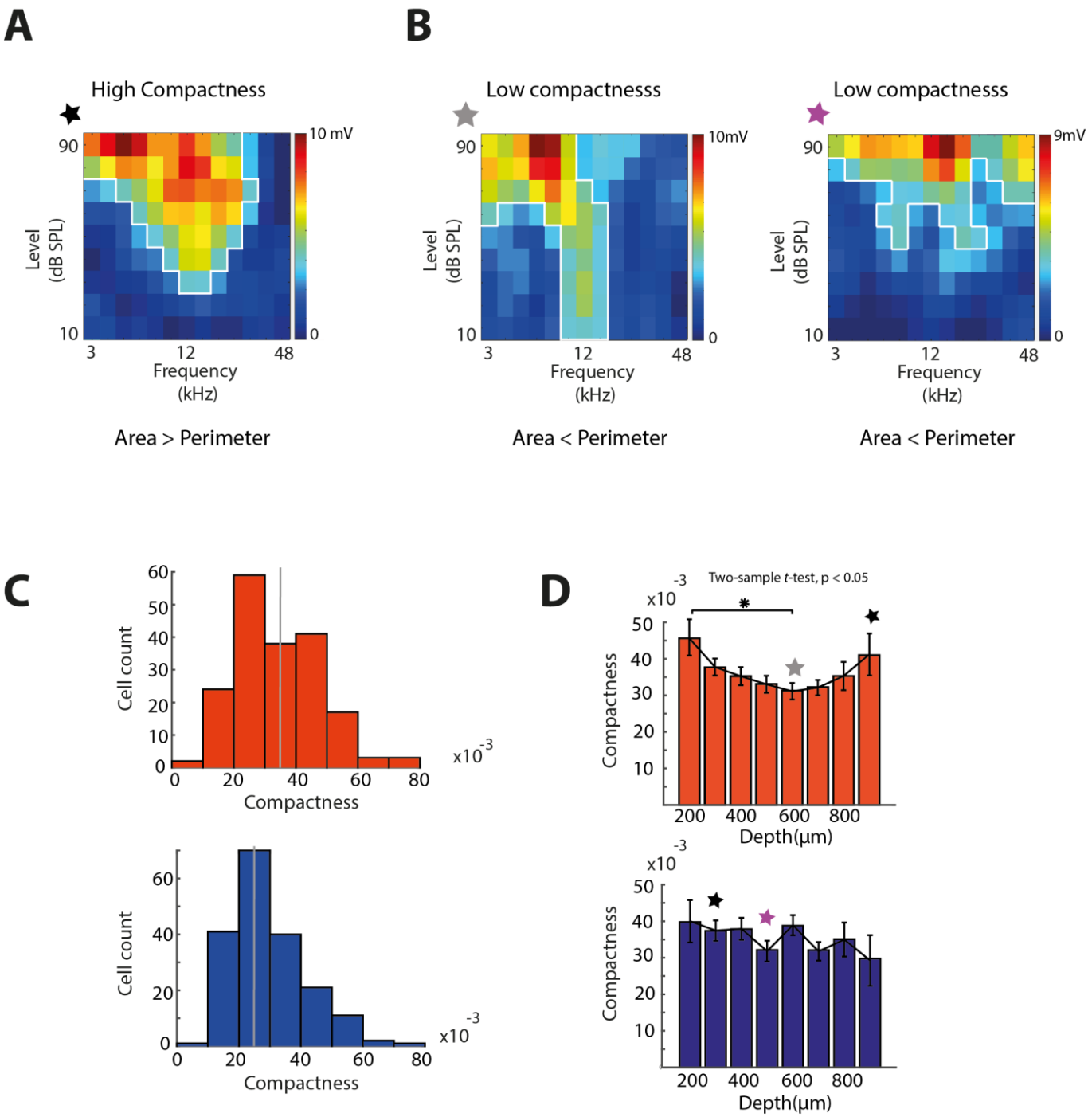

Figure 3.9

Onset frequency tuning becomes more narrow across depth

The compactness parameter is defined as the area bounded by the tuning curve (in terms of pixels) divided by the square of the length of its perimeter. **A** Example of a compact FRA (large value), with a perimeter (white boundary) that is smaller than the area contained by it **B** Two types of low compactness (low value) FRAs (left), Example of a narrowly tuned cell with a low compactness, where the Perimeter is larger than the area. (Right) example of another FRA with low compactness, where the Perimeter is larger than the area. **C** Comparison of compactness measure for onset (left) and offset (right) responses, mean (grey line). **D** Comparison of compactness measure across depth for onset (left) and offset (right) responses. Onset responses showed a significant decrease in compactness across depth, where the type of FRA responsible for this trend are narrowly tuned (grey star) cells. In contrast offset responses showed no significant trend across depth where most neurons had diffuse FRAs (purple star)

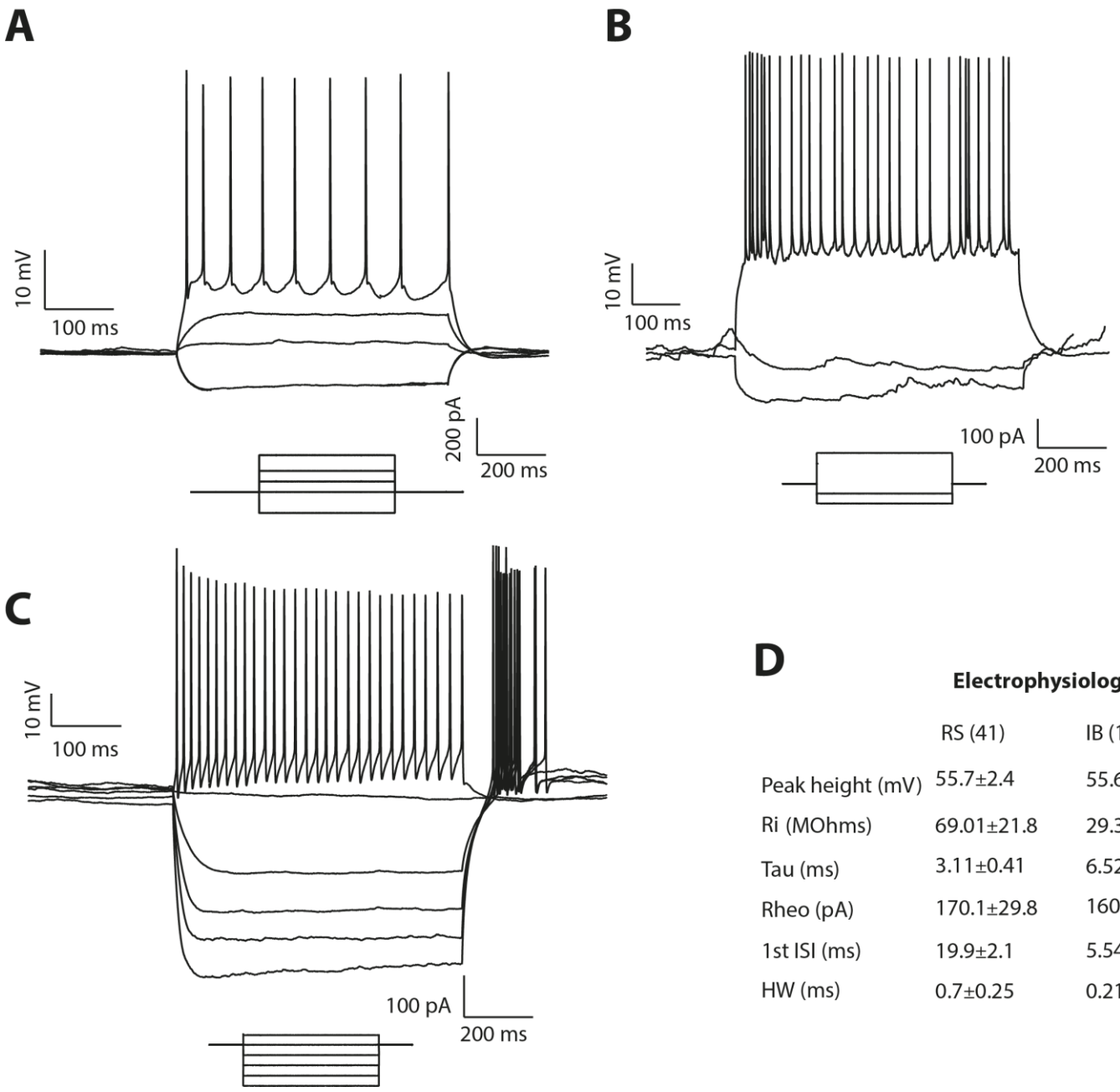

Figure 3.10

Intrinsic response properties A Response of an regular spiking (RS) cell to hyperpolarising and depolarising current steps **B** Response of a intrinsic burst (IB) cell to hyperpolarising and depolarising current steps. **C** Response of a fast spiking (FS) cell to hyperpolarising and depolarising current steps. **D** Table of intrinsic measures. Peak height, input resistnace (Ri), membrane time constant (Tau), current required to elicit a spike or rheobase (Rheo), 1st inter spike interval (1st ISI) and Spike half-width (HW).

D

Electrophysiological classes (n)

	RS (41)	IB (13)	FS (2)
Peak height (mV)	55.7±2.4	55.6±3.6	41.4±6.7
Ri (MOhms)	69.01±21.8	29.3±12.3	76.3±5.6
Tau (ms)	3.11±0.41	6.52±0.5	2.8±1.3
Rheo (pA)	170.1±29.8	160.2±12.3	51.3±4.4
1st ISI (ms)	19.9±2.1	5.54±2.87	3.2±0.8
HW (ms)	0.7±0.25	0.21±0.17	0.18±0.06

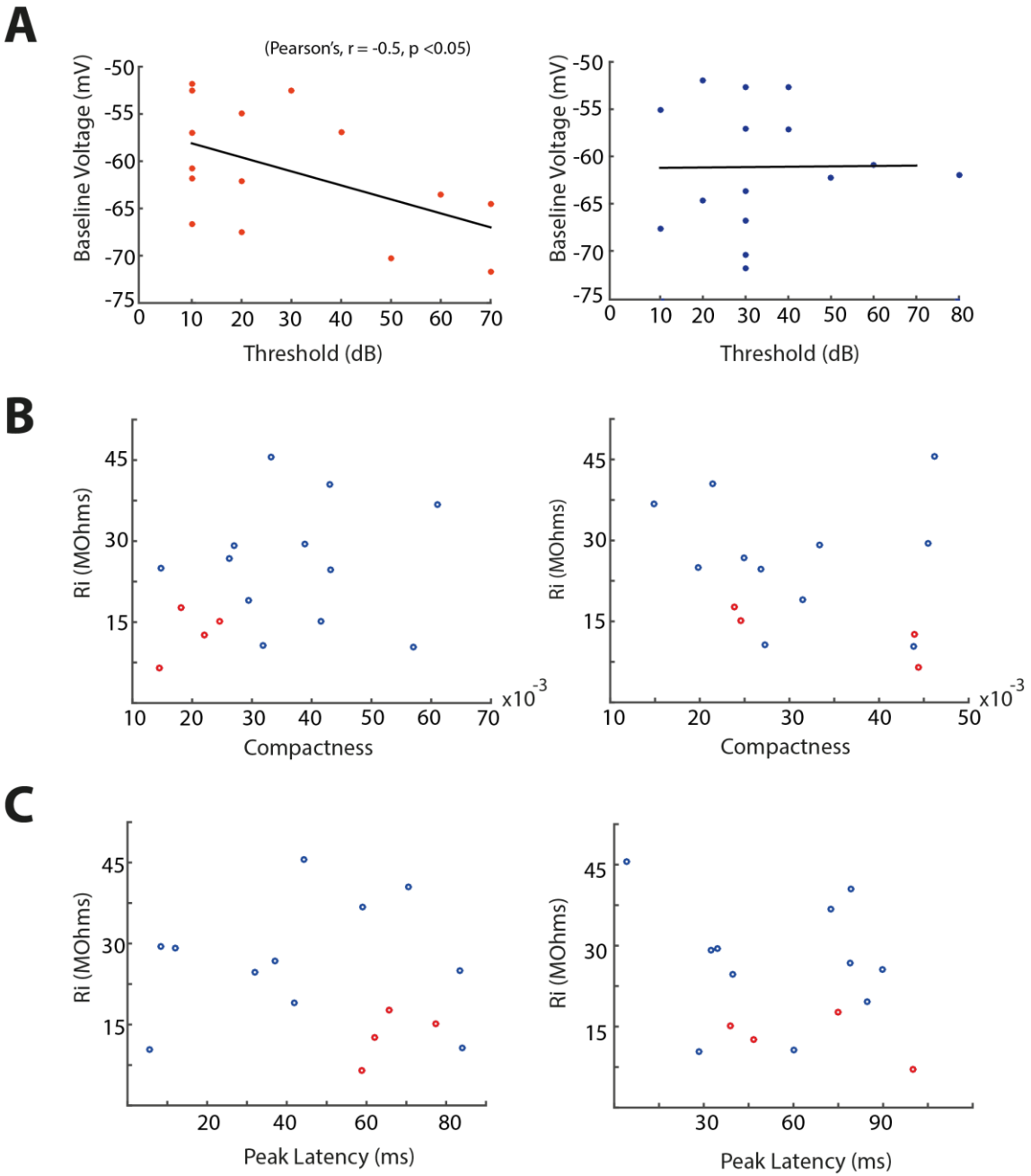

Figure 3.11

Dichotomy of response profiles between IB and RS cells **A** Onset Frequency tuning threhsolds at isnegatively correlated with a neurons resting membrane potential (left) but not for offset responses (right) **B** Onset FRA compactness is positively correlated with a neurons input resistance (left) but negatively correlated for offset (right) **C** Onset peak-latency and input resistance exhibits a weak negative correlation with a neurons input resistance (left), where this trend is also observed for offsets (right)

4 mGRASP: A UNIQUE TOOL FOR IDENTIFYING DEFINED SYNAPTIC INPUTS ONTO INDIVIDUAL NEURONS

4.1 INTRODUCTION

The main pathway responsible for the transfer of auditory information from lower order nuclei to cortex is between the ventral division of the medial geniculate body (MGBv) and primary auditory cortex (AI). The classical view of thalamus is that it simply acts as a relay nucleus (Walker, 1938), targeting cortical neurons in layers IV and VI (Sousa-Pinto, 1973) in a topographic manner, (Miller et al., 2001; Kahee Niimi & Matsuoka, 1979; Velenovsky et al., 2003) with minimal functional transformations (K Niimi & Kuwahara, 1973). However recent findings suggest a departure from these widely held conclusions.

Studies involving the use of biotinylated dextran amine (BDA), revealed that thalamus projects to several layers other than the classic input layer IV, where interestingly the largest axons resided in Layer I (Burton & Jones, 1976; M. Wilson et al., 1969). This indicates that specific input to the superficial cortex could play a functional role, such as affecting temporal feedforward and feedback processes (Matsubara & Phillips, 1988; Mitani et al., 1985). Furthermore recent slice studies revealed that thalamic input to different layers of AI drives functionally distinct responses (Viaene et al., 2011a, 2011b), where stimulation of MGB evoked EPSPs of a different amplitude and time course depending on the cortical neurons laminar location. This apparent heterogeneous degree of thalamic input has been shown to extend beyond laminar distribution and include cortical cell class (Ji et al., 2015). Optogenetic stimulation of MGB identified varying degrees of excitation amongst cortical cell classes within the same layer. These results combined indicate a complex network of thalamic contributions to cortical processing which could suggest a greater functional transformation than previously thought.

In order to generate a deeper understanding of thalamocortical transformations it is necessary to quantify thalamic inputs onto cortical neurons whilst simultaneously performing an electrophysiological and functional characterisation. Beyond simply quantifying the number of thalamic inputs a neuron receives an overlooked, yet extremely relevant factor that can influence the processing of spectral information and hence a receptive field, is their distribution. A simplistic view of a neuron's role is

to translate incoming synaptic signals into an output, in the form of an action potential. The process through which a neuron achieves this is synaptic integration (Jack et al., 1975; Mainen et al., 1996; Rall, 1967; Rall et al., 1967). Synaptic integration involves combining membrane potential changes caused by single or multiple pre-synaptic sources, and transforming them into an overall voltage deflection. More specifically, this process involves integrating the amplitude of the EPSP, its temporal characteristics (temporal summation) and finally the location along the dendritic arbor at which the depolarisation occurs (spatial summation). The relative impact of each component is still widely debated (Chadderton et al., 2014; London & Häusser, 2005; Rall, 1967). However previous studies have shown that spatially non-uniform distributions of synapses, such as clustering, influence dendritic summation and could be involved in plasticity (Harvey & Svoboda, 2007; Losonczy et al., 2008) or influence a neuron's ability to selectively respond to spatiotemporal patterns (Branco et al., 2010; Gasparini & Magee, 2006; Poirazi et al., 2003; Spruston, 2008). These studies suggest that there could be an underlying causal role for synaptic distribution.

The advent of a novel technique, mammalian GFP reconstitution across synaptic partners (mGRASP) (Kim et al., 2012), has made it possible to investigate, for the first time, the subcellular distribution of defined populations of synapses with standard fluorescent microscopy. The mGRASP technique involves the fusion of two complementary split-GFP fragments (called GFP1–10 and GFP11) where one portion is tethered to the presynaptic membrane and the other to the postsynaptic membrane of two synaptically linked neurons. To achieve this one spatially distinct brain region must be transfected with an *aavCAG-pre-mGRASP-mCerulean* and the other with transfected with *post-mGRASP-2A-dTomato.* Successfully labelled neurons AI will appear red and axons from thalamus will appear blue. Green fluorescence will only be visualised when a successful synaptic contact has been made. This technique is more efficient and accurate than EM methods, which involve identifying the degree of overlap between axonal and dendritic arbors in a small volume of tissue to infer the presence of a synapse (Braitenberg & Schüz, 2013; Peters & Feldman, 1976; Sotelo, 2003), where this has been shown to greatly overestimate the number of synaptic contacts (Mishchenko et al., 2010) (Bock et al., 2011).

Here I have applied this method to explore direct thalamic contributions to the processing of acoustic stimuli in primary auditory cortex. Utilising this powerful tool I

quantified and determined the distribution patterns of thalamic synaptic contacts on different cortical cell classes and layers in AI. I investigated for the first time how influential synaptic distributions are on spectral tuning, by performing whole cell recordings *in vivo* whilst simultaneously delivering the *post-mGRASP-2A-dTomato* plasmid (Rancz et al., 2011). This allowed for the identification and quantification of thalamic inputs on a single cell whilst also acquiring the labelled neurons spectral tuning and intrinsic electrophysiology. Its thalamic input profile could then be compared to other recovered single cells and the gross viral average, in order to determine if any correlates exist.

4.2 RESULTS

4.2.1 Viral labelling of MGB and AI

Retrograde tracer studies identified that AI receives 17% of its input (extrinsic and intrinsic) from the ventral portion of the medial geniculate body (MGBv) (Andersen et al., 1980; Colwell, 1977; Lee & Winer, 2011; Merzenich et al., 1982). Therefore in order to quantify thalamic synapses on AI neurons, both MGB and AI must be robustly located and transfected using the dual viral technique of mGRASP (Kim et al., 2012). This firstly allowed me to determine how axonal input from MGB is distributed across cortex, and relate this distribution to the number of identified synapses. It also allowed me to investigate the subcellular distribution of synapses in order to establish whether thalamic input is 'random' or 'clustered'. The post-mGRASP virus is stereo-tactically injected into primary auditory cortex (AI) and the pre-mGRASP virus is injected into the medial geniculate body (MGB) of an anaesthetised mouse (Figure 4.1 A). The pre- portion of mGRASP encodes cerulean (blue fluorescent protein responsible for identifying pre- infected cells) (Figure 4.1 B top panel) and a portion of green fluorescent protein, GFP. The post portion of mGRASP encodes, dtomato (a red fluorescent protein responsible for identifying post- infected cells) (Figure 4.1 B bottom panel) and the second portion of GFP required to form the complete fusion protein. When the two portions of GFP are close enough (20 nm), they fuse resulting in the green fluorescence characteristic of GFP.

Three steps are followed in order to confirm successful stereotactically directed expression of the Pre-viral load in MGB. Firstly, the presence of labelled cell bodies at the location of MGB based on the 'Allen brain atlas', secondly the presence of axons in primary auditory cortex and finally the presence of axons being most prominent in the internal granular layer of cortex (Figure 4.1 B,C,D) (Herkenham, 1986; Jones, 1981; Kemper & Galaburda, 1984). I firstly quantified the viral spread of the pre-virus in MGB, were I confirmed that MGB was sufficiently labelled (0.37 ± 0.02 mm^3). A larger volume of 300 nl was used to ensure sufficient labelling of MGB, given its difficulty locating it in the brain. I therefore quantified the laminar distribution of thalamic axons (n=4) by calculating the total labelled area in a 100x100 µm space across layers (Figure 4.1 D), where cortical layers were determined based on cell types, density and thalamic input (Brodmann, 1909; Douglas & Martin, 2004; Gilbert & Wiesel, 1979; D. LORENTE, 1949; Zilles & Amunts, 2010). Layer IV had the highest axonal input (5846 ± 201 μm^2), followed by layer VI (3527 ± 156 μm^2), Layer I

(3353 ± 51.4 μm^2), Layer V (1664 ± 320 μm^2) and finally Layers II/III (1492 ± 128 μm^2). The difference between layers that received the most input (IV, VI, and I) and layers that received the least (II/III and V) was significant (ANOVA, $F = 1.17$ $p < 0.05$). This result confirms that the lemniscal pathway, MGB to AI, can be successfully labelled - as Layer IV, the internal granular layer, was identified as receiving the most axonal input.

4.2.2 Layer and Cell class

Recent work has shown that thalamic input onto cortical layers of AI drives functionally distinct responses (Viaene et al., 2011a, 2011b). Further optogenetic studies revealed that different cortical cell classes across laminae had different levels of thalamic innervation (Ji et al., 2015). I therefore utilised the post-mGRASP virus to not only recover synaptic contacts but also their morphologies in order to establish cell classes. A much smaller viral titre of 50 nl was used to label neurons with the post virus in order minimize viral spread (0.067 ± 0.001 mm^3) and subsequently avoid labelling cells outside the field of AI. Across all experiments (N=9) neurons that were not located in a densely labelled cluster and sufficiently labelled by the Post-mGRASP virus (n=24) had their morphologies reconstructed using Neutube (Figure 4.2A) and their depths determined. Two cell classes were established based on somatic and dendritic shape, where pyramidal neurons have a characteristically large triangular shaped soma with biconically radiating dendrites (Megıas et al., 2001); pyramidal (n=15) and non-pyramidal (n=9) (Figure 4.2 B). Based on these distinctions, Pyramidal neurons (202.4 ± 19.4 μm^2) had on average larger soma than Non –pyramidal neurons (154.2 ± 21.1 μm^2), however these two classes based on soma size just fall short of significance (ANOVA, $F = 2.1$ $p = 0.1$). Comparing the dendritic area the difference is clearer, with Pyramidal neurons having larger dendritic arbours (1841.1 ± 420 μm^2) than Non-pyramidal neurons (1376.1 ± 342 μm^2). For this measure the difference between the two classes is significant (ANOVA, $F=1.25$ $p < 0.05$). In terms of laminar distribution a majority of cells were located in layer IV, 50%, with 33.3% in layers II/III, 16.6% layer V, 8.3% layer I and none in layer VI (Figure 4.2 D). This result confirms that the Post-virus can express sufficient quantities of fluorescent protein to reconstruct neuronal morphology and hence establish two distinct morphological classes based on their dendritic area, in this data set.

4.2.3 Process of synapse identification

Given that both components of the mGRASP virus can successfully transfect thalamic and cortical neurons, I then developed a technique to automatically quantify all synaptic contacts. Previous techniques that used the 'Peter's rule' (Braitenberg & Schüz, 2013; Peters & Feldman, 1976) were shown to greatly overestimate the number of true synaptic contacts (Mishchenko et al., 2010). The principle authors of the mGRASP technique propose that it overcomes this drawback as synaptic identification can only be achieved when the two portions of GFP are close enough (Kim et al., 2012). Given the nature of the mGRASP technique I was able to compare the two methods; as a prerequisite for successfully labelled GFP synapses, is the overlap of a dendrite with an axon. I therefore developed an automated process (Matlab) whereby stack images acquired from a fluorescence microscope are deconstructed. Overlaid images were split into each component channel (red and blue). A threshold is set to remove artefact from the image where subsequently the total number of pixels were calculated and each given the same unitary value (Figure 4.3 A). The two 'pixel extracted' channels are then combined and an image is formed only where there is an overlap of the red and blue channel (± 1µm) (Figure 4.3 B). The resulting pixel counts are then converted into area. On average neurons had a much smaller overlap area (81.4 ± 21.3 μm^2) than the average axonal area (3120 ± 722.3 μm^2) and neuronal area (1725 ± 289.3μm^2) in the field of view. This is expected as depending on the image acquired, certain regions may be axon dense where there is no Post-labelled cell. Even though neurons in Layer IV, as expected, had the highest overlap area (107 ± 17.2μm^2), interestingly the amount of overlap was not significantly different across layer. When comparing the amount of overlap between cell classes pyramidal neurons (82.5 ± 31 μm^2) were just as likely to receive overlap than Non-pyramidal neurons (79.5 ± 25.8 μm^2), (ANOVA, $F= 2.8$ $p = 0.9$). These results indicate that even though certain cortical layers receive more axonal innervation, they don't necessarily lead to more dendro-axonal overlap. Furthermore, this overlap is equally present in pyramidal and non-pyramidal cell classes. Based on previous techniques, this overlap area qualifies as 'successful' synaptic contacts.

The image was analysed further in order to compare detected mGRASP with predicted synapses (based on overlap area). Once blue and red fluorescence are overlapping (±1 µm) the green channel was then observed. If there is green fluorescence at the point of overlap (meets the criteria described in Methods) then a synapse is identified. Fig 4.4 A is an example layer IV pyramidal neuron that receives

a typical level of axonal thalamic innervation for its laminar position. On the left lower panel we have a Neutube reconstruction of the apical trunk where red indicates the portion of labelled neuron and the green spheres (n=26) are identified synapses. This procedure is then carried out across the entirety of the labelled neuron, in order to construct a complete synaptic map of thalamic inputs. I then compared 'actual' (mGRASP) synapses to the predicted number of synapses, which are determined by the overlap of labelled axon and dendrite. The data confirms that there is mismatch between the expected number of synapses and the actual number of synapses observed on neurons, where the correlation is mildly positive (Pearson correlation coefficient, $r = 0.3$ $p < 0.05$) (Figure 4.3 C) as you would expect, however there is ~100 fold difference between the expected (2000 ± 398 synapses) and actual number of synapses (15.6 ± 4.3 synapses). This result suggests that overlap is not as accurate an indicator as mGRASP for quantifying the actual number of synapses present on a neuron. However there does remain the possibility of false negatives, although this rarely occurs (< 1%) (Kim et al., 2012)

4.2.4 Quantification of Thalamocortical synapses

Recent studies have suggested that thalamic inputs that innervate certain layers of cortex can evoked functionally distinct responses in AI neurons (Viaene et al., 2011a, 2011b). Given that I can successfully label thalamic contacts on AI neurons using the mGRASP technique, I quantified the number of synapses present on cells across depth. Layer I (56 synapses) on average had the most synapses followed by Layer IV (34 ± 15.6 synapses), Layer II/III (7.5 ± 1.2 synapses) and Layer V (7.2 ± 1.2 synapses). The number of synapses across layer was significant (ANOVA $F= 2.6$, $p < 0.03$), which confirms previous work that suggests that laminar location most likely determines the number of thalamic synapses a neuron receives (Figure 4.4B). Previous work identified that different cortical cell classes across laminae had different levels of thalamic innervation (Ji et al., 2015). This could suggest that not only do thalamic inputs target specific layers more than others but they're also cell class selective. I then compared the total number of synapses between two morphologically distinct cell classes. On average Pyramidal neurons had more synapses (20.1 ± 6.7 synapses) than Non pyramidal neurons (10.4 ± 6.7 synapses), however this difference was not statistically significant.

Given that synaptic contacts can be axo-somatic or axo-dendritic and that Pyramidal neurons have larger dendritic areas than Non-pyramidal neurons, I segregated the

number of synapses that occurred on the soma and dendrites and compared the difference again between the two classes (Figure 4.4D). Exactly 50% (n=11) of neurons had synapses present on their soma (4.3 ± 0.6 synapses) where there appeared to be a strong linear correlation between the number of synapses on the soma and the number of synapses on the dendrite (10.2 ± 3 synapses) ($r = 0.75$, $p < 0.01$) across the overall population (Figure 4.4C). Interestingly, Pyramidal neurons had significantly (unpaired t-test, $p < 0.05$) more synapses on their dendrites (18.3 ± 6.2 synapses) than Non-pyramidal neurons (5.6 ± 3.3 synapses). Instead Non-pyramidal neurons had on average more somatic synapses (3.2 ± 1.1 synapses) than Pyramidal neurons (1.8 ± 0.7 synapses). These results could suggest that axonal innervation from thalamus is not only layer dependent but also preferentially synapses onto dendrites Pyramidal cells. I previously observed a significant difference between Pyramidal and Non-pyramidal dendritic area, so investigated the possibility that neurons with far reaching dendritic arbors are more likely to form synapses (Figure 4.4E). When comparing dendritic area and the number of synapses, the data indicates that neurons with long dendritic arbors are more likely to have more synapses ($r = 0.2$, $p > 0.05$).

4.2.5 Thalamocortical inputs are somatocentric

Even though Pyramidal neurons have more dendritic synapses and that longer dendrites are more likely to have more synapses we don't know how distributed those synapses are across dendritic arbors, where previous work highlighted the potential importance of spatial summation and its subsequent impact on synaptic integration (Branco et al., 2010; Jack et al., 1975; Mainen et al., 1996; Rall, 1967; Rall et al., 1967). As mGRASP is such a novel technique, there have been very few studies that have been able to probe functionally connected regions and quantify synaptic distributions (Druckmann et al., 2014). Therefore I quantified synaptic distributions and compared them amongst neuronal class and depth. Synapses in both neuronal classes had to be normalised relative to the dendritic location. Synaptic distance is directly traced through the dendrite back to the centre of the soma and then normalised relative to the total length of dendrite to which the synapse is located (Figure 4.5 A). This then yields two types of distribution, somato-centric and distal distributions (Figure 4.5 B). Given that laminar location determines the number of thalamic synapses a neuron is likely to have, I compared normalised synaptic distances across the entire neuronal population within different layers of cortex (Figure 4.5 C). Interestingly, there was also a significant difference between

cells located in layer IV (0.28 ± 0.1) and the other layers (0.2 ± 0.1) (unpaired t-test, $p<0.05$). These results combined suggest that neurons located in layer IV are more likely to have synapses than other layer but those synapses are also less somato-centric than other cortical layers. When comparing normalised synaptic distance between cell class across layer however there was no significant difference. Therefore thalamic axons innervating layer IV do not have unique distributions between cell class.

Having determined that Pyramidal (0.2 ± 0.06) and Non-Pyramidal neurons (0.18 ± 0.1) on average had similar normalised synaptic distance, I therefore wished to clarify whether this effect was correlated with a neurons size and the number of synapses it receives. Surprisingly the data indicates that in both cell classes, neurons that are more somatocentric (smaller normalised distances) have more synapses (Figure 4.5 D). Furthermore when comparing dendritic area and normalised distance for pyramidal neurons, there was a strong negative correlation ($r = -0.55$, $p < 0.1$) (Figure 4.5 D), however it must be noted that the trend just falls short of significance. The opposite trend was observed in non-pyramidal neurons, where the correlation was positive between normalised synaptic distance and dendritic area ($r = 0.92$, $p < 0.01$). Firstly these results indicate that thalamic convergence onto neurons in AI regardless of cell class is relatively somato-centric and secondly that thalamic input is targeted closer to the soma the larger a pyramidal neuron is whereas the opposite trend exists for Non-pyramidal cells, where the larger the dendritic area the more likely those thalamic synapses are going to be located further from the soma.

4.2.6 Whole cell in-vivo transfection

Synapses for both Pyramidal and Non-pyramidal neurons appear to be somato-centric, meaning that thalamic contacts preferentially synapse onto proximal branches. The most intriguing question remains, is there any functional relevance to this apparent non-random synaptic distribution. By performing the mGRASP labelling technique on a single cell level whilst obtaining its electrophysiological profile, I can establish if certain synaptic distributions impact a neurons integration of frequency information. Whole-cell transfection (Rancz et al., 2011) provides us with a unique way of inserting DNA into a single cell whilst performing standard electrophysiological recordings. In this case, Post-mGRASP plasmid DNA is added to the recording solution and during the recording it passively diffuses from the internal solution to the inside of the cell (Figure 4.6 A). Once a successful recording

from one neuron is achieved, the pipette is slowly retracted and the animal recovered in order to prevent labelling of false positives. A successful incubation period lasts 52 hours and then the neuron is subsequently imaged. Biocytin-streptavidin-cy3 was initially used to demonstrate that single neuronal morphology could be recovered, 24hrs after a recording (n=6). Once single cells could be identified using biocytin, plasmid GFP was used (n=3) in order to prove that individual cells could be successfully transfected. Finally, pCAG-Post-mgrasp was used to prove that a plasmid form of the Post virus could be successful transfected (n=4) (Figure 4.6 B). Whole cell transfection is a necessary but extremely low yield technique, where a sequence of events must occur in order to increase the success rate (Figure 4.6 C). A high plasmid titre, negative voltage injection, Long incubation period and low access resistance all appear to be crucial in recovering single cell morphologies at a reasonable success rate of 25%.

4.2.7 Thalamocortical contributions to spectral tuning

Prior to electrophysiological recordings, MGB was stereo-tactically injected with pre-Virus and allowed to incubate for 2 weeks in order to sufficiently label axons in primary auditory cortex (AI). Neurons in AI were then recorded and labelled with pCAG-Post-mGRASP via whole cell transfection. Cortical neuronal morphologies and thalamic innervations were successfully recovered via this labelling technique (Figure 4.7 A). Recovered single cells were compared to their viral bulk counterparts. These neurons were identified as Pyramidal cells (layer IV and VI), where on average their somatic (106 ±17 μm^2) and dendritic areas (1283 ±760 μm^2) were not significantly different from viral recovered morphologies of the same class. Again as expected the single cells also showed a disproportionately higher number of expected synapses in comparison to the total number of actual synapses where they also received similar levels of thalamic input (12 ±8.5 synapses) when compared to the viral average (Figure 4.8 A). Normalised synaptic distances were then calculated and compared to the viral average for Pyramidal cells. Interestingly both recovered neurons had similar somatic centric distributions of their synapses when compared to the viral average (Figure 4.8 B).

These neurons individual electrophysiological and spectral tuning profiles were compared with its thalamic synaptic distribution profile, in order to identify any functional correlates. Given that single cell morphologies and synaptic distributions did not deviate significantly from the virally labelled population, some functional

correlates can be extrapolated. As in chapter 3, a full functional characterisation was performed (Figure 4.9 A), this included determining electrophysiological cell class by injecting hyperpolarising/depolarising current steps and frequency response area. Intrinsic properties and frequency, for the first time, were compared to its thalamic synaptic distribution profile, which included the quantification of thalamic synapses and their distribution. Given that both recovered cells were Regular spiking neurons (RS), I could not compare them to other electrophysiological cell classes. I therefore selected input resistance (Ri) as we have previously seen in Chapter 3, that intrinsic burst firing (IB) neurons can be distinguished based on this parameter. There appeared to be a mild positive trend between the input resistance and synaptic distribution (Figure 4.9 B). A positive trend was also observed between the number of synapses and Bandwidth at 40dB above threshold, where the Layer VI neuron had a larger bandwidth (1.8 oct) than the layer IV neuron (1 oct) (Figure 4.9 C left). This trend was also reflected when comparing bandwidth to the synaptic distribution. A positive trend was also observed between the number of synapses and Peak latency, where the Layer VI neuron had a faster peak latencies (26 ms) than the layer IV neuron (28 ms) (Figure 4.9 D left). As seen in the previous chapter both neurons had similar peak latencies to the population data. Finally a positive trend was also observed between the number of synapses and Peak amplitude, where the Layer VI neuron narrowly had larger EPSPs (5 mV) than the layer IV neuron (4.6 mV) (Figure 4.9 E left). Interestingly both neurons had similar smaller peak amplitudes in comparison to the population data acquired in chapter 3. When comparing normalised synaptic distance the same positive trends were observed across all measures (Figure 4.9 B-E, right). Given such a small sample size, no conclusions can be made. Although an extremely promising technique more recordings are required to investigate any correlation that may exist between thalamocortical synaptic distributions and synaptic integration of auditory stimuli.

4.3 DISCUSSION

In auditory neuroscience, determining which receptive field properties are enhanced, passively inherited and synthesized in auditory cortex are key questions that must be answered. The synaptic mechanisms and neural circuitry involved in spectral integration remain a mystery. Previous studies have suggested that thalamic input could play more a complex functional role in cortical processing than simply a feed into the canonical circuit of auditory cortex (Matsubara & Phillips, 1988; Mitani et al., 1985; Viaene et al., 2011a, 2011b; M. Wilson et al., 1969). The amount of thalamic input a cortical neuron receives has been shown to drive functionally distinct responses (Ji et al., 2015; Viaene et al., 2011a, 2011b). The distribution of thalamic synapses on cortical neurons has never been performed in auditory cortex. By evaluating a neuron's functional response profile and combining those observations with thalamic distributions it may be possible to shed light on this apparent functional dichotomy. Previous methods used to identify functional synapses were proven to be inaccurate (Mishchenko et al., 2010; Sotelo, 2003) or extremely time consuming (Navlakha et al., 2013). The mGRASP technique overcomes these issues, allowing for efficient and accurate synapse identification. There is a growing body of evidence that suggests that pre and postsynaptic connectivity patterns are not as random as previously thought (Brown & Hestrin, 2009; Y. Li et al., 2012; Yu et al., 2009), where clustering of functional homologues occur on specific dendrites (Kleindienst et al., 2011; Makino & Malinow, 2011; McBride et al., 2008; Takahashi et al., 2012). How this apparent non-random distributions effect the overall representation of a stimulus is widely debated (Jack et al., 1975; Mainen et al., 1996; Rall, 1967; Rall et al., 1967). For the first time in auditory cortex I applied the mGRASP technique, in an attempt to tackle the role of thalamus in frequency tuning integration. In this chapter I discovered that thalamic axons preferentially but not exclusively synapse onto layer IV neurons in a somatocentric manner, independent of cell class. Furthermore I identify interesting trends regarding the size of pyramidal and non-pyramidal dendritic arbors and the distribution of thalamic input. For the first time in auditory cortex I whole cell *in vivo* transfection was performed in order to identify a neuron's frequency response profile to the type of thalamic input it receives. In order to establish if observed differences in thalamic distribution impact cortical tuning curves further investigation is required.

4.3.1 Identifying thalamocortical synapses using mGRASP

I successfully applied the mGRASP technique to identify thalamic inputs on cortical neurons in AI. Even though this technique proved to be more efficient and accurate than previously reported studies, drawbacks do exist. Successfully labelling the lemniscal pathway to AI has its challenges and a limiting factor of this technique is that you cannot restrict the Pre-viral payload to exclusively label MGBv. As a result other thalamic sub regions such as, MGBd and parts of LGB, are inevitably labelled and could contribute to some axonal innervation observed in AI. However the positioning of the Post virus in theory should minimize the chance of labelling synapses from other thalamic regions, which may have been labelled via unavoidable spread of the pre-virus from its initial site of injection in MGB. Furthermore ~90% of thalamic innervation into AI is from MGBv, as a result it is unlikely that false-positives that occur due to pre-viral spread into other regions of thalamus will occur (J. A. Winer, 1984). The spread of the post-virus must be controlled more accurately, where in most cases labelled neurons were located within 100 µm of the injection site. This was achieved in part by reducing the titre to 50 nl (Kim et al., 2012). The timing of Post-mGRASP viral incubation also presented a challenge, where if it was left for too long cell necrosis and debris ensued or if terminated too early, cells were insufficiently labelled and could not be analysed properly. However given these drawbacks and strict analytical criteria (see Methods), a population of synaptic data was achieved (n=24). This population could be divided into two classes, pyramidal and non-pyramidal (Fig 4.2 B). This classification was based on soma and dendritic morphology, where given the size of labelled population, this decision to define only two morphological classes seemed reasonable. The mGRASP technique not only allowed for the comparison of morphological classes but another important aspect of cortical circuitry, a cells laminar location (Binzegger et al., 2004; Callaway, 1998; Fitzpatrick, 1996; Kagan et al., 2002; Lund et al., 1979; Ringach et al., 2002).

4.3.2 Quantification of thalamocortical synapses in AI

Having proved that thalamus and cortex can be successfully labelled by each respective virus, thalamocortical contacts were inspected by identifying the presence of GFP. Neutube reconstruction of dendrites and axons assisted in a robust identification of ‘true’ synaptic contacts. Cell debris and channel bleed through of other fluorophores can lead to false positives being identified. In order to overcome this issue only green fluorescence at the point of overlap between the red and blue

channel is considered to be a true synaptic contact. A rolling ball radius of 0.25μm is applied in order to identify individual puncta. As previously mentioned, prior techniques involved simply using overlap as a marker for synapse formation, therefore actual synapses, identified via the mGRASP technique, were then compared to the predicted number of synapses, estimated based on overlap alone. My data demonstrated a significant over prediction of the expected number of synapses (~ 100 fold) confirming the result of previous studies (Mishchenko et al., 2010; Sotelo, 2003) which suggests that overlap technique is not an accurate indicator for the number of actual synapses. However the value presented in this data set is also 10 fold lower than Mishchenko, Hu et al. 2010, which could indicate that the criteria used in this analysis could be too restrictive. Therefore to overcome this underestimation of thalamic contacts, the degree of overlap could be extended. Another interesting observation is that the relative amount of overlap was uniformal across depth and cell class. This would directly contradict previous studies that indicate thalamic input predominantly form synaptic contacts in layer IV (A. Kimura et al., 2003; LeDoux et al., 1985; Romanski & LeDoux, 1993). Again these results prove that, in the case of mGRASP, overlap is not the best indication of true synaptic formation. Finally the issue of false negatives was addressed in the techniques original publication and other light microscope based techniques (Kim et al., 2012). The combination of false negatives and overly restrictive criteria performed in these analyses would mean that the estimates/distributions I have presented are lower than the 'true' number of thalamic synapses on AI cortical neurons. The issue could be clarified by pharmacologically silencing cortex, whilst performing two-photon calcium imaging of neurons in AI whilst simultaneously driving thalamus. Although admittedly an arduous control experiment it does present the obvious benefit over electron microscopy as previously mentioned, as functional synaptic contacts can be identified. Furthermore when comparing the neuronal area in this chapter with other reports they appear low (Sarid et al., 2007), which could be due to insufficient labelling of all dendrites.

4.3.3 Non-uniformal distributions of synapses across layer

The next step is to identify how these synapses are distributed across cortical layers. Thalamic axons preferentially form synaptic contacts on deep Layer III and Layer IV neurons (A. Kimura et al., 2003; LeDoux et al., 1985; Romanski & LeDoux, 1993). In this data set we see that Layer IV does indeed receive the most input. However other cortical layers such as V and I also received a significant amount of input. This result

confirms previous reports of thalamic innervation of other cortical layers beside layer IV (Ji et al., 2015; Viaene et al., 2011a, 2011b). It has been suggested that these layer dependent inputs could play specific roles. In the case of layer I innervation, thalamocortical axons could drive responses on apical dendrites prior to activation from the lemniscal pathway via the classic canonical route (S. Sherman & Guillery, 2006). This path could play role in feedforward and feedback processes (Matsubara & Phillips, 1988). Regarding innervation into other cortical layers, it has been proposed that it could affect, intralaminar circuitry, cortico-fugal and cortico-cortical circuits (Kitzes & Doherty, 1994). How this data fits into new models suggesting that the cortex actually can be represented as two distinct processing units that receive the same sensory information yet process it differently remains unclear (Constantinople & Bruno, 2013; Feldmeyer, 2015; Sarid et al., 2007). We know that neurons present in the upper layer and lower layers of cortex have distinct morphologies and channel expressions, yet what acts as the main 'enabler' for them to process the information differently could be explained by the distinct synaptic distributions that have been indicated in my dataset. Through further experimentation we can confirm the power of the mGRASP technique and begin to answer the basis for these distinct processing strategies and its potential role in behaviour and perception.

4.3.4 Thalamocortical synaptic distributions

Where these thalamic projections synapse on auditory cortical neurons up until now has not been researched. In this neuronal population 50% had synapses on their soma. The functional consequence of these synapses is unclear, as typically somatic synapses are typically inhibitory (Mitchell & Silver, 2003). This result, if true is interesting because thalamic projections to cortex are predominantly excitatory. The spatial arrangement of thalamic synapses on target dendrites was then analysed, revealing a somato-centric distribution (Figure 4.5). The location of a synapse was normalised relative to the length of its dendrite. For both neuronal classes a vast majority of synapses were located on distal dendritic branches. Interestingly, even though larger pyramidal neurons, as previously reported had more synapses, these results suggest that these same large pyramidal neurons were more likely to have more somato-centric distributions. The opposite trend was observed in non-pyramidal neurons, where larger cells were more likely to have more proximal synapses, relatively speaking. In combination with somatic synapses, there is a strong indication that thalamic inputs synapse close to or on the soma. The functional

significance of this trend has never been investigated. The neuronal classification of non-pyramidal and pyramidal, as previously mentioned, isn't ideal as identifying neuronal class based on morphology alone can lead to subjective interpretations and can be improved with relative ease. By incorporating immunohistology and electrophysiology it is possible to not only determine cell class more definitively but also identify subclasses.

4.3.5 Comparing a neurons individual electrophysiological profile with its synaptic distribution

In order to determine whether there was any functional underpinning to the observed synaptic distributions, the mGRASP technique was combined with *in vivo* whole cell electrophysiology. This was achieved using whole cell transfection, where an electrophysiological characterisation is performed followed by a characterisation of thalamic synapses. MGB was stereo-tactically injected with pre-Virus and subsequent recordings were made in AI, where recorded neuron is transfected with pCAG-Post-mgrasp via passive diffusion through the pipette. It proved to be an extremely low yield technique, however minor adjustments were made (Fig 4.6 C) in order to achieve a final success rate of 25%. In total 4 neurons were recovered using this technique, however due to low intrinsic fluorescence, 2 cells were excluded from the analysis as morphological and synaptic profiling was not possible. This proved to be an inherent issue with this technique, as due to the nature of the plasmid construct common immune-histochemical protocols used to boost a signal would not work. Therefore to increase the sample population more research is required to identify the best incubation period for this plasmid construct. This method allowed us for the first time to compare possible thalamic distributions to functional output. Although due to the sample size, only casual observations can be made. There appeared to be a mild positive trend between the input resistance and synaptic distribution where this positive trend was less evident when comparing the membrane time constant (Fig 4.9 B). A positive trend was also observed between the number of synapses and the frequency tuning bandwidth at 40dB. However as this data falls short of significance no definitive conclusions as of yet can be made.

A final point to make is that dendritic and somatic areas calculated do appear low (Benavides-Piccione et al., 2006). This could be as a result of insufficient labelling relative to other techniques or alternative analyses used. Further experimentation on this new technique will help improve its robustness.

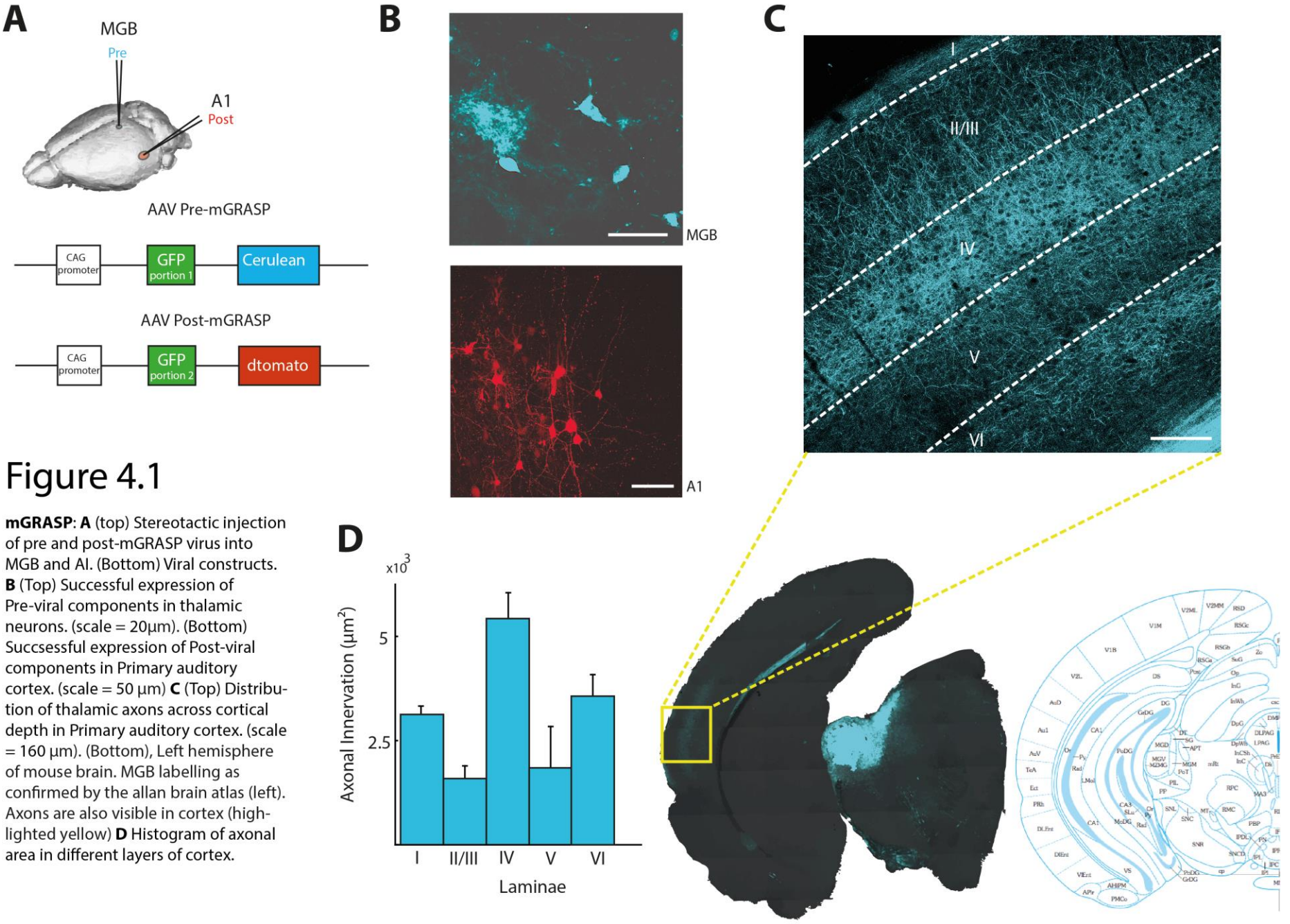

Figure 4.1

mGRASP: **A** (top) Stereotactic injection of pre and post-mGRASP virus into MGB and AI. (Bottom) Viral constructs. **B** (Top) Successful expression of Pre-viral components in thalamic neurons. (scale = 20µm). (Bottom) Succsessful expression of Post-viral components in Primary auditory cortex. (scale = 50 µm) **C** (Top) Distribution of thalamic axons across cortical depth in Primary auditory cortex. (scale = 160 µm). (Bottom), Left hemisphere of mouse brain. MGB labelling as confirmed by the allan brain atlas (left). Axons are also visible in cortex (highlighted yellow) **D** Histogram of axonal area in different layers of cortex.

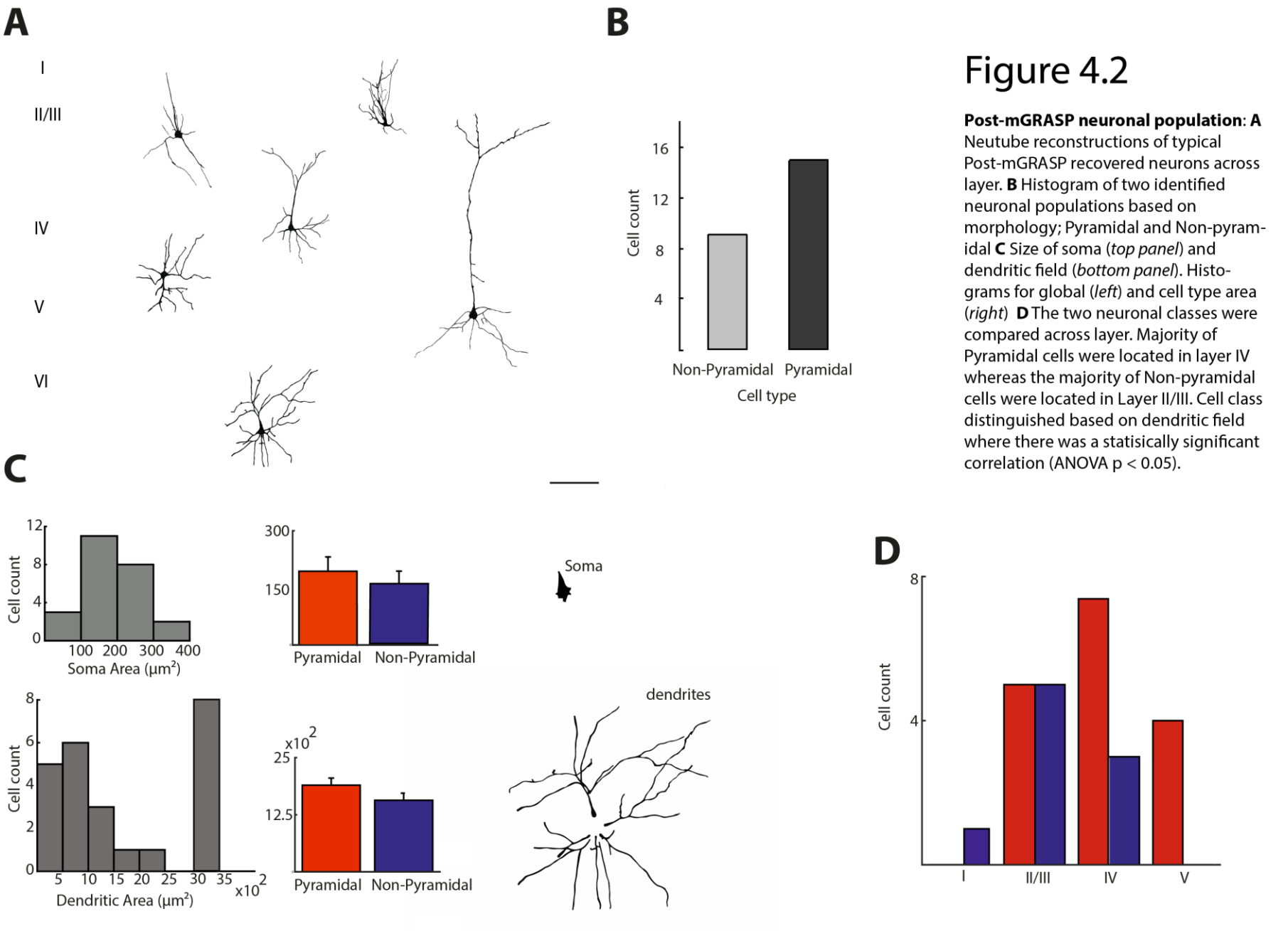

Figure 4.2

Post-mGRASP neuronal population: **A** Neutube reconstructions of typical Post-mGRASP recovered neurons across layer. **B** Histogram of two identified neuronal populations based on morphology; Pyramidal and Non-pyramidal **C** Size of soma (*top panel*) and dendritic field (*bottom panel*). Histograms for global (*left*) and cell type area (*right*) **D** The two neuronal classes were compared across layer. Majority of Pyramidal cells were located in layer IV whereas the majority of Non-pyramidal cells were located in Layer II/III. Cell class distinguished based on dendritic field where there was a statisically significant correlation (ANOVA $p < 0.05$).

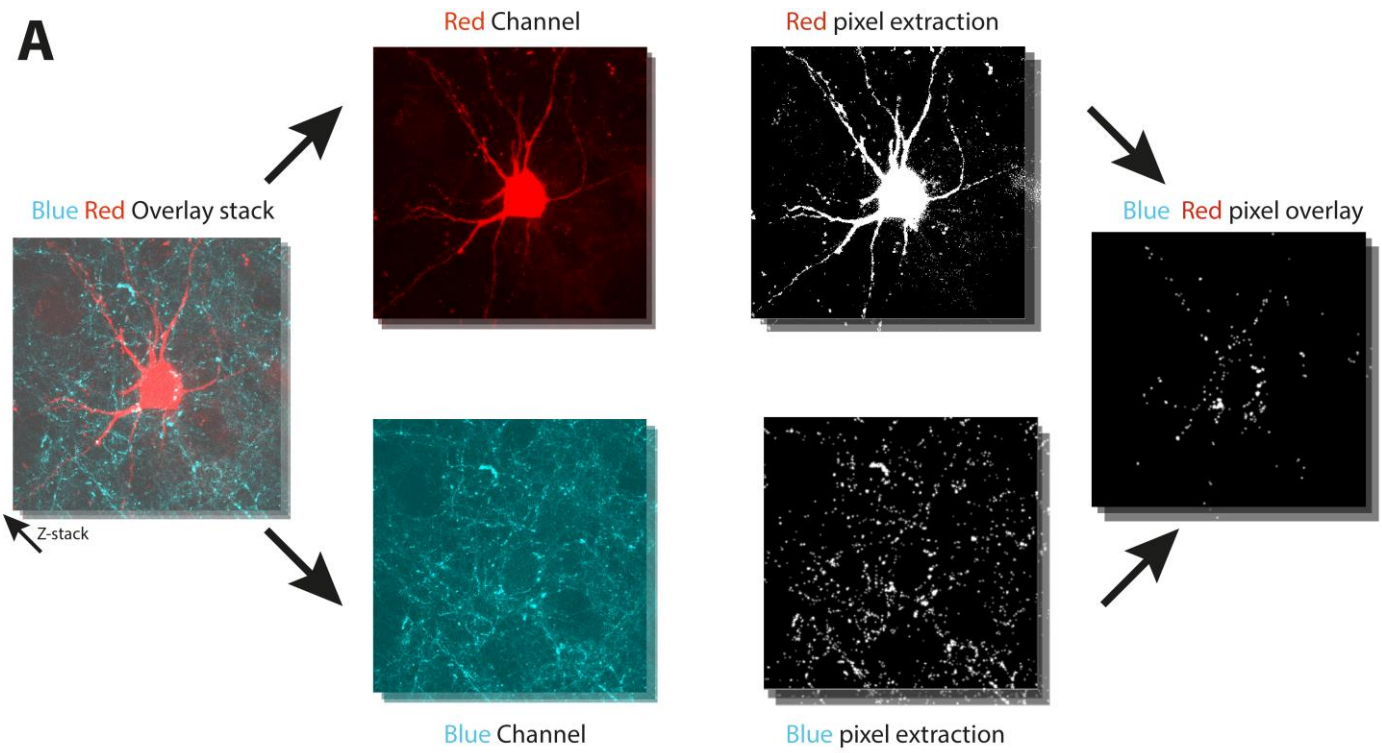

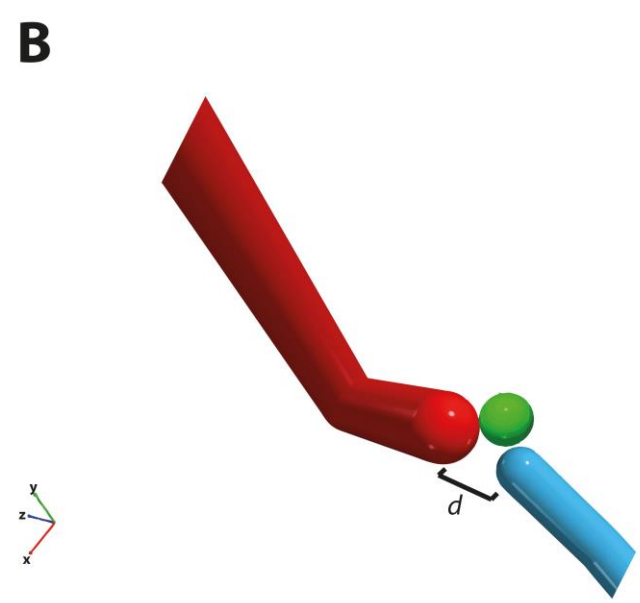

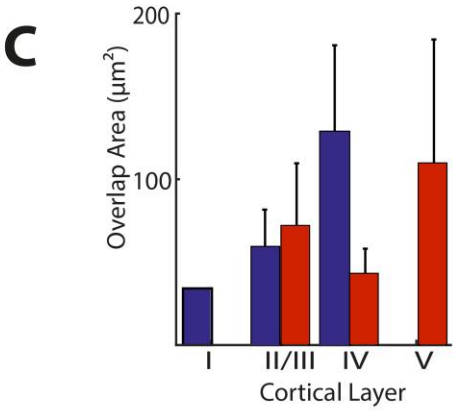

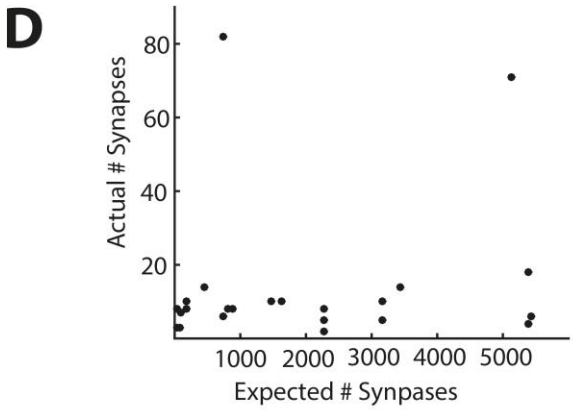

Figure 4.3

Synapse identification: **A** Process of overlap detection, blue (*bottom panel*) and red (*top panel*) channels are segregated and given identical pixel values. Images are recombined and overlay determined. **B** Neutube reconstruction of dendrite (red) and axon (blue) whereby distance (d) is close enough for synapse formation. Green channel is then observed and if fluorescence is present, a 'true' synapse is identified **C** Overlaps are comapred across depth for two neuronal classes, Pyramidal and Non-pyramidal. Across layer no statistically significant correlation was found for either cell population. **D** Comparison between the expected number of synapses and the actual number of synapses based on mGRASP detection.

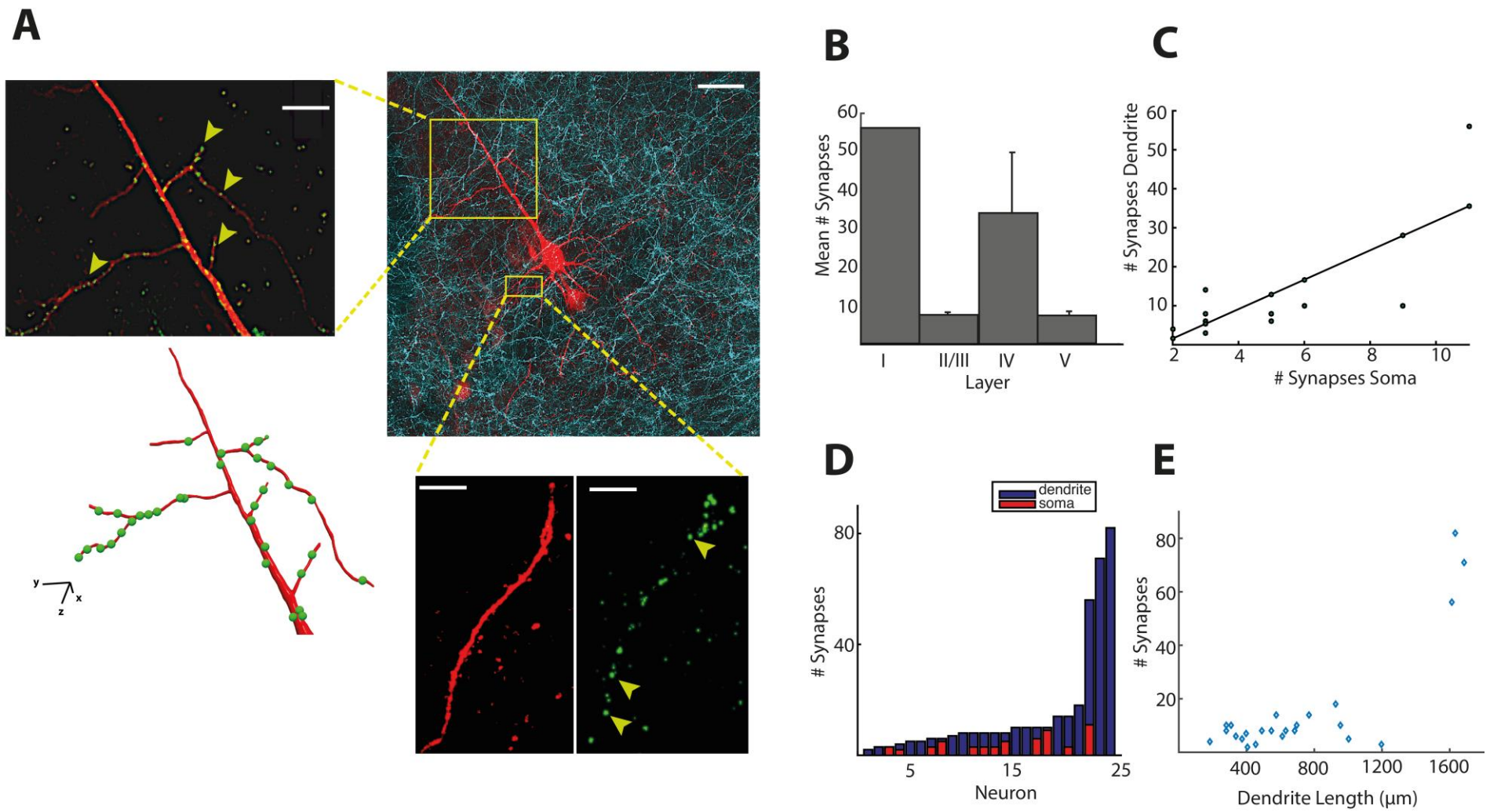

Figure 4.4

Puncta quantification: **A** Example 1 Layer IV pyramidal neuron. *Top right* panel shows overlap of thalamic input onto a cell (scale = 30µm) . *Top left* panel is a zoom of a portion of the apical dendrite (scale = 10µm), where the *bottom left* is a Neutube reconstruction of a portion of the apical dendrite with identified synaptic contacts represented as green spheres. These spheres are not a proportional representation of the size of identified synapses. *Bottom left,* zoom of the basal dendrites, highlighting some contacts on basal dendrites (yellow arrrows), red channel on the left and green channel on the right (scale = 5 µm). **B** Quantification of synapses across depth, where there is a non-uniformal distribution across depth (ANOVA p <0.05). **C** Comparison of recorded synaptic contacts on soma versus the number of contacts made on the soma. **D** Half of the neural population had synaptic contacts on the soma. **E** Number of synapses across a neuron is compared to total dendrite length .

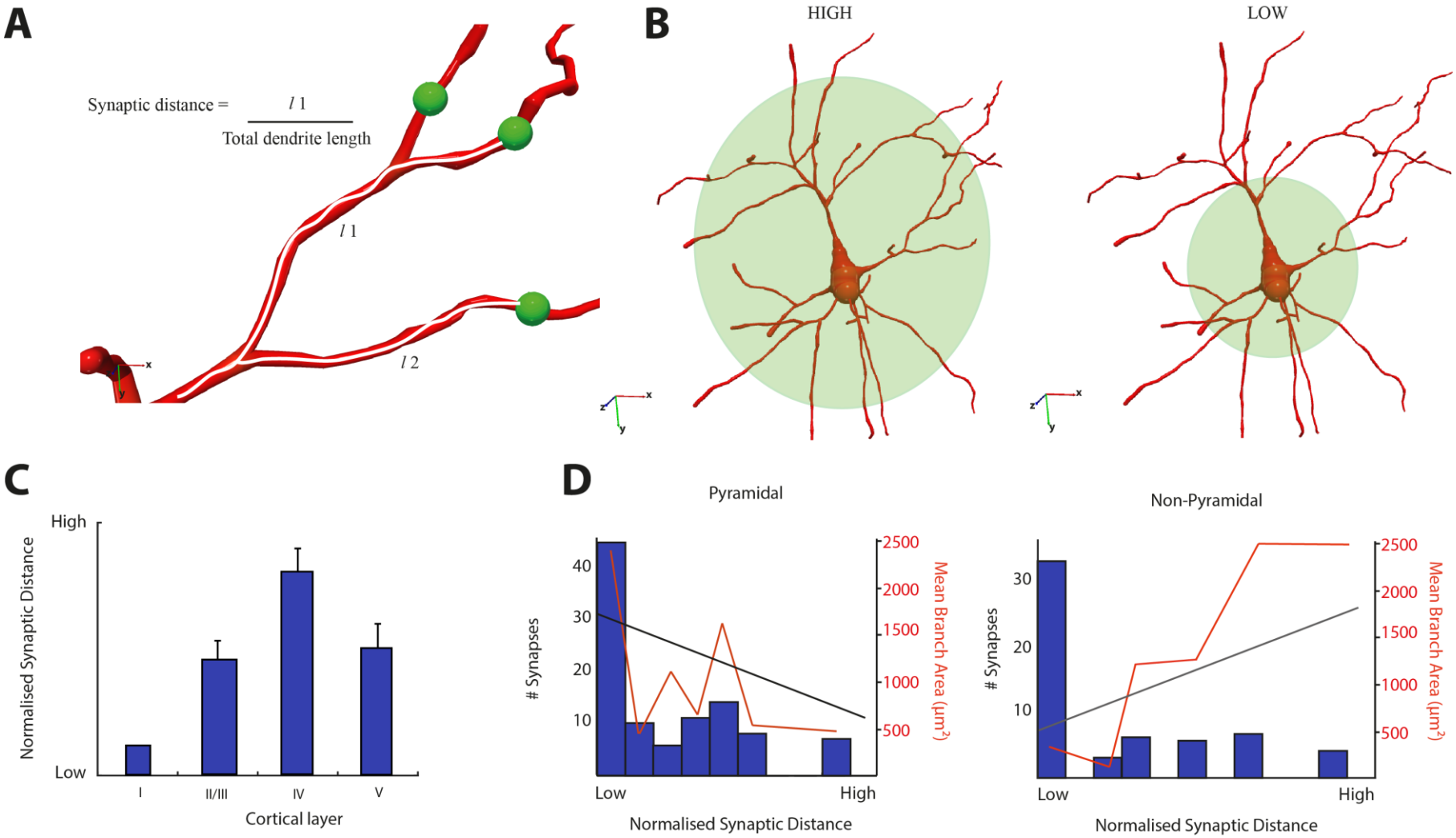

Figure 4.5

Synaptic distribution: **A** Method for normalising synapses. Each synapse is normalised relative to the dendritic branch it is located on, where 'l' denotes the distance of the synapse from the soma. **B** Normalised synatpic distances yeild two distributions. When the normalised synaptic distance is high, synapses are distributed proximally, whereas if it is low synapses are distributed distally. **C** Normalised synaptic distance was compared across cortical layer **D** Normalised synaptic distances are compared to the total number of synpases and the mean dendritic branch area for two neuronal populations, Pyramidal and Non-pyramidal.

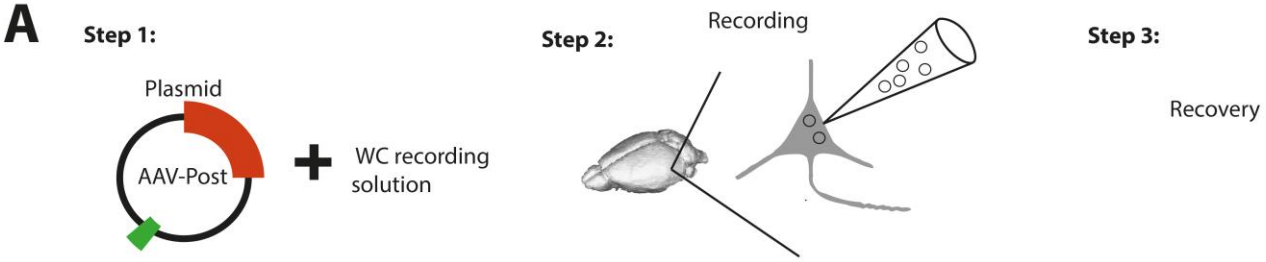

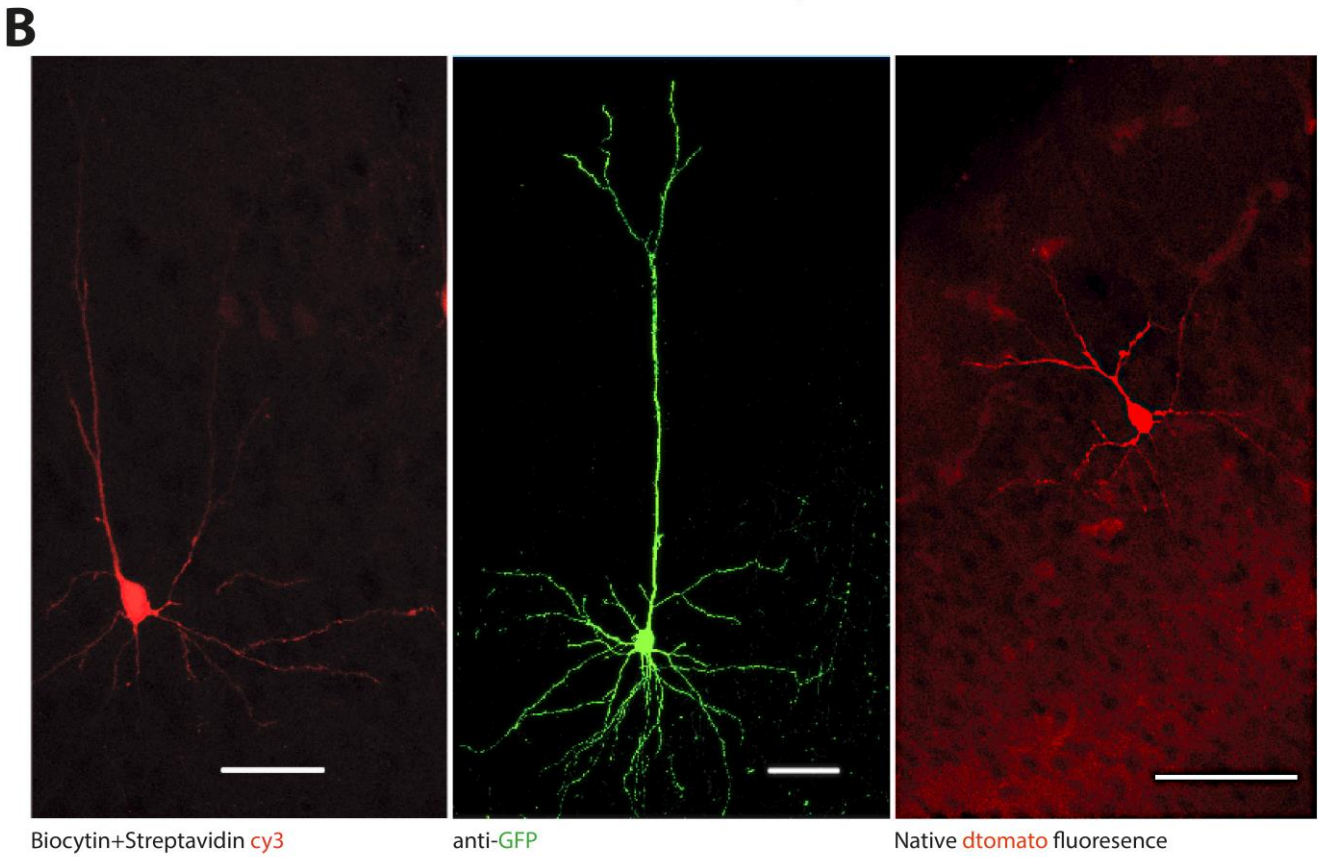

C

Incubation time (hr)	Plasmid Titre (ng/µL)	Voltage Injection (-1V)	Access Resistance (MΩ)	Attempts	Succes Rate (%)
12	Low	None	83.4 (±24.3)	31	-
24	Low	None	62.1 (±30.7)	32	-
36	Low	None	64.4 (±21.3)	28	-
36	High	None	51.6 (±15.5)	44	-
48	High	None	47.4 (±14.7)	53	-
52	High	Yes	27 (±10.3)	26	25

Figure 4.6

Whole-cell transfection: **A** Three step process. Correct concentration of plasmid is added to the recording solution. Whole cell recordings are performed with plasmid containing internal solution and via passive diffusion the plasmid enters the neuron. Pipette is slowly withrawn from the recorded cell completing the transfection process **B** *left panel*, biocytin included in normal recording solution and conjegated with Steptaviding-cy3 for detection, neuron left to incubate for 24hrs in order to prove that an individual cell can be successfully recovered . *Middle panel*, pCAG-GFP replaces Biocytin in internal solution in order to prove that single cells can be successfullly transfected. Signal is boosted using anti-GFP antibody. Right panel, native fluorescence from pCAG-POST-mGRASP (scale 20µm). **C** Table of success. Transfection attempts were monitored under different conditions in order to determine the parameter that will lead to successful transfection.

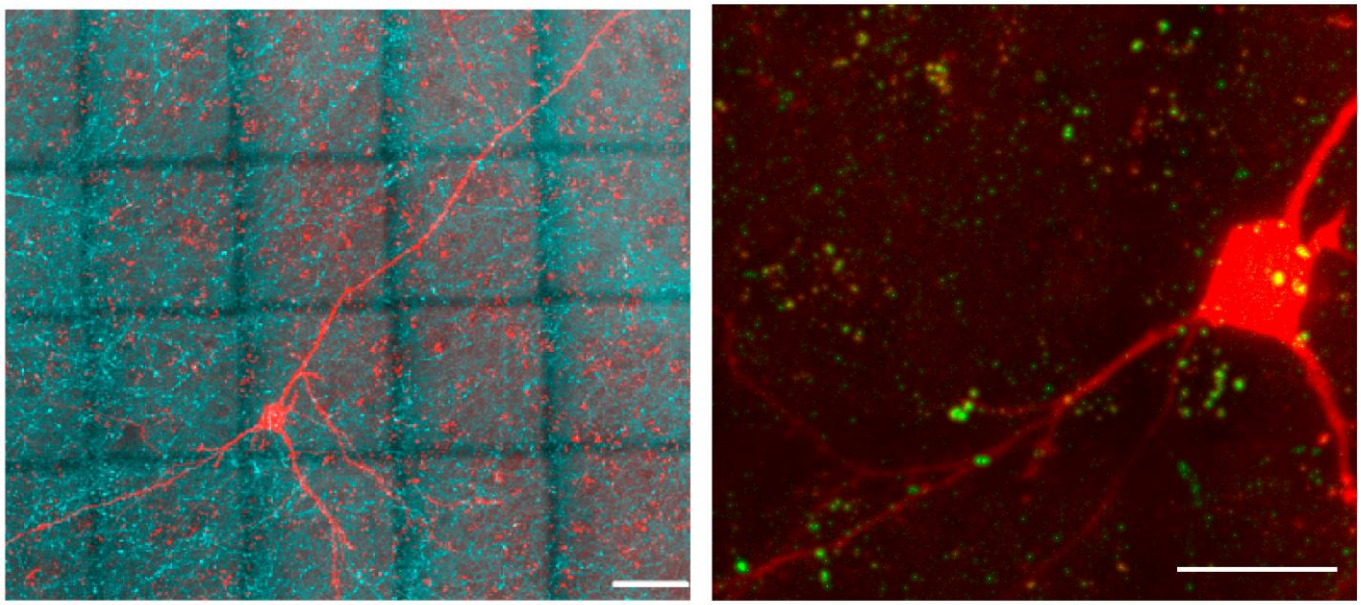

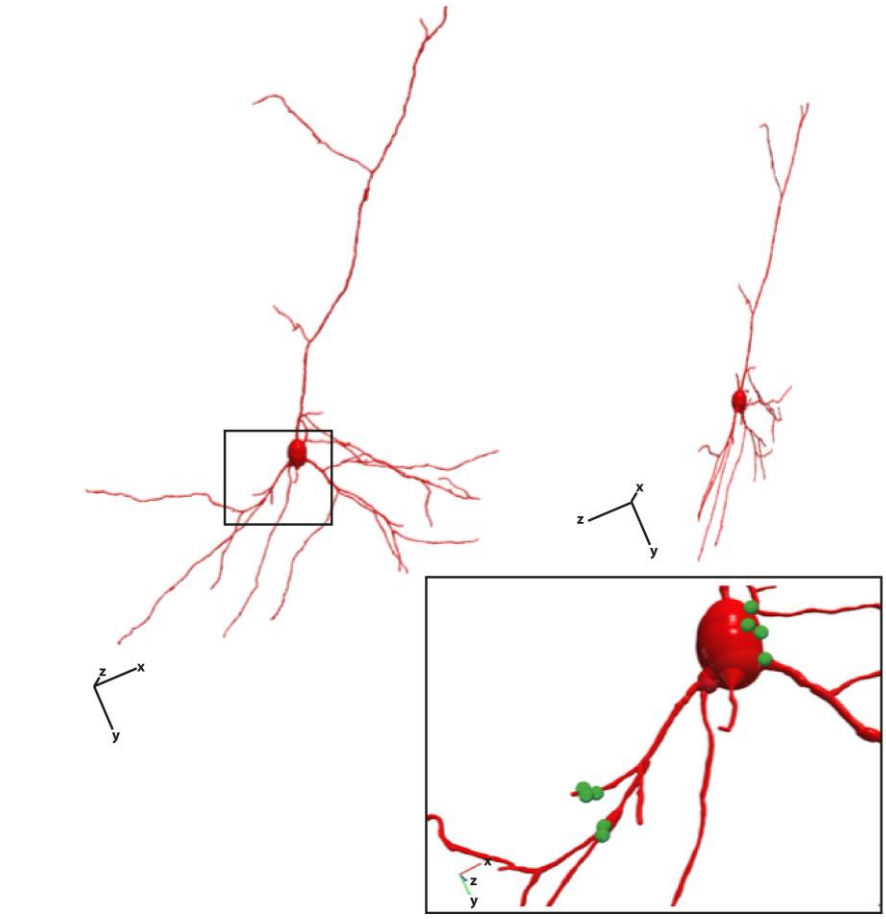

Figure 4.7

Single cell mGRASP: **A (***op panel* Post-mGRASP labelled single cell achieved via whole cell transfection. Axons visible (blue) labelled by stereotactic injection of pre-mGRASP into MGB (scale 20µm). *bottom panel* Red and green channel with syanpses visible on soma and basal dendrites (scale 20µm). **B** Neutube reconstruction of single cell at two different angles. Bottom panel, zoom on basal dendrites and soma, where thalamic synapses are visible in green.

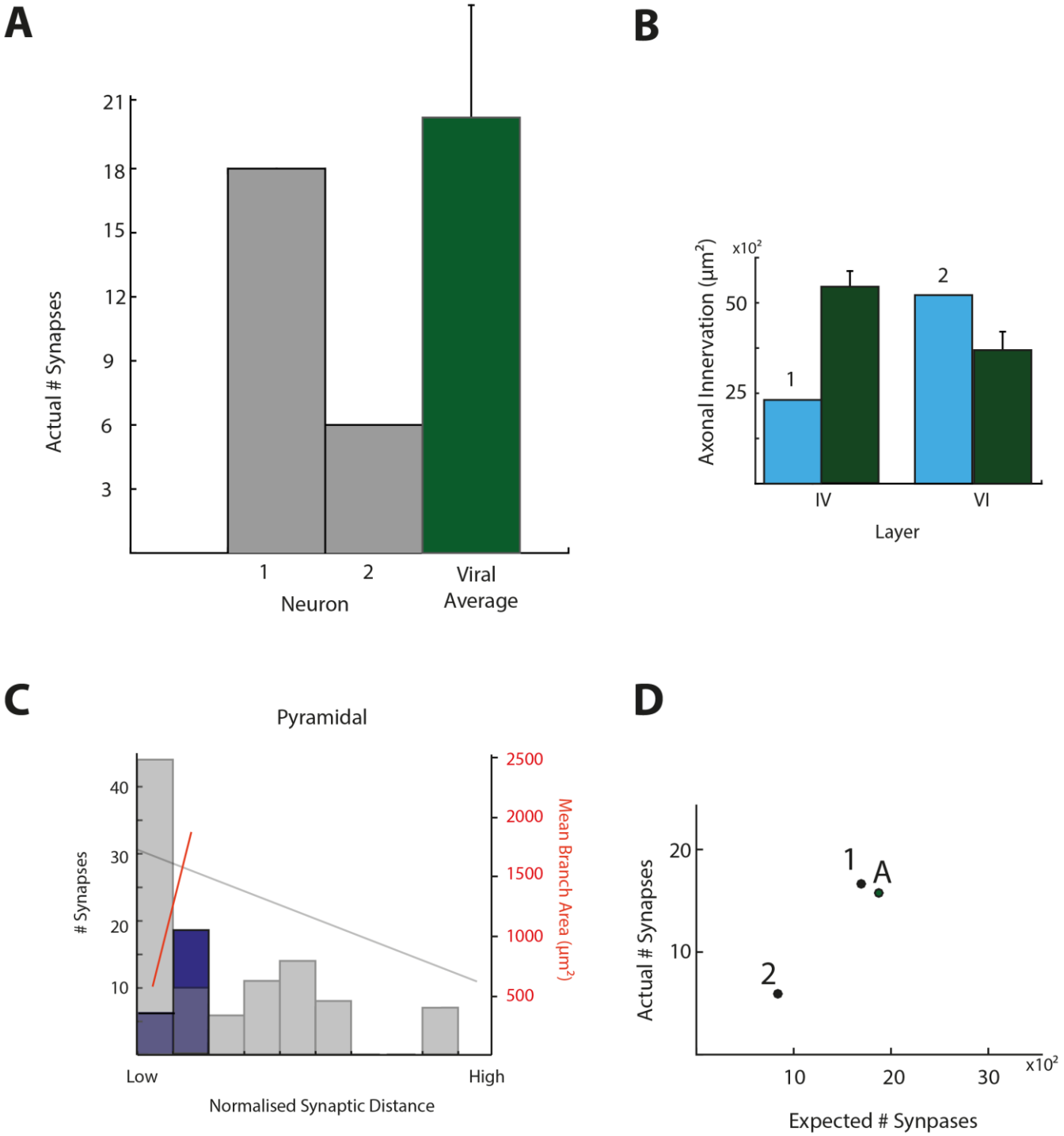

Figure 4.8

Comparing of single cell and viral bulk data: **A** Total number of synapses compared for two single cells and viral bulk, where differences are not statistically significant. (*left panel*) Axonal input for the layer IV single cell was lower than the viral bulk for that layer whereas the layer VI neurons received more axonal input that its virul bulk equivalent **B** Noramilsed synaptic distances for both single cells were similar to pyramidal viral bulk, indicating that the distribution of synapses is just as soma centric. (*left panel*) expected number fo synapses for single cells reflects the trend observed in the viral average, where although linear, there is ~100 fold difference between predicted and actual number of synapses.

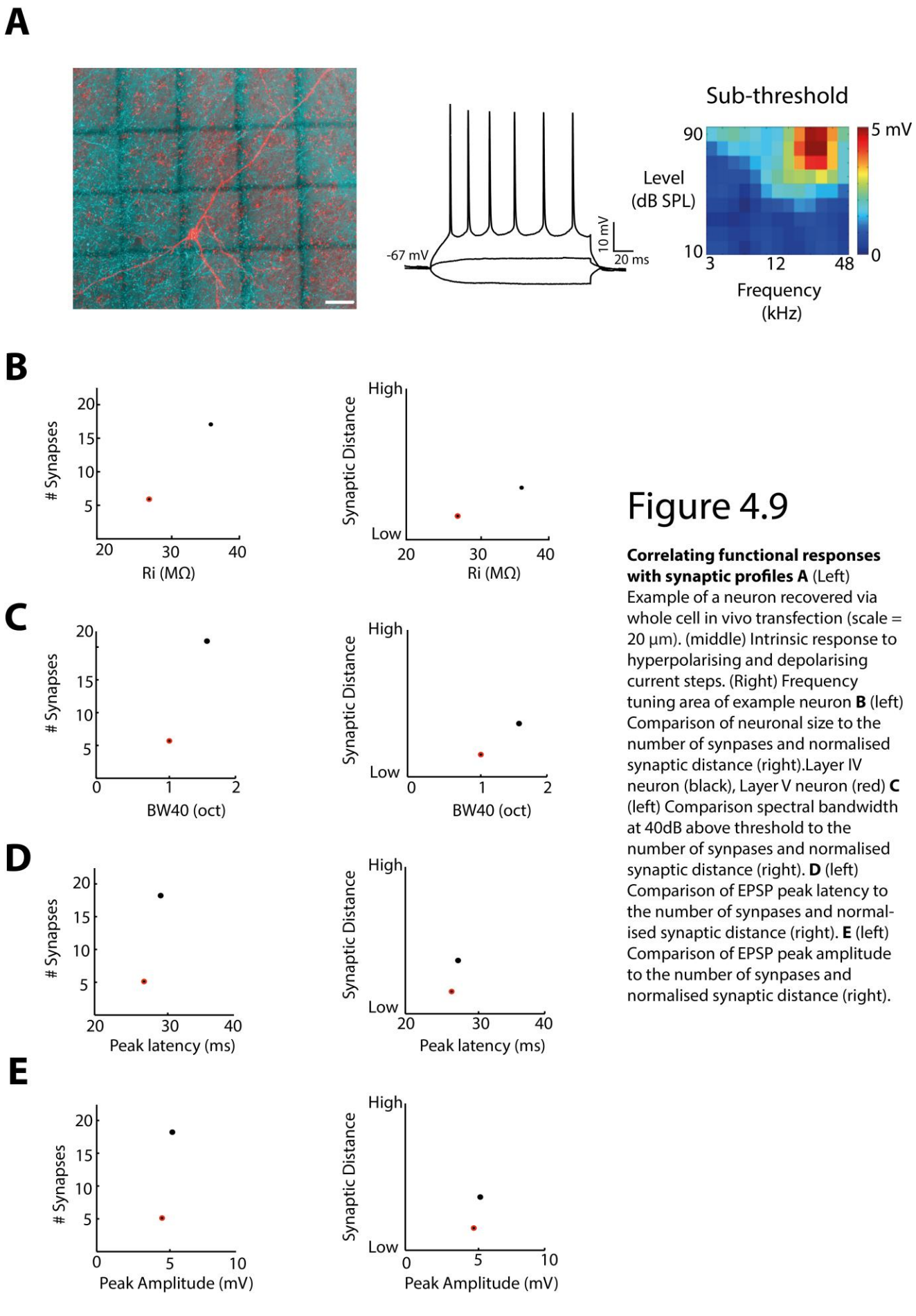

Figure 4.9

Correlating functional responses with synaptic profiles A (Left) Example of a neuron recovered via whole cell in vivo transfection (scale = 20 µm). (middle) Intrinsic response to hyperpolarising and depolarising current steps. (Right) Frequency tuning area of example neuron **B** (left) Comparison of neuronal size to the number of synpases and normalised synaptic distance (right).Layer IV neuron (black), Layer V neuron (red) **C** (left) Comparison spectral bandwidth at 40dB above threshold to the number of synpases and normalised synaptic distance (right). **D** (left) Comparison of EPSP peak latency to the number of synpases and normalised synaptic distance (right). **E** (left) Comparison of EPSP peak amplitude to the number of synpases and normalised synaptic distance (right).

5 CORRELATES OF CMR IN AI OF THE MOUSE

5.1 INTRODUCTION

Natural auditory environments are complex, where natural sounds are both spectrally and temporally complex. Pure tones are often used to probe the auditory system, as this stimulus is the basic building block of more complex naturalistic sounds. Animals have evolved the ability to detect salient sounds in complex background noise, a process crucial to survival (communication, hunting and evasion). This process requires segregation of perceptual objects by monitoring intensity changes across frequency ranges over time. Changes in such spectro-temporal patterns, are detected by the auditory system to a remarkably high resolution (Klumpp & Eady, 1956; Rosenblith & Stevens, 1953). The auditory system employs pattern recognition when monitoring these spectro-temporal changes (McDermott et al., 2013), to improve sound processing (Yaron et al., 2012). One such pattern prevalent in nature (vocalisation and running water) is coherent amplitude fluctuations across frequencies (Comodulation) (Nelken et al., 1999). Such a phenomenon could act as a cue in the auditory system for object formation and segregation (McDermott et al., 2013).

A psychoacoustic phenomenon known as, Comodulation masking release (CMR), involves adding comodulation to an existing masker to improve signal detection (Hall et al., 1984). This is a somewhat surprising effect, as typically adding noise decreases signal detection (Fletcher, 1940). There are two types of CMR; *within-channel* CMR, where the modulated noise is similar in frequency to the signal and *across-channel* CMR, where the modulated noise and signal frequencies are dissimilar. A mechanistic explanation of within-channel CMR has been demonstrated in the auditory periphery whereas *across-channel* CMR, instead has been attributed to an auditory grouping effect performed in the brain (Buss et al., 2009; T Dau et al., 2004; Torsten Dau et al., 2009; Verhey et al., 2012). However the precise mechanism and location in the auditory pathway where this process is carried out is not well understood.

The temporal history of the masker affects the magnitude of *across-channel* CMR (T Dau et al., 2004; Grose et al., 2009; Grose & Hall III, 1993; Grose et al., 2005; McFadden & Wright, 1992; Verhey et al., 2012). Increasing the duration of the masker (history) prior to the signal enhances CMR has also been shown to reduce

detection thresholds (Hatch et al., 1995; McFadden & Wright, 1990, 1992). Conversely asynchronous across channel noise modulation produces no masking release (Grose et al., 2009; Grose & Hall III, 1993; Grose et al., 2005). These findings would suggest that: 1) the history of the noise masker and 2) the importance of synchronous spectro-temporal dynamics are fundamental to *across-channel* CMR. Given that these are psychoacoustic observations the exact location in the auditory system that produces this effect is unclear. However these processes are suggestive of higher order processing that may involve auditory cortex. A handful of multi-unit and single unit extracellular studies have investigated CMR in the brain. These studies have been conducted in the cochlear nucleus (the first auditory nucleus) and auditory cortex (one of the last auditory processing stations), where most confirmed the effects of within-channel CMR (Nelken, Rotman et al. 1999, Nieder and Klump 2001, Hofer and Klump 2003, Las, Stern et al. 2005).

In this chapter I attempted to confirm the presence of *across-channel* CMR in primary auditory cortical (AI) neurons by performing whole cell recordings in the anaesthetised mouse. Having established its presence I then assessed the influence of noise history (through the addition of a precursor) and determine whether it enhances the effect of CMR. I then determined if this enhancement involved cortical circuitry or whether any improvement is passively inherited from subcortical nuclei. In order to determine this auditory cortex was silenced during the precursor using optogenetics. This was achieved by targeting the expression of Channelrhodopsin-2, a light gated ion channel, to the membranes of PV+ interneurons in AI. PV+ interneurons are a subgroup of fast spiking GABAergic interneurons, that target the perisomatic region of pyramidal cells and therefore when activated will inhibit their activity. Whole cell recordings were performed during this stimulus paradigm in AI of PV-cre mouse lines and the resulting activity is monitored.

5.2 RESULTS

5.2.1 Cortical correlates of CMR in mouse AI

My first aim was to establish whether neural correlates of CMR are present in individual neurons of the mouse auditory cortex. Psychoacoustic CMR is characterised by increased detectability (reduced detection threshold) of a signal embedded in noise that lies within the same auditory filter. This type of noise is referred to as a narrowband masker (NB). The degree of masking release is dependent on (i) the amount of extra noise energy (bandwidth) encompassing the signal frequency (broadband), and (ii) the envelope of this additional noise energy is coherently modulated with respect to the NB masker. Therefore both conditions should be met in order to observe masking release of signal-evoked neuronal activity. In order to assess the relative contribution of additional noise energy and degree of co-modulation, a 'modulated broadband masker' must be presented. It is comprised of amplitude-modulated 'flanking bands' of pure tones, added to the NB masking stimulus (6 pure tones split into low and high frequency flanking bands). The modulation phase of flanking noise bands are presented either incoherently (incoherent modulation, IM), or coherently (coherent modulation, CM) (Figure 5.1A), with respect to the NB masker. Whole cell patch clamp recordings were made in AI of anaesthetised mice, where evoked activity to pure tone stimuli is recorded in order to establish a frequency response area. By determining a neurons FRA it then becomes possible to adjust the signal and masker frequencies in the CMR stimulus so that it represents the range of inputs onto individual cells. Finally, evoked activity was measured during the presentation of the pure tone signals embedded in masking noise at a variety of signal-to-noise ratios (SNRs; range: -10 to +20 dB, 5dB steps) for each co-modulated condition. Across the population, evoked responses were observed to both signal and co-modulated masker, including a wide variety of firing profiles to the masking noise alone (Fig 5.1 B). Thus by comparing signal detection between three distinct noise conditions (NB, IM, CM), I could measure the influence of across-frequency coherence on signal detectability in auditory cortex (Figure 5.1 B-C).

5.2.2 CM-condition produces larger EPSPs and reduces threshold relative other conditions

A majority of neurons demonstrated a simple relationship between evoked activity and SNR, whereby increased signal levels evoked larger and faster EPSPs across

all conditions, however there were clear observable differences between conditions (Figure 5.1 C-D). For each condition had ten repeats across all eight different SNR conditions (see Methods 2.2.2). The ten repeats were averaged in order to produce a mean trace across the entire stimulus window (2 s) at each SNR. Each mean trace was then subtracted from the mean trace for the noise alone condition, in order to isolate signal-evoked activity. Finally signal evoked activity across SNR was measured in terms of mean membrane potential (MMP) and peak latency (PL) of evoked EPSPs during the signal window of the entire trace. Interestingly, when comparing MMP across SNR, on average the CM condition evoked larger EPSPs than (2.2 ± 0.76 mV), IM (1.1 ± 0.6 mV) and NB (1.7 ± 0.8 mV). This trend was reflected in the peak latency where EPSPs in the CM condition were faster than (13.6 ± 3.76 ms), IM (18.6 ± 5.9 ms) and NB (16.1 ± 5.7 ms), where the difference was significant (ANOVA, $F=1.9$, $p=0.05$).

This result shows that the CM condition evokes significantly faster and larger responses relative to IM and NB conditions, which suggest that it is more likely to elicit spike activity. However given that CMR concerns the reduction of threshold, I then compared signal detection thresholds across condition so see if these larger EPSPs occur at lower SNRs. This was achieved by determining the minimum sound level, otherwise known as threshold, at which signal-evoked responses can be observed (> 0.5 mV). Interestingly there was a significant difference across SNR between conditions in both MMP and Peak time (MANOVA, $p = 0.05$) where the NB (9.5 ±1 dB SNR) and IM (8±1 dB SNR) conditions showed similar activity, whereas signal evoked responses in coherently modulated broadband (4±1.6 dB SNR) noise were detected at significantly lower SNRs (Figure 5.1 D-E). Given that there were only small differences in signal-evoked responses between NB and broadband IM maskers it suggests that adding sound energy alone to a masking noise neither improves nor impairs the detectability of low-level signals. On the other hand CM of flanking noise bands produced significant enhancements in signal-evoked subthreshold activity, which suggests that these results correspond to true masking release reported in previous psychoacoustic measurements. From a biophysical perspective, it could suggest that inputs driven by IM and NB stimuli integrate on a neurons dendrite, overlapping in time so that channels are opened simultaneously (temporal summation). This could result in a ‘leakier’ cell (low resistance R) and hence less able to store charge (C), resulting in attenuation of the driving force. This difference in temporal summation of synaptic contacts across a cell could explain the reduction in threshold observed under the CM condition.

5.2.3 Centering a neurons receptive field at the signal improves CMR

Frequency selectivity is an elemental property of auditory cortical neurons, fundamental in determining individual neuronal sensitivity to tone signals. Most psychoacoustic studies have centred the noise and signal frequency around the minimal threshold response in an audiogram (Buus, 1985; Hall III & Grose, 1988; Hall et al., 1984). Recent extracellular studies report within-channel CMR correlates in cat AI (Nelken et al., 1999) and across-channel CMR in mouse AI (Sollini et al., 2014). It has been suggested that a neurons frequency tuning impacts signal detectability (Sollini et al., 2014). In order to confirm this effect, a neurons characteristic frequency (CF) was identified by determining its FRA and two types of CMR stimulus are presented i) where the embedded signal, as previously presented, matches its CF and the second ii) changing the signal frequency. The signal frequency was altered ± 1 oct from CF, and evoked activity compared (n = 8). As expected, on average the On-CF response showed an improvement over Off-CF for all measures (Fig 5.3 C-E) (MMP 1.8 ± 0.5 mV and Peak time 28.4 ± 18.2 ms). There was also a significant reduction in threshold when the signal frequency is set at CF vs off-CF (unpaired t-test, $p < 0.05$). These results suggest that frequency tuning plays a crucial role in signal detection.

5.2.4 Noise history improves CMR

Psychoacoustic studies have shown that the temporal history of the masker is known to affect the magnitude of *across-channel* CMR (T Dau et al., 2004; Grose et al., 2009; Grose & Hall III, 1993; Grose et al., 2005; McFadden & Wright, 1992; Verhey et al., 2012), however a correlate of this effect has only been observed recently in the mouse (Sollini et al., 2014). The original coherently modulated noise signal had its early noise portion removed resulting in two stimulus conditions, a long and a short CM (Figure 5.2 A). There was a significant difference (unpaired t-test, $p<0.05$) between both measures where EPSPs were on average larger (MMP, 1.55 ± 3.76 mV) and faster (PL, 4.8 ± 1.7 ms) in the long condition than the short CM condition (Figure 5.2 C). The difference in threshold was as significant across SNR (MANOVA, $p < 0.05$), where thresholds were on average lower in the long condition (4 dB SNR) (Figure 5.2 D). Overall, this result demonstrates that the noise history enhances the effect of CMR at the level of cortex.

5.2.5 Cortex contributes to CMR

Adaptation to coherently modulated maskers could manifest at several stages in the ascending auditory pathway. To determine whether it is an effect passively inherited from subcortical regions or is formulated at the level of cortex a paradigm to transiently and selectively inactivate neuronal activity in the auditory cortex during early sound processing while leaving activity in subcortical processing centres intact was employed. To achieve this a protocol involved was used to selectively express channelrhodopsin (ChR2) in Parvalbumin-positive (PV+) interneurons using viral injections of the FLEXed ChR2 construct into auditory cortex of PV-Cre mice (Figure 5.4). ChR2 was successfully expressed in PV+ neurons (96.6 ± 0.8 %), however there were instances PV- and YFP+ labelled cells. Given that so few were observed, activation of a handful of other cells types (pyramidal and SOM) most likely will no impact the overall effect of cortical inactivation produced by PV+ interneurons. Blue light stimulation (150ms, 473nm, 5mW) of cortical tissue caused transient activation of PV+ cells (Figure 5.4 D), which in turn produced strong inhibition of cortical pyramidal cells (Weible et al., 2014) (Figure 5.4 D). This method enabled fast temporal inactivation, and more importantly, recovery of auditory cortical processing, indicating that any potential leakage into other cell types had no observable impact. This stimulus protocol was first tested on the short duration masker (CM), where laser inactivation of cortex occurred prior to the presentation of the modulated masker and signal (n=32).

Signal-evoked responses measured in MMP (0.7 ± 0.4 mV) and PT (2.7 ± 1.77 ms) were unchanged following cortical disruption demonstrating that cortex could reliably recover following laser inactivation (MMP MANOVA, $p = 0.5$ and PT, MANOVA, $p = 0.9$). For the long-CM condition the result is unclear as the two measures produced conflicting effects. When looking at differences in peak latency of EPSPs under each condition, there is a significant increase in latency under the cortically inactivated condition (3.58 ± 1.5 ms), whereas there was an insignificant decrease in MMP (0.7 ± 0.1 mV) (Fig 5.5 C). This trend was also observed across SNR, where there was no significant change between the two conditions in terms of MMP whereas for PT there was (MANOVA, $p << 0.01$). Therefore, based on this data selective optogenetic inactivation of auditory cortex caused a significant reduction in signal-evoked response when measured in PT but not MMP, possibly demonstrating that auditory cortical processing of the early sound portion could be critical for large across-channel CMR. To confirm this hypothesis further experimentation is required as thresholds did appear to increase to similar levels between the long-CM opto condition and the short CM condition (Figure 5.5 D). Laser stimulation during the

presentation of the early sound portion also resulted in a large significant change in threshold, increasing thresholds by 5.4 dB (from 0.2 to 5.6 dB SNR). Therefore in conclusion selective optogenetic inactivation of auditory cortex caused a significant reduction in signal-evoked response, demonstrating that auditory cortical processing of the early sound portion most likely plays a critical in large across-channel CMR.

5.3 DISCUSSION

The auditory system has the ability to identify salient sounds in noisy backgrounds; the mechanism through which it evolves into a sensory perception is best explained through across-channel CMR. In this chapter, a potential neural correlate of CMR has been identified in AI of the mouse, where the largest effect involved adding more frequency information and coherently modulating it (Fig 5.1). Interestingly, 'priming' auditory cortical processing with an extension of noise (precursor) increased CMR at the level of cortex. Silencing cortex had the effect of on average increasing thresholds and hence diminishing the effect of CMR. These results would imply that primary auditory cortex plays a role in the formation of *across-channel* CMR, however further experiments will need to be carried out to test the validity of this statement.

5.3.1 Across-channel CMR

It has been suggested that across channel CMR occurs when the embedded noise encompasses frequency information beyond a single auditory filter. I therefore measured the impact of adding coherent and incoherent modulated flanking noise bands, outside of a mouse auditory filter, on cortical detection of embedded pure tones. This was achieved by performing whole cell recordings in AI of anaesthetised mice where subthreshold activity was recorded in response to different stimulus conditions. Subthreshold activity can be very informative regarding the type of inputs a neuron receives where two critical EPSP dynamics involved in achieving suprathreshold activity can be easily determined (amplitude and timing). Of the three stimulus conditions (NB, IM, CM), the incoherently comodulated noise didn't improve signal detection significantly from the narrowband condition. The comodulated condition did significantly reduce threshold and on average (across SNR) where it also evoked larger and faster responses to the signal (higher MMP and shorter PL),

suggesting that this most likely translates to spike activity. These results would suggest two things: Firstly that in the IM condition, even though more sound energy has been added to the noise, a requirement for improving CMR, there is no observed improvement in signal detection thresholds which could indicate that frequency channels in AI do not integrate and act independently. Secondly in the case of the CM condition, the modulation phase appeared crucial in enhancing the effect additional noise energy, as there was a large decrease in detection threshold. This most likely suggests that across-frequency integration occurs when sound energy is synchronised across frequency channels.

5.3.2 Noise history improves signal detection

Psychoacoustic experiments have shown that CMR was sensitive to the spectro-temporal history prior to signal presentation (Buss et al., 2009; T Dau et al., 2004; Grose & Hall III, 1993). My results agree and confirm that presentation of an extended portion of the noise prior to signal presentation improved detectability (Figure 5.3). This effect was observed firstly in EPSP dynamics where the MMP was on average larger in the long CM condition than the short CM condition. Secondly the long condition evoked faster EPSP's on average than the short condition. Combined with this, differences thresholds were significantly increased in the short condition (4 dB SNR). Several mechanisms have been proposed that could explain this effect (Sollini et al., 2014) such as synaptic plasticity and complex inhibition. Stimulus specific adaption (Ulanovsky et al., 2003) appears to be a common feature in AI where the plasticity has been shown to evolve and change neuronal responses over rapid timescales (Fritz et al., 2005). It has been suggested that this This dynamic model of AI could serve a means of improving performance during perceptual learning (Polley et al., 2006; Schnupp et al., 2006) where this mechanism could be attributed to the influence that AI has on subcortical processing, (King et al., 2007; Suga, 2008).

5.3.4 Contribution of Auditory Cortex to CMR

As you ascend through the auditory system feature selectivity becomes more apparent, such as increased receptive filed dimensionality, frequency specificity (Atencio et al., 2012) and the increasing effect of stimulus history (Wehr & Zador, 2005). Some of these features are known to be involved in object formation at the level of cortex and beyond (Bizley & Cohen, 2013). *Across-channel* CMR is heavily

reliant on stream segregation and subsequent object formation, but to what extent auditory nuclei contribute to its effect remains unknown (T Dau et al., 2004; Torsten Dau et al., 2009; Verhey et al., 2012). The optogenetic study attempts to answer the contribution that Primary auditory cortex has on observed CMR (Figure 5.5). Transient activation of PV+ neurons temporarily disrupts the cortical network by inhibiting excitatory pyramidal neurons that they synapse onto, which in turn has a cascade effect. Given that a majority of input onto cortical neurons is cortico-cortical, pyramidal neurons are left with distant cortical and thalamic input. By silencing one of the key components in cortical processing it is possible to abolish any across frequency integration or an alternative unknown network effect that mostly likely evolves at the level of cortex. To determine the benefit of noise history auditory cortex was silenced during the priming period of the stimulus, which was shown to act as a key cue in signal detection (Figure 5.3). The data implies that on average auditory cortex enhances the effect of CMR but is not responsible for it, as noise and signal evoked activity is still detected in the laser condition, albeit diminished. This would suggest that auditory cortex augments an inherited precortical effect.

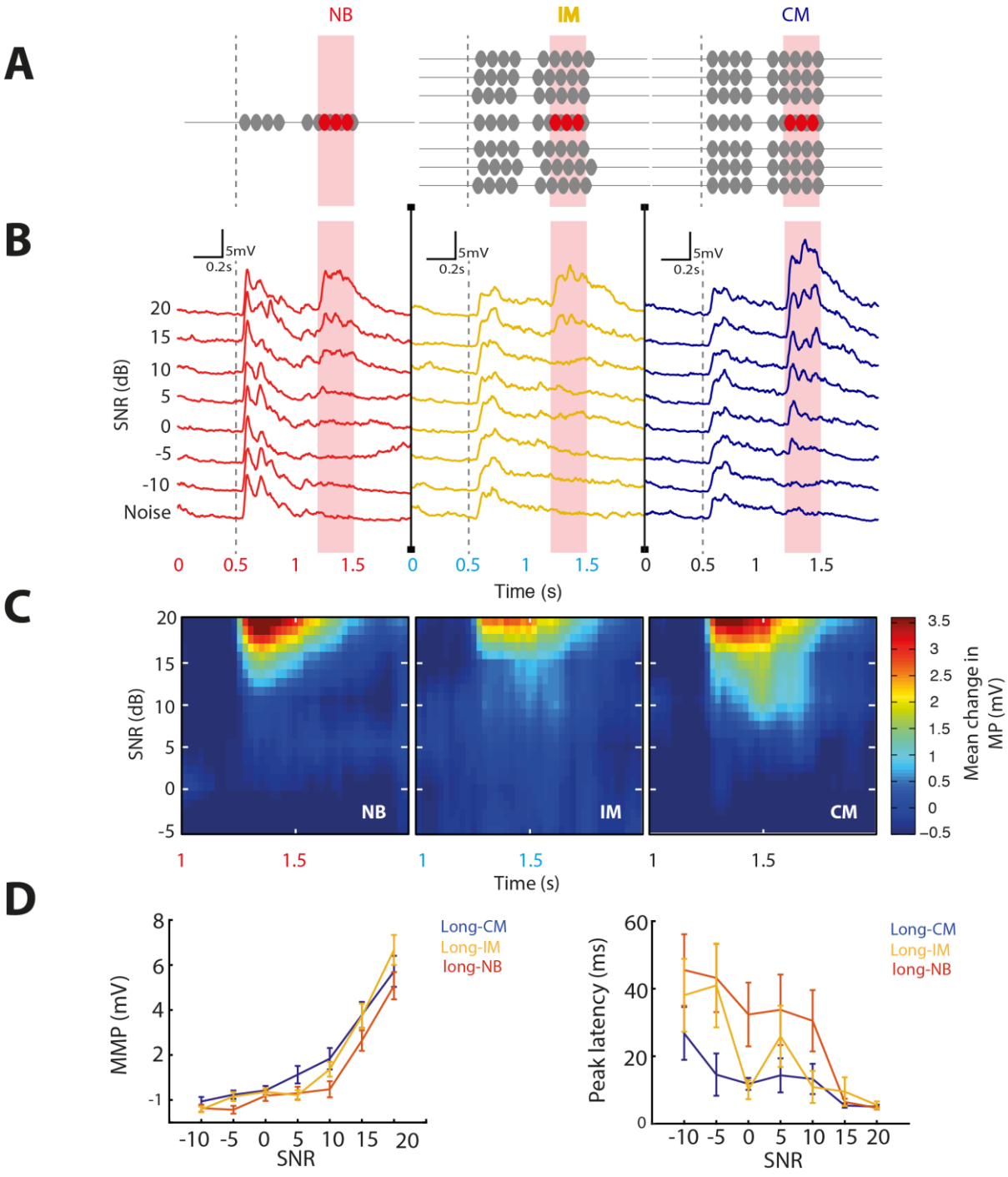

Figure 5.1

Subthreshold signal detection in the presence of different maskers. A Stimulus design, Pure tone signals were presented in three different noise backgrounds: narrowband (NB, red), broadband with incoherent modulation (IM, yellow) and broadband with comodulated envelopes (CM, blue). **B** Example cell, average responses (10 repeats) to each condition where the noise envelope was presented alone and in the presence of three tone pips at a number of different signal-to-noise ratios (SNR). Grey dashed lines indicate the beginning of the noise. Pink backgrounds indicate the tone presentation window. **C** Change in mean membrane potential at between two time points (1-1.5) for the 3 conditions presented. **D** (left) Plot fo mean membrane potential (MMP) across SNR for each condition.(Right) Plot of peak latency across SNR for each condition. **E** Histogram of average threshold SNR across each condition.

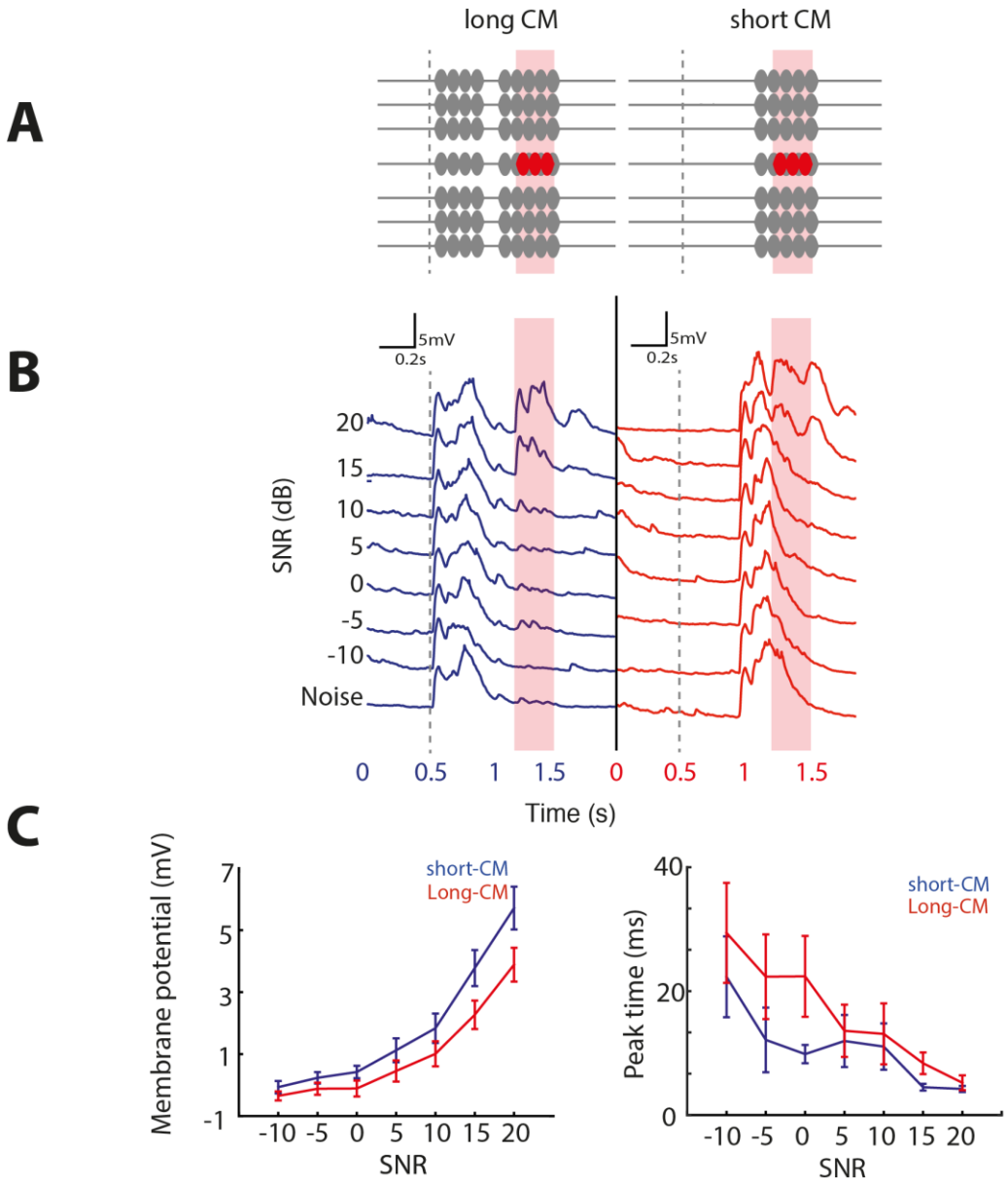

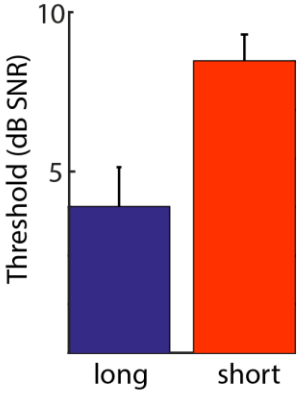

Figure 5.2

Effect of noise history on signal detection A Stimulus design: broadband with comodulated envelopes (CM-long, blue as before) and broadband with comodulated envelopes without noise history (CM-short, red) . **B** Example cell, average responses (10 repeats) to each condition where the noise envelope was presented alone and in the presence of three tone pips at a number of different signal-to-noise ratios (SNR). Grey dashed lines indicate the beginning of the noise. Pink backgrounds indicate the tone presentation window. **C** (left) Plot fo mean membrane potential (MMP) across SNR for each condition. (Right) Plot of peak latency across SNR for each condition. **D** Histogram of average threshold SNR across each condition.

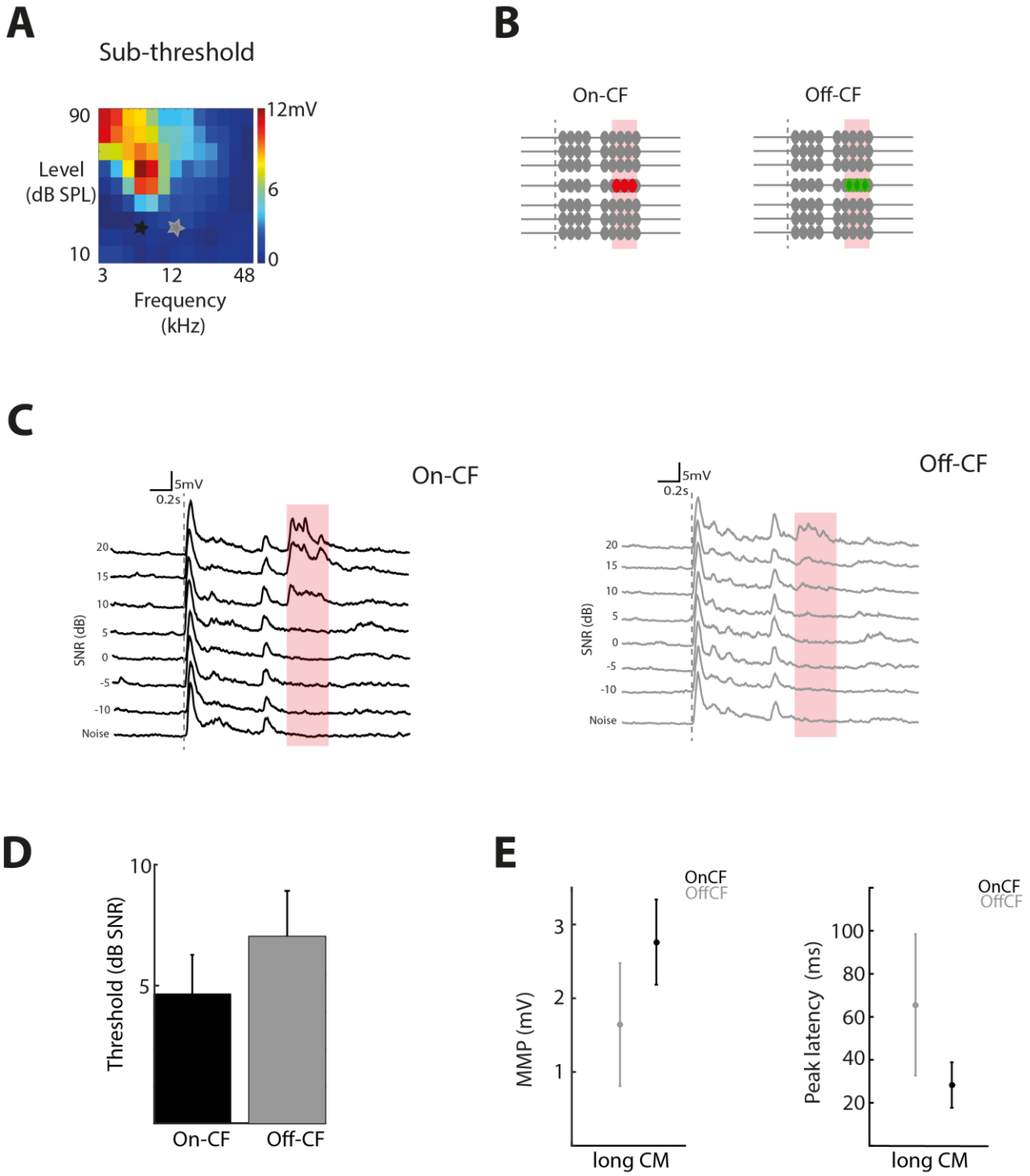

Figure 5.3

Effect of changing signal and envelope frequency to off-CF A An example cells frequency response area (FRA), when CF is selected (black star) and Off-CF is selected 1 octave away (grey star). **B** Stimulus design: broadband with comodulated envelopes based on cells CF (CM On-CF, red) and broadband with comodulated envelopes based away from cells CF (CM, CM Off-CF, green). **C** Example cell, average responses (10 repeats) to each condition where the noise envelope was presented alone and in the presence of three tone pips at a number of different signal-to-noise ratios (SNR). Grey dashed lines indicate the beginning of the noise. Pink backgrounds indicate the tone presentation window. (left) On-CF evoked responses (black), (right) Off-CF evoked responses. **D** Histogram of average threshold SNR across each condition. **E** (left) Compasionsof mean membrane potential at threshold between On-CF (black) and Off-CF (grey) trials. (Right) Compasionsof Peak latencies at threshold between On-CF (black) and Off-CF (grey) trials.

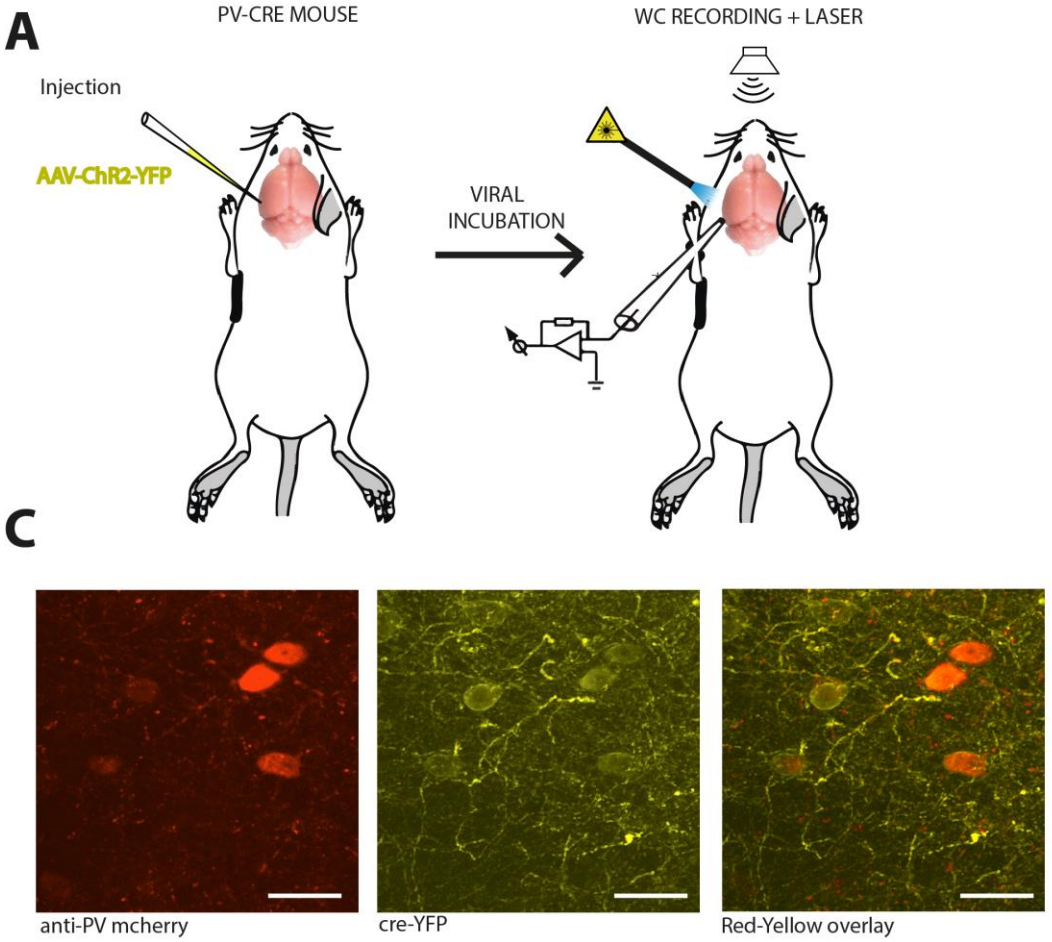

Figure 5.4

PV directed inactivation of cortex A Schematic of experimental procedure. AAV-FLEX-ChR2 was injected into the auditory cortex of PV+ cre mice. After a given incubation period laser stimulation stimulates PV cell firing thus inactivation cortical contribution during stimulus presentation. **B** Left hemisphere, identifying successfull YFP fluoresence at a confirmed AI location. **C** Specific infection of PV+ cells was confrmed via co-expression (merged image, right) of ChR2 (yellow, middle) and PV-antibody (left, middle), scale 25µm **D** Physiological confirmation of ChR2 expression. Two responses during laser stimulation, (top) excitatory responses in PV+ cell and (bottom) an inhibitory responses in a PV- cell.

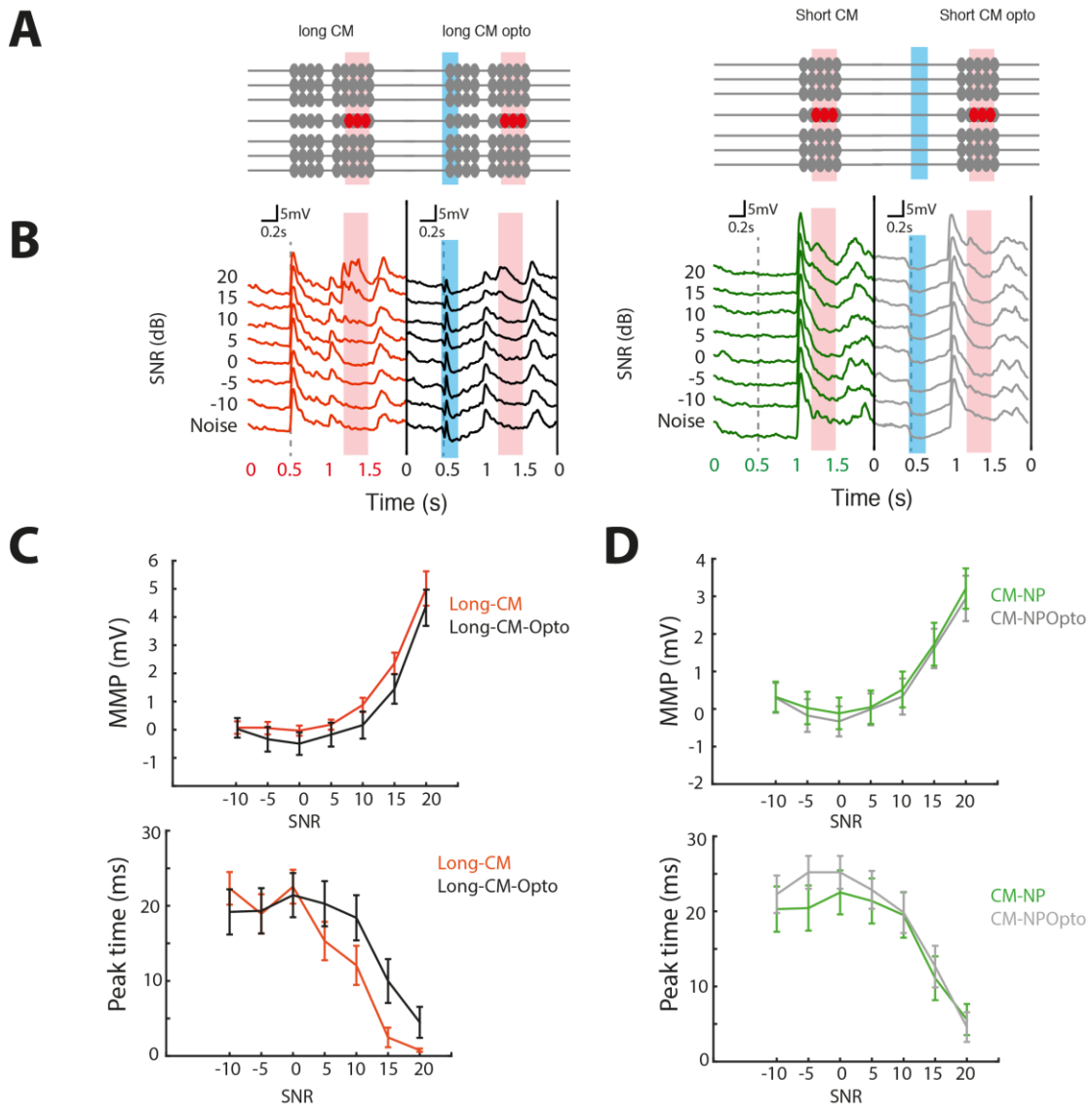

Figure 5.5

Evoked responses during cortical inactivation A Stimulus design: The role of A1 in the build-up of CMR was tested by inactivating AI during the early noise period (left), CM-Long; CM-long with A1 inactive during precursor. The blue bar indicates laser on. (Right) CM-short was also presented in order to confirm a similar responses to the CM-long opto condition. CM-short ;CM-long with A1 inactive during precursor. **B** Example cell, average responses (10 repeats) to each condition where the noise envelope was presented alone and in the presence of three tone pips at a number of different signal-to-noise ratios (SNR). Grey dashed lines indicate the beginning of the noise. Pink backgrounds indicate the tone presentation window and blue indicates laser stimulation period. **C** CM-long (top) Plot fo mean membrane potential (MMP) across SNR for each condition. (bottom) Plot of peak latency across SNR for each condition. **D** CM-short (top) Plot fo mean membrane potential (MMP) across SNR for each condition. (bottom) Plot of peak latency across SNR for each condition. **E** Histogram comparing mean threshold SNR across stimulus condition

6 GENERAL DISCUSSION & FUTURE WORK

6.1 Probing selectivity in sensory cortices

Auditory cortex plays a critical role in further integrating the spectral and temporal information it receives from subcortical nuclei (Linden & Schreiner, 2003; Volkov & Galazjuk, 1991). My main aim in chapter 3 was to acquire the basic receptive field properties of cortical neurons in the mouse. Previous research in AI describes receptive-field properties of neurons obtained by single/multi-unit recordings in anaesthetized or awake animals. The limitations to this approach, as previously mentioned, are uncertainties regarding the class of cell that is firing and its underlying synaptic activity. In this regard very little is known about auditory cortical responses in the mouse. The work in this thesis identified and confirmed interesting trends regarding frequency responses and how cells respond to their cessation (onset and offset responses) in the anaesthetised mouse. In summary: subthreshold receptive fields were broad, sometimes with bandwidths of 4 octaves. Onset responses were more frequency selective than offset responses. Even though onset and offset suprathreshold bandwidths were similar, EPSP dynamics were not; with onset evoked EPSPs peak amplitude and latency were larger and faster respectively. I also confirmed that frequency tuning of both Onset and Offset responses is complex, where a majority of neurons exhibited mismatches between onset and offset CF tuning. This complexity most likely occurred as a result of the heterogeneous shapes of frequency response areas in both onset and offset responses Although preliminary, my data suggests that there could be functional differences between IB and RS cells in the mouse AI, however more experiments must be carried out to establish these trends.

All in all, these recordings represent a narrow spectrum of what would be a full characterisation of the type of stimulus information auditory cortical neurons can encode. Although non-homogeneous there appear to be representations of binaurality (Middlebrooks et al., 1980), intensity information (D. Phillips et al., 1994; Polley et al., 2007), gradients for sharpness of tuning (Read et al., 2001) and response timing (Cheung et al., 2001). Therefore by expanding the stimuli presented to neurons it may be possible to identify more precisely the exact transformations that auditory cortex performs. Furthermore the utilisation of the patch clamp technique in these set of experiments allowed for partial characterisation of neuronal

responses to simple tonal stimuli in AI. Although insightful, determining cell class based solely on its electrophysiological profile is insufficient. Therefore a simple addition to the experimental design would be to add Biocytin and recover the recorded cells morphology. This would enable more accurate identification of cell type and depth, and hence the role those individual units might play in overall network function. However presenting all of these stimuli whilst maintaining cellular viability would be quite challenging. Therefore less invasive and long-term recordings must be employed. Two-photon calcium imaging, offers the best means to further our understanding, as the dynamics of calcium indicators and ability to record at deeper cortical locations is being constantly improved.

6.2 High throughput approaches for identifying functional and anatomical correlates

The gross viral labelling technique identified interesting synaptic distributions of thalamic inputs onto cortical cells. Irrespective of cell class, the data presented in this thesis would suggest that these synapses cluster on distal dendrites. Furthermore I was also able to establish two distinct morphological classes, where there appear to be interesting trends regarding subtle differences in synaptic clustering. However as previously mentioned there are several drawbacks; such as isolating neuronal processes to individual cells, overestimating viral incubation which can result in cellular debris that interferes with puncta detection and false positives. The very strict criteria I employed to avoid these inherent issues, though lead to a smaller dataset and potential underestimation of 'true puncta'. By carrying out further experiments using the same methodology it will be possible to increase the size of the dataset and test the validity of my observations. This would enable one to generate interesting hypotheses such as; does the non-uniformal distribution of thalamic input across cortical layers yield distinct synaptic distributions? And do those synaptic distributions vary between cell classes within those layers? Furthermore by applying post-hoc immunhisotchemical labelling (PV, SOM, CR, CCK and VIP) it may be possible to increase the repertoire and serve as an affirmation of neuronal classes beyond morphological inspection (X. Xu et al., 2010).

How these interesting synaptic distributions from thalamus contribute to receptive-field properties of neurons remains elusive. The mGRASP technique doesn't necessarily tell you how a particular input contributes to integration; it does offer useful insight from which one can make inferences. I approached this problem by

marrying mGRASP with single-unit recordings by applying the *in vivo* whole cell transfection technique for the first time in the mouse. Although an extremely low yield technique, I proved that by adjusting certain parameters it is possible to recover the synaptic map and receptive field of a neuron in 1 in every 4 experiments. I attempted to identify what aspect of the technique prevented any further increase in yield by performing two-photon guided patch clamp experiments with Alex-Fluor 594 on anaesthetised mice. I confirmed that neuronal death did not occur immediately after recordings even with rapid retrieval of the patch pipette, as neuronal morphologies were visible for up to 30 minutes (Figure 6.1). This would suggest that neural death occurs as a result of long-term damage, possibly as a result of ionic imbalance or lipid peroxidation (Lu et al., 2002).

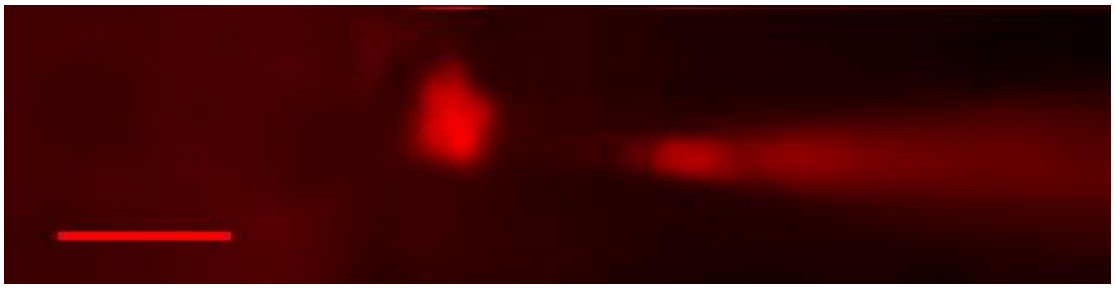

Figure 6.1

Two-photon guided patch. Neuron located in auditory cortex visualised using Alex Fluor 594. The image is taken after pull off, with the cell still visible after 20 minutes. This would suggest that the membrane was no ruptured during the patching and pull off process (scale = 15µm).

It would appear that the best strategy involves performing the gross viral labelling method first followed, by two-photon guided patch clamp recordings. By selecting spatially distinct neurons it could be possible to retrieve receptive fields and then correlate them to post-hoc imaging of their synaptic maps. Alternatively, one could inject each respective virus in MGB and AI replace patch clamp recordings with calcium imaging and using juxta-cellular labelling identify recorded neurons post hoc. Beyond identifying thalamic inputs it would be of great interest to segregate the type of synaptic input further and identify which inputs the most prominent. By using specific cre mouse lines it could be possible to express the pre portion of the virus in certain neuronal cell classes, such as SOM or PV interneurons, and then quantify their synaptic contributions and correlate them potential functional implications.

6.3 Identifying and deciphering cortical circuits involved in across channel CMR

In chapter 5 I confirmed a physiological correlate of CMR at the level of primary auditory cortex. Furthermore this correlate can only be accounted for through *across-channel* effects. By cortically silencing via laser stimulating PV cells expressing ChR2, it is possible to identify if this correlate of CMR at the level of cortex is merely occurs as a result of passive inheritance. My data indicates that there is an increase in threshold when cortex is silenced. However the trend just falls short of significance, therefore it is necessary to perform more experiments in order to confirm if cortex definitively contributes. The next obvious question is how cortex contributes. Assuming that auditory cortex augments an inherited precortical effect, as my results suggest, one possible mechanism that it could rely on, is stream segregation. Stream segregation, although a vaguely understood concept most likely involves complex feed forward and other inhibitory mechanisms. Therefore it may be possible to silence or enhance inhibitory circuits in cortex and identify if the action of certain inhibitory circuits are responsible or not. This can only be achieved by selectively transfecting specific inhibitory neuronal classes such as SOM and PV with ArchT or ChR2, in order to perturb the circuit and monitor the resulting activity. Furthermore most CMR studies have been restricted to Extracellular recordings. Whole cell recordings provide us with a potentially unique insight into the type of neurons that encode CMR, an aspect due to time constraints, not explored in this thesis. Of the auditory evoked recordings (n=80), 32 (dataset in chapter 5) were classed as having significant responses to CMR. This could suggest that certain subtypes/classes of neuron are recruited into a specific circuit involved in CMR. To test this hypothesis it would be necessary to identify morphological and electrophysiological properties of recorded neurons and directly compare them to CMR response profiles. By combining these two approaches it may be possible to begin building perceptual circuits.

7 Bibliography:

Abeles, M., & Goldstein, M. H. (1972). Responses of single units in the primary auditory cortex of the cat to tones and to tone pairs. *Brain research, 42*(2), 337-352.

Andersen, R. A., Knight, P. L., & Merzenich, M. M. (1980). The thalamocortical and corticothalamic conections of AI, AII, and the anteriior auditory field (AFF) in the cat: Evidence ofr two largely sergregarted systems of connections. *Journal of Comparative Neurology, 194*(3), 663-701.

Arnott, R. H., Wallace, M. N., Shackleton, T. M., & Palmer, A. R. (2004). Onset neurones in the anteroventral cochlear nucleus project to the dorsal cochlear nucleus. *Journal of the Association for Research in Otolaryngology, 5*(2), 153-170.

Atencio, C. A., Sharpee, T. O., & Schreiner, C. E. (2012). Receptive field dimensionality increases from the auditory midbrain to cortex. *Journal of neurophysiology, 107*(10), 2594-2603.

Bacon, S. P., Fay, R. R., & Popper, A. N. (2004). *Compression: from cochlea to cochlear implants*: Springer.

Bandyopadhyay, S., Shamma, S. A., & Kanold, P. O. (2010). Dichotomy of functional organization in the mouse auditory cortex. *Nature neuroscience, 13*(3), 361-368.

Bar-Yosef, O., & Nelken, I. (2007). The effects of background noise on the neural responses to natural sounds in cat primary auditory cortex. *Frontiers in Computational Neuroscience, 1*, 3.

Bartlett, E. L., Sadagopan, S., & Wang, X. (2011). Fine frequency tuning in monkey auditory cortex and thalamus. *Journal of neurophysiology, 106*(2), 849-859.

Bartlett, E. L., & Smith, P. H. (1999). Anatomic, intrinsic, and synaptic properties of dorsal and ventral division neurons in rat medial geniculate body. *Journal of neurophysiology, 81*(5).

Baumgarte, F. (1997). *A physiological ear model for auditory masking applicable to perceptual coding.* Paper presented at the Audio Engineering Society Convention 103.

Benavides-Piccione, R., Hamzei-Sichani, F., Ballesteros-Yáñez, I., DeFelipe, J., & Yuste, R. (2006). Dendritic size of pyramidal neurons differs among mouse cortical regions. *Cerebral cortex, 16*(7), 990-1001.

Binzegger, T., Douglas, R. J., & Martin, K. A. (2004). A quantitative map of the circuit of cat primary visual cortex. *The Journal of Neuroscience, 24*(39), 8441-8453.

Bizley, J. K., & Cohen, Y. E. (2013). The what, where and how of auditory-object perception. *Nature Reviews Neuroscience, 14*(10), 693-707.

Bizley, J. K., Nodal, F. R., Nelken, I., & King, A. J. (2005). Functional organization of ferret auditory cortex. *Cerebral cortex, 15*(10), 1637-1653.

Blackburn, C. C., & Sachs, M. B. (1990). The representations of the steady-state vowel sound/e/in the discharge patterns of cat anteroventral cochlear nucleus neurons. *Journal of neurophysiology, 63*(5), 1191-1212.

Bock, D. D., Lee, W.-C. A., Kerlin, A. M., Andermann, M. L., Hood, G., Wetzel, A. W., . . . Reid, R. C. (2011). Network anatomy and in vivo physiology of visual cortical neurons. *Nature, 471*(7337), 177-182.

Boudreau, J. C., & Tsuchitani, C. (1969). Cat superior olive S-segment cell discharge to tonal stimulation. *Contributions to sensory physiology, 4*, 143-213.

Boyden, E. S., Zhang, F., Bamberg, E., Nagel, G., & Deisseroth, K. (2005). Millisecond-timescale, genetically targeted optical control of neural activity. *Nature neuroscience, 8*(9), 1263-1268.

Braitenberg, V., & Schüz, A. (2013). *Cortex: statistics and geometry of neuronal connectivity*: Springer Science & Business Media.

Branco, T., Clark, B. A., & Häusser, M. (2010). Dendritic discrimination of temporal input sequences in cortical neurons. *Science, 329*(5999), 1671-1675.

Brand, A., Urban, R., & Grothe, B. (2000). Duration tuning in the mouse auditory midbrain. *Journal of neurophysiology, 84*(4), 1790-1799.

Brawer, J. R., Morest, D. K., & Kane, E. C. (1974). The neuronal architecture of the cochlear nucleus of the cat. *Journal of Comparative Neurology, 155*(3), 251-299.

Bregman, A. S. (1994). *Auditory scene analysis: The perceptual organization of sound*: MIT press.

Brodmann, K. (1909). Vergleichende Lokalisationslehre der Gro hirnrinde.

Brown, S. P., & Hestrin, S. (2009). Intracortical circuits of pyramidal neurons reflect their long-range axonal targets. *Nature, 457*(7233), 1133-1136.

Burton, H., & Jones, E. (1976). The posterior thalamic region and its cortical projection in New World and Old World monkeys. *Journal of Comparative Neurology, 168*(2), 249-301.

Buss, E., Grose, J. H., & Hall III, J. W. (2009). Features of across-frequency envelope coherence critical for comodulation masking release. *The Journal of the Acoustical Society of America, 126*(5), 2455-2466.

Buus, S. (1985). Release from masking caused by envelope fluctuations. *J. Acoust. Soc. Am, 78*(6), 1958-1965.

Calford, M., & Semple, M. (1995). Monaural inhibition in cat auditory cortex. *Journal of neurophysiology, 73*(5), 1876-1891.

Calford, M., & Webster, W. (1981). Auditory representation within principal division of cat medial geniculate body: an electrophysiological study. *Journal of neurophysiology, 45*(6), 1013-1028.

Calford, M. B., Webster, W. R., & Semple, M. M. (1983). Measurement of frequency selectivity of single neurons in the central auditory pathway. *Hearing research, 11*(3), 395-401.

Callaway, E. M. (1998). Local circuits in primary visual cortex of the macaque monkey. *Annual review of neuroscience, 21*(1), 47-74.

Campbell, A. W. (1905). *Histological studies on the localisation of cerebral function*: University Press.

Cardin, J. A., Carlén, M., Meletis, K., Knoblich, U., Zhang, F., Deisseroth, K., . . . Moore, C. I. (2009). Driving fast-spiking cells induces gamma rhythm and controls sensory responses. *Nature, 459*(7247), 663-667.

Cardin, J. A., Carlén, M., Meletis, K., Knoblich, U., Zhang, F., Deisseroth, K., . . . Moore, C. I. (2010). Targeted optogenetic stimulation and recording of

neurons in vivo using cell-type-specific expression of Channelrhodopsin-2. *Nature protocols, 5*(2), 247-254.
Castro, J. B., & Kandler, K. (2010). Changing tune in auditory cortex. *Nature neuroscience, 13*(3), 271.
Chadderton, P., Schaefer, A. T., Williams, S. R., & Margrie, T. W. (2014). Sensory-evoked synaptic integration in cerebellar and cerebral cortical neurons. *Nature Reviews Neuroscience, 15*(2), 71-83.
Chechik, G., Anderson, M. J., Bar-Yosef, O., Young, E. D., Tishby, N., & Nelken, I. (2006). Reduction of information redundancy in the ascending auditory pathway. *Neuron, 51*(3), 359-368.
Chen, X., Leischner, U., Rochefort, N. L., Nelken, I., & Konnerth, A. (2011). Functional mapping of single spines in cortical neurons in vivo. *Nature, 475*(7357), 501-505.
Cheung, S. W., Bedenbaugh, P. H., Nagarajan, S. S., & Schreiner, C. E. (2001). Functional organization of squirrel monkey primary auditory cortex: responses to pure tones. *Journal of neurophysiology, 85*(4), 1732-1749.
Chi, T., Ru, P., & Shamma, S. A. (2005). Multiresolution spectrotemporal analysis of complex sounds. *The Journal of the Acoustical Society of America, 118*(2), 887-906.
Christopher deCharms, R., Blake, D. T., & Merzenich, M. M. (1998). Optimizing sound features for cortical neurons. *Science, 280*(5368), 1439-1444.
Clarke, S., Bellmann, A., Meuli, R. A., Assal, G., & Steck, A. J. (2000). Auditory agnosia and auditory spatial deficits following left hemispheric lesions: evidence for distinct processing pathways. *Neuropsychologia, 38*(6), 797-807.
Code, R. A., & Winer, J. A. (1985). Commissural neurons in layer III of cat primary auditory cortex (AI): Pyramidal and non‐pyramidal cell input. *Journal of Comparative Neurology, 242*(4), 485-510.
Cohen, M. F. (1991). Comodulation masking release over a three octave range. *The Journal of the Acoustical Society of America, 90*(3), 1381-1384.
Colwell, S. A. (1977). *Corticothalamic Projections from Physiologically Defined Loci Within Primary Auditory Cortex in the Cat: Reciprocal Structure in the Medial*: University Microfilms.
Constantinople, C. M., & Bruno, R. M. (2013). Deep cortical layers are activated directly by thalamus. *Science, 340*(6140), 1591-1594.
Crawford, A., & Fettiplace, R. (1980). The frequency selectivity of auditory nerve fibres and hair cells in the cochlea of the turtle. *The Journal of physiology, 306*(1), 79-125.
Creutzfeldt, O., Hellweg, F.-C., & Schreiner, C. (1980). Thalamocortical transformation of responses to complex auditory stimuli. *Experimental brain research, 39*(1), 87-104.
Dau, T., Ewert, S., & Oxenham, A. (2004). Auditory signal processing: physiology, psychoacoustics, and models.
Dau, T., Ewert, S., & Oxenham, A. J. (2009). Auditory stream formation affects comodulation masking release retroactivelya). *The Journal of the Acoustical Society of America, 125*(4), 2182-2188.
Davis, K. A. (2005). Contralateral effects and binaural interactions in dorsal cochlear nucleus. *Journal of the Association for Research in Otolaryngology, 6*(3), 280-296.

De Martino, F., Moerel, M., Ugurbil, K., Goebel, R., Yacoub, E., & Formisano, E. (2015). Frequency preference and attention effects across cortical depths in the human primary auditory cortex. *Proceedings of the National Academy of Sciences, 112*(52), 16036-16041.

de Ribaupierre, F., Goldstein, M. H., & Yeni-Komshian, G. (1972). Intracellular study of the cat's primary auditory cortex. *Brain research, 48*, 185-204.

Dean, C., & Dresbach, T. (2006). Neuroligins and neurexins: linking cell adhesion, synapse formation and cognitive function. *Trends in neurosciences, 29*(1), 21-29.

Dégenètais, E., Thierry, A.-M., Glowinski, J., & Gioanni, Y. (2002). Electrophysiological properties of pyramidal neurons in the rat prefrontal cortex: an in vivo intracellular recording study. *Cerebral cortex, 12*(1), 1-16.

Douglas, R. J., & Martin, K. A. (2004). Neuronal circuits of the neocortex. *Annu. Rev. Neurosci., 27*, 419-451.

Druckmann, S., Feng, L., Lee, B., Yook, C., Zhao, T., Magee, Jeffrey C., & Kim, J. (2014). Structured Synaptic Connectivity between Hippocampal Regions. *Neuron, 81*(3), 629-640. doi:http://dx.doi.org/10.1016/j.neuron.2013.11.026

Dubno, J. R., & Dirks, D. D. (1989). Auditory filter characteristics and consonant recognition for hearing‐impaired listeners. *The Journal of the Acoustical Society of America, 85*(4), 1666-1675.

Durlach, N. I. (1963). Equalization and Cancellation Theory of Binaural Masking‐Level Differences. *The Journal of the Acoustical Society of America, 35*(8), 1206-1218.

Eccles, J. C., Ito, M., & Szentágothai, J. (1967). The mossy fiber input into the cerebellar cortex and its inhibitory control by Golgi cells *The cerebellum as a neuronal machine* (pp. 116-155): Springer.

Eggermont, J. (1996). How homogeneous is cat primary auditory cortex? Evidence from simultaneous single-unit recordings. *Auditory Neuroscience, 2*(1), 79-+.

Erulkar, S. (1972). Comparative aspects of spatial localization of sound. *Physiological Reviews, 52*(1), 237-360.

Evans, E., & Whitfield, I. (1964). Classification of unit responses in the auditory cortex of the unanaesthetized and unrestrained cat. *The Journal of physiology, 171*(3), 476.

Fairless, R., Masius, H., Rohlmann, A., Heupel, K., Ahmad, M., Reissner, C., . . . Missler, M. (2008). Polarized targeting of neurexins to synapses is regulated by their C-terminal sequences. *The Journal of Neuroscience, 28*(48), 12969-12981.

Feinberg, E. H., VanHoven, M. K., Bendesky, A., Wang, G., Fetter, R. D., Shen, K., & Bargmann, C. I. (2008). GFP Reconstitution Across Synaptic Partners (GRASP) defines cell contacts and synapses in living nervous systems. *Neuron, 57*(3), 353-363.

Feldmeyer, D. (2015). Excitatory neuronal connectivity in the barrel cortex. *Wiring Principles of Cerebral Cortex*, 66.

Ferragamo, M. J., Golding, N. L., & Oertel, D. (1998). Synaptic inputs to stellate cells in the ventral cochlear nucleus. *Journal of neurophysiology, 79*(1), 51-63.

Ferster, D., & Jagadeesh, B. (1992). EPSP-IPSP interactions in cat visual cortex studied with in vivo whole-cell patch recording. *The Journal of Neuroscience, 12*(4), 1262-1274.

Fetcho, J. R., Cox, K. J., & O'Malley, D. M. (1998). Monitoring activity in neuronal populations with single-cell resolution in a behaving vertebrate. *The Histochemical journal, 30*(3), 153-167.

Fitzpatrick, D. (1996). The functional organization of local circuits in visual cortex: insights from the study of tree shrew striate cortex. *Cerebral cortex, 6*(3), 329-341.

Fletcher, H. (1940). Auditory patterns. *Reviews of modern physics, 12*(1), 47.

Fritz, J. B., Elhilali, M., & Shamma, S. A. (2005). Differential dynamic plasticity of A1 receptive fields during multiple spectral tasks. *The Journal of Neuroscience, 25*(33), 7623-7635.

Fuzessery, Z., & Hall, J. (1996). Role of GABA in shaping frequency tuning and creating FM sweep selectivity in the inferior colliculus. *Journal of neurophysiology, 76*(2), 1059-1073.

Gaese, B. H., & Ostwald, J. (2001). Anesthesia changes frequency tuning of neurons in the rat primary auditory cortex. *Journal of neurophysiology, 86*(2), 1062-1066.

Galambos, R., & Davis, H. (1943). The response of single auditory-nerve fibers to acoustic stimulation. *Journal of neurophysiology, 6*(1), 39-57.

Games, K. D., & Winer, J. A. (1988). Layer V in rat auditory cortex: projections to the inferior colliculus and contralateral cortex. *Hearing research, 34*(1), 1-25.

Gao, W. J., & Zheng, Z. H. (2004). Target‐specific differences in somatodendritic morphology of layer V pyramidal neurons in rat motor cortex. *Journal of Comparative Neurology, 476*(2), 174-185.

Gasparini, S., & Magee, J. C. (2006). State-dependent dendritic computation in hippocampal CA1 pyramidal neurons. *The Journal of Neuroscience, 26*(7), 2088-2100.

Gilbert, C. D., & Wiesel, T. N. (1979). Morphology and intracortical projections of functionally characterised neurones in the cat visual cortex. *Nature, 280*(5718), 120-125.

Glasberg, B. R., & Moore, B. C. (1990). Derivation of auditory filter shapes from notched-noise data. *Hearing research, 47*(1-2), 103-138.

Golding, N. L., Ferragamo, M. J., & Oertel, D. (1999). Role of intrinsic conductances underlying responses to transients in octopus cells of the cochlear nucleus. *The Journal of Neuroscience, 19*(8), 2897-2905.

Grose, J. H., Buss, E., & Hall III, J. W. (2009). Within-and across-channel factors in the multiband comodulation masking release paradigm. *The Journal of the Acoustical Society of America, 125*(1), 282-293.

Grose, J. H., & Hall III, J. W. (1993). Comodulation masking release: Is comodulation sufficient? a). *The Journal of the Acoustical Society of America, 93*(5), 2896-2902.

Grose, J. H., Hall III, J. W., Buss, E., & Hatch, D. R. (2005). Detection of spectrally complex signals in comodulated maskers: Effect of temporal fringe. *The Journal of the Acoustical Society of America, 118*(6), 3774-3782.

Grutzendler, J., Kasthuri, N., & Gan, W.-B. (2002). Long-term dendritic spine stability in the adult cortex. *Nature, 420*(6917), 812-816.

Hall III, J. W., & Grose, J. H. (1988). Comodulation masking release: Evidence for multiple cues. *The Journal of the Acoustical Society of America, 84*(5), 1669-1675.

Hall, J. W., Haggard, M. P., & Fernandes, M. A. (1984). Detection in noise by spectro‐temporal pattern analysis. *The Journal of the Acoustical Society of America, 76*(1), 50-56.

Hamill, O. P., Marty, A., Neher, E., Sakmann, B., & Sigworth, F. (1981). Improved patch-clamp techniques for high-resolution current recording from cells and cell-free membrane patches. *Pflügers Archiv, 391*(2), 85-100.

Harvey, C. D., & Svoboda, K. (2007). Locally dynamic synaptic learning rules in pyramidal neuron dendrites. *Nature, 450*(7173), 1195-1200.

Hatch, D. R., Arné, B. C., & Hall III, J. W. (1995). Comodulation masking release (CMR): Effects of gating as a function of number of flanking bands and masker bandwidth. *The Journal of the Acoustical Society of America, 97*(6), 3768-3774.

Hattox, A. M., & Nelson, S. B. (2007). Layer V neurons in mouse cortex projecting to different targets have distinct physiological properties. *Journal of neurophysiology, 98*(6), 3330-3340.

He, J., Hashikawa, T., Ojima, H., & Kinouchi, Y. (1997). Temporal integration and duration tuning in the dorsal zone of cat auditory cortex. *The Journal of Neuroscience, 17*(7), 2615-2625.

Heffner, H. E., & Heffner, R. S. (1986). Hearing loss in Japanese macaques following bilateral auditory cortex lesions. *Journal of neurophysiology, 55*(2), 256-271.

Heil, P. (1997). Auditory cortical onset responses revisited. II. Response strength. *Journal of neurophysiology, 77*(5), 2642-2660.

Heil, P., Rajan, R., & Irvine, D. R. (1992). Sensitivity of neurons in cat primary auditory cortex to tones and frequency-modulated stimuli. II: Organization of response properties along the 'isofrequency'dimension. *Hearing research, 63*(1), 135-156.

Herkenham, M. (1986). New perspectives on the organization and evolution of nonspecific thalamocortical projections *Sensory-Motor Areas and Aspects of Cortical Connectivity* (pp. 403-445): Springer.

Hirsch, J. A., & Martinez, L. M. (2006). Circuits that build visual cortical receptive fields. *Trends in neurosciences, 29*(1), 30-39.

Hoffmann, S., Firzlaff, U., Radtke-Schuller, S., Schwellnus, B., & Schuller, G. (2008). The auditory cortex of the bat Phyllostomus discolor: Localization and organization of basic response properties. *BMC neuroscience, 9*(1), 65.

Hudspeth, A. (2008). Making an effort to listen: mechanical amplification in the ear. *Neuron, 59*(4), 530-545.

Imaizumi, K., Priebe, N. J., Crum, P. A., Bedenbaugh, P. H., Cheung, S. W., & Schreiner, C. E. (2004). Modular functional organization of cat anterior auditory field. *Journal of neurophysiology, 92*(1), 444-457.

Issa, J. B., Haeffele, B. D., Agarwal, A., Bergles, D. E., Young, E. D., & Yue, D. T. (2014). Multiscale optical Ca 2+ imaging of tonal organization in mouse auditory cortex. *Neuron, 83*(4), 944-959.

Jack, J. J. B., Noble, D., & Tsien, R. W. (1975). *Electric current flow in excitable cells*: Clarendon Press Oxford.

Jean‐Baptiste, M., & Morest, D. K. (1975). Transneuronal changes of synaptic endings and nuclear chromatin in the trapezoid body following cochlear ablations in cats. *Journal of Comparative Neurology, 162*(1), 111-133.

Ji, X.-y., Zingg, B., Mesik, L., Xiao, Z., Zhang, L. I., & Tao, H. W. (2015). Thalamocortical innervation pattern in mouse auditory and visual cortex: laminar and cell-type specificity. *Cerebral cortex*, bhv099.

Jiang, D., Palmer, A. R., & Winter, I. (1996). Frequency extent of two-tone facilitation in onset units in the ventral cochlear nucleus. *Journal of neurophysiology, 75*(1), 380-395.

Joachimsthaler, B., Uhlmann, M., Miller, F., Ehret, G., & Kurt, S. (2014). Quantitative analysis of neuronal response properties in primary and higher‐order auditory cortical fields of awake house mice (Mus musculus). *European Journal of Neuroscience, 39*(6), 904-918.

Jones, E. (1981). Functional subdivision and synaptic organization of the mammalian thalamus. *International review of physiology, 25*, 173.

Joris, P., Schreiner, C., & Rees, A. (2004). Neural processing of amplitude-modulated sounds. *Physiological Reviews, 84*(2), 541-577.

Kaas, J. H. (2011). The evolution of auditory cortex: the core areas *The auditory cortex* (pp. 407-427): Springer.

Kaas, J. H., & Hackett, T. A. (2000). Subdivisions of auditory cortex and processing streams in primates. *Proceedings of the National Academy of Sciences, 97*(22), 11793-11799.

Kaas, J. H., Hackett, T. A., & Tramo, M. J. (1999). Auditory processing in primate cerebral cortex. *Current opinion in neurobiology, 9*(2), 164-170.

Kagan, I., Gur, M., & Snodderly, D. M. (2002). Spatial organization of receptive fields of V1 neurons of alert monkeys: comparison with responses to gratings. *Journal of neurophysiology, 88*(5), 2557-2574.

Kamondi, A., Acsády, L., & Buzsáki, G. (1998). Dendritic spikes are enhanced by cooperative network activity in the intact hippocampus. *The Journal of Neuroscience, 18*(10), 3919-3928.

Kaur, S., Lazar, R., & Metherate, R. (2004). Intracortical pathways determine breadth of subthreshold frequency receptive fields in primary auditory cortex. *Journal of neurophysiology, 91*(6), 2551-2567.

Kayser, C., Petkov, C. I., & Logothetis, N. K. (2007). Tuning to sound frequency in auditory field potentials. *Journal of neurophysiology, 98*(3), 1806-1809.

Kemper, T., & Galaburda, A. (1984). Principles of cytoarchitectonics. *Cerebral cortex, 1*, 35-57.

Kim, J., Zhao, T., Petralia, R. S., Yu, Y., Peng, H., Myers, E., & Magee, J. C. (2012). mGRASP enables mapping mammalian synaptic connectivity with light microscopy. *Nat Meth, 9*(1), 96-102. doi:10.1038/nmeth.1784

http://www.nature.com/nmeth/journal/v9/n1/abs/nmeth.1784.html - supplementary-information

Kimura, A., Donishi, T., Sakoda, T., Hazama, M., & Tamai, Y. (2003). Auditory thalamic nuclei projections to the temporal cortex in the rat. *Neuroscience, 117*(4), 1003-1016.

Kimura, M., & Eggermont, J. J. (1999). Effects of acute pure tone induced hearing loss on response properties in three auditory cortical fields in cat. *Hearing research, 135*(1), 146-162.

King, A. J., Bajo, V. M., Bizley, J. K., Campbell, R. A., Nodal, F. R., Schulz, A. L., & Schnupp, J. W. (2007). Physiological and behavioral studies of spatial coding in the auditory cortex. *Hearing research, 229*(1), 106-115.

King, A. J., & Nelken, I. (2009). Unraveling the principles of auditory cortical processing: can we learn from the visual system? *Nature neuroscience, 12*(6), 698-701.

Kitzes, L., & Doherty, D. (1994). Influence of callosal activity on units in the auditory cortex of ferret (Mustela putorius). *Journal of neurophysiology, 71*(5), 1740-1751.

Kleindienst, T., Winnubst, J., Roth-Alpermann, C., Bonhoeffer, T., & Lohmann, C. (2011). Activity-dependent clustering of functional synaptic inputs on developing hippocampal dendrites. *Neuron, 72*(6), 1012-1024.

Klumpp, R. G., & Eady, H. R. (1956). Some Measurements of Interaural Time Difference Thresholds. *The Journal of the Acoustical Society of America, 28*(5), 859-860. doi:doi:http://dx.doi.org/10.1121/1.1908493

Koay, G., Heffner, R. S., & Heffner, H. E. (2002). Behavioral audiograms of homozygous med J mutant mice with sodium channel deficiency and unaffected controls. *Hearing research, 171*(1), 111-118.

Kozlov, A. S., & Gentner, T. Q. (2014). Central auditory neurons display flexible feature recombination functions. *Journal of neurophysiology, 111*(6), 1183-1189.

Le Bé, J.-V., Silberberg, G., Wang, Y., & Markram, H. (2007). Morphological, electrophysiological, and synaptic properties of corticocallosal pyramidal cells in the neonatal rat neocortex. *Cerebral cortex, 17*(9), 2204-2213.

LeDoux, J. E., Ruggiero, D. A., & Reis, D. (1985). Projections to the subcortical forebrain from anatomically defined regions of the medial geniculate body in the rat. *Journal of Comparative Neurology, 242*(2), 182-213.

Lee, C. C., & Winer, J. A. (2011). Convergence of thalamic and cortical pathways in cat auditory cortex. *Hearing research, 274*(1), 85-94.

Li, X., Gutierrez, D. V., Hanson, M. G., Han, J., Mark, M. D., Chiel, H., . . . Herlitze, S. (2005). Fast noninvasive activation and inhibition of neural and network activity by vertebrate rhodopsin and green algae channelrhodopsin. *Proceedings of the National Academy of Sciences of the United States of America, 102*(49), 17816-17821.

Li, Y., Lu, H., Cheng, P.-l., Ge, S., Xu, H., Shi, S.-H., & Dan, Y. (2012). Clonally related visual cortical neurons show similar stimulus feature selectivity. *Nature, 486*(7401), 118-121.

Liberman, M. C. (1982). The cochlear frequency map for the cat: Labeling auditory‐nerve fibers of known characteristic frequency. *The Journal of the Acoustical Society of America, 72*(5), 1441-1449.

Liberman, M. C., Gao, J., He, D. Z., Wu, X., Jia, S., & Zuo, J. (2002). Prestin is required for electromotility of the outer hair cell and for the cochlear amplifier. *Nature, 419*(6904), 300-304.

Linden, J. F., & Schreiner, C. E. (2003). Columnar transformations in auditory cortex? A comparison to visual and somatosensory cortices. *Cerebral cortex, 13*(1), 83-89.

Logothetis, N. K., & Wandell, B. A. (2004). Interpreting the BOLD signal. *Annu. Rev. Physiol., 66*, 735-769.

London, M., & Häusser, M. (2005). Dendritic computation. *Annu. Rev. Neurosci., 28*, 503-532.

LORENTE, D. (1949). Cerebral cortex: architecture, intracortical connections, motor projections. In." Physiology of the Nervous System: London: Oxford University Press.

Lorente, d. N. (1947). A study of nerve physiology. *Studies from the Rockefeller institute for medical research. Reprints. Rockefeller Institute for Medical Research, 131*, 1.

Losonczy, A., Makara, J. K., & Magee, J. C. (2008). Compartmentalized dendritic plasticity and input feature storage in neurons. *Nature, 452*(7186), 436-441.

Lu, C., Chan, S. L., Fu, W., & Mattson, M. P. (2002). The lipid peroxidation product 4-hydroxynonenal facilitates opening of voltage-dependent Ca2+ channels in neurons by increasing protein tyrosine phosphorylation. *Journal of Biological Chemistry, 277*(27), 24368-24375.

Lund, J., Henry, G., MacQueen, C., & Harvey, A. (1979). Anatomical organization of the primary visual cortex (area 17) of the cat. A comparison with area 17 of the macaque monkey. *Journal of Comparative Neurology, 184*(4), 599-618.

Machens, C. K., Wehr, M. S., & Zador, A. M. (2004). Linearity of cortical receptive fields measured with natural sounds. *The Journal of Neuroscience, 24*(5), 1089-1100.

Mainen, Z. F., Carnevale, N. T., Zador, A. M., Claiborne, B. J., & Brown, T. H. (1996). Electrotonic architecture of hippocampal CA1 pyramidal neurons based on three-dimensional reconstructions. *Journal of neurophysiology, 76*(3), 1904-1923.

Makino, H., & Malinow, R. (2011). Compartmentalized versus global synaptic plasticity on dendrites controlled by experience. *Neuron, 72*(6), 1001-1011.

Margrie, T. W., Brecht, M., & Sakmann, B. (2002). In vivo, low-resistance, whole-cell recordings from neurons in the anaesthetized and awake mammalian brain. *Pflügers Archiv, 444*(4), 491-498.

Masterton, B., Thompson, G. C., Bechtold, J. K., & RoBards, M. J. (1975). Neuroanatomical basis of binaural phase-difference analysis for sound localization: a comparative study. *Journal of comparative and physiological psychology, 89*(5), 379.

Matsubara, J. A., & Phillips, D. (1988). Intracortical connections and their physiological correlates in the primary auditory cortex (AI) of the cat. *Journal of Comparative Neurology, 268*(1), 38-48.

McBride, T. J., Rodriguez-Contreras, A., Trinh, A., Bailey, R., & DeBello, W. M. (2008). Learning drives differential clustering of axodendritic contacts in the barn owl auditory system. *The Journal of Neuroscience, 28*(27), 6960-6973.

McDermott, J. H., Schemitsch, M., & Simoncelli, E. P. (2013). Summary statistics in auditory perception. *Nature neuroscience, 16*(4), 493-498.

McFadden, D., & Wright, B. A. (1990). Temporal decline of masking and comodulation detection differences. *The Journal of the Acoustical Society of America, 88*(2), 711-724.

McFadden, D., & Wright, B. A. (1992). Temporal decline of masking and comodulation masking release. *The Journal of the Acoustical Society of America, 92*(1), 144-156.

Megıas, M., Emri, Z., Freund, T., & Gulyas, A. (2001). Total number and distribution of inhibitory and excitatory synapses on hippocampal CA1 pyramidal cells. *Neuroscience, 102*(3), 527-540.

Merzenich, M. M., Colwell, S. A., & Andersen, R. A. (1982). Auditory forebrain organization *Cortical sensory organization* (pp. 43-57): Springer.

Merzenich, M. M., Knight, P. L., & Roth, G. L. (1975). Representation of cochlea within primary auditory cortex in the cat. *Journal of neurophysiology, 38*(2), 231-249.

Meyer, G., Castañeyra-Perdomo, A., & Ferres-Torres, R. (1984). A type of apparently axonless granule cell in the cat auditory cortex. *Anatomy and embryology, 170*(3), 319-320.

Micheyl, C., Tian, B., Carlyon, R. P., & Rauschecker, J. P. (2005). Perceptual organization of tone sequences in the auditory cortex of awake macaques. *Neuron, 48*(1), 139-148.

Middlebrooks, J. C., Dykes, R. W., & Merzenich, M. M. (1980). Binaural response-specific bands in primary auditory cortex (AI) of the cat: topographical organization orthogonal to isofrequency contours. *Brain research, 181*(1), 31-48.

Miller, L. M., Escabı, M. A., & Schreiner, C. E. (2001). Feature selectivity and interneuronal cooperation in the thalamocortical system. *The Journal of Neuroscience, 21*(20), 8136-8144.

Mishchenko, Y., Hu, T., Spacek, J., Mendenhall, J., Harris, K. M., & Chklovskii, D. B. (2010). Ultrastructural analysis of hippocampal neuropil from the connectomics perspective. *Neuron, 67*(6), 1009-1020.

Mitani, A., Shimokouchi, M., Itoh, K., Nomura, S., Kudo, M., & Mizuno, N. (1985). Morphology and laminar organization of electrophysiologically identified neurons in the primary auditory cortex in the cat. *Journal of Comparative Neurology, 235*(4), 430-447.

Mitchell, S. J., & Silver, R. A. (2003). Shunting Inhibition Modulates Neuronal Gain during Synaptic Excitation. *Neuron, 38*(3), 433-445. doi:http://dx.doi.org/10.1016/S0896-6273(03)00200-9

Moore, A. K., & Wehr, M. (2013). Parvalbumin-Expressing Inhibitory Interneurons in Auditory Cortex Are Well-Tuned for Frequency. *The Journal of Neuroscience, 33*(34), 13713-13723. doi:10.1523/JNEUROSCI.0663-13.2013

Moore, B. C., & Glasberg, B. R. (1983). Suggested formulae for calculating auditory‐filter bandwidths and excitation patterns. *The Journal of the Acoustical Society of America, 74*(3), 750-753.

Moshitch, D., Las, L., Ulanovsky, N., Bar-Yosef, O., & Nelken, I. (2006). Responses of Neurons in Primary Auditory Cortex (A1) to Pure Tones in the Halothane-Anesthetized Cat. *Journal of neurophysiology, 95*(6), 3756-3769. doi:10.1152/jn.00822.2005

Nadol, J. B., Burgess, B. J., & Reisser, C. (1990). Morphometric analysis of normal human spiral ganglion cells. *Annals of Otology, Rhinology & Laryngology, 99*(5), 340-348.

Narayan, S. S., Temchin, A. N., Recio, A., & Ruggero, M. A. (1998). Frequency tuning of basilar membrane and auditory nerve fibers in the same cochleae. *Science, 282*(5395), 1882-1884.

Navlakha, S., Suhan, J., Barth, A. L., & Bar-Joseph, Z. (2013). A high-throughput framework to detect synapses in electron microscopy images. *Bioinformatics, 29*(13), i9-i17.

Neher, E., & Sakmann, B. (1992). The patch clamp technique. *Sci Am, 266*(3), 44-51.

Nelken, I., Fishbach, A., Las, L., Ulanovsky, N., & Farkas, D. (2003). Primary auditory cortex of cats: feature detection or something else? *Biological cybernetics, 89*(5), 397-406.

Nelken, I., Rotman, Y., & Yosef, O. B. (1999). Responses of auditory-cortex neurons to structural features of natural sounds. *Nature, 397*(6715), 154-157.

Nelken, I., & Ulanovsky, N. (2007). Mismatch negativity and stimulus-specific adaptation in animal models. *Journal of Psychophysiology, 21*(3-4), 214-223.

Niedermeyer, E., & da Silva, F. L. (2005). *Electroencephalography: basic principles, clinical applications, and related fields*: Lippincott Williams & Wilkins.

Niimi, K., & Kuwahara, E. (1973). The dorsal thalamus of the cat and comparison with monkey and man. *Journal für Hirnforschung, 14*(3), 303.

Niimi, K., & Matsuoka, H. (1979). Thalamocortical organization of the auditory system in the cat studied by retrograde axonal transport of horseradish peroxidase. *Advances in anatomy, embryology, and cell biology, 57*, 1.

Nobre, M. J., Sandner, G., & Brandão, M. L. (2003). Enhancement of acoustic evoked potentials and impairment of startle reflex induced by reduction of GABAergic control of the neural substrates of aversion in the inferior colliculus. *Hearing research, 184*(1), 82-90.

Noreña, A., & Eggermont, J. J. (2002). Comparison between local field potentials and unit cluster activity in primary auditory cortex and anterior auditory field in the cat. *Hearing research, 166*(1), 202-213.

Nowak, L. G., Azouz, R., Sanchez-Vives, M. V., Gray, C. M., & McCormick, D. A. (2003). Electrophysiological classes of cat primary visual cortical neurons in vivo as revealed by quantitative analyses. *Journal of neurophysiology, 89*(3), 1541-1566.

Osen, K. K. (1969). Cytoarchitecture of the cochlear nuclei in the cat. *Journal of Comparative Neurology, 136*(4), 453-483.

Ozen, S., Sirota, A., Belluscio, M. A., Anastassiou, C. A., Stark, E., Koch, C., & Buzsáki, G. (2010). Transcranial electric stimulation entrains cortical neuronal populations in rats. *The Journal of Neuroscience, 30*(34), 11476-11485.

Pandya, P. K., Rathbun, D. L., Moucha, R., Engineer, N. D., & Kilgard, M. P. (2008). Spectral and temporal processing in rat posterior auditory cortex. *Cerebral cortex, 18*(2), 301-314.

Pelleg-Toiba, R., & Wollberg, Z. (1989). Tuning properties of auditory cortex cells in the awake squirrel monkey. *Experimental brain research, 74*(2), 353-364.

Peters, A., & Feldman, M. L. (1976). The projection of the lateral geniculate nucleus to area 17 of the rat cerebral cortex. I. General description. *Journal of neurocytology, 5*(1), 63-84.

Petersen, C. C., & Crochet, S. (2013). Synaptic computation and sensory processing in neocortical layer 2/3. *Neuron, 78*(1), 28-48.

Pfeiffer, R. R., & Molnar, C. E. (1970). Cochlear nerve fiber discharge patterns: relationship to the cochlear microphonic. *Science, 167*(3925), 1614-1616.

Phillips, D., Semple, M., Calford, M., & Kitzes, L. (1994). Level-dependent representation of stimulus frequency in cat primary auditory cortex. *Experimental brain research, 102*(2), 210-226.

Phillips, D. P. (1995). Central auditory processing: a view from auditory neuroscience. *Otology & Neurotology, 16*(3), 338-352.

Poirazi, P., Brannon, T., & Mel, B. W. (2003). Pyramidal neuron as two-layer neural network. *Neuron, 37*(6), 989-999.

Polley, D. B., Read, H. L., Storace, D. A., & Merzenich, M. M. (2007). Multiparametric auditory receptive field organization across five cortical fields in the albino rat. *Journal of neurophysiology, 97*(5), 3621-3638.

Polley, D. B., Steinberg, E. E., & Merzenich, M. M. (2006). Perceptual learning directs auditory cortical map reorganization through top-down influences. *The Journal of Neuroscience, 26*(18), 4970-4982.

Pressnitzer, D., Meddis, R., Delahaye, R., & Winter, I. M. (2001). Physiological correlates of comodulation masking release in the mammalian ventral cochlear nucleus. *The Journal of Neuroscience, 21*(16), 6377-6386.

Prieto, J. J., Peterson, B. A., & Winer, J. A. (1994). Laminar distribution and neuronal targets of GABAergic axon terminals in cat primary auditory cortex (AI). *Journal of Comparative Neurology, 344*(3), 383-402.

Prieto, J. J., & Winer, J. A. (1999). Layer VI in cat primary auditory cortex: Golgi study and sublaminar origins of projection neurons. *Journal of Comparative Neurology, 404*(3), 332-358.

Qin, L., Chimoto, S., Sakai, M., Wang, J., & Sato, Y. (2007). Comparison Between Offset and Onset Responses of Primary Auditory Cortex on–off Neurons in Awake Cats. *Journal of neurophysiology, 97*(5), 3421-3431. doi:10.1152/jn.00184.2007

Rall, W. (1967). DISTINGUISHING THEORETICAL SYNAPTIC POTEN-TIALS COMPUTED FOR DIFFERENT SOMA-DEN-DRITIC DISTRIBUTIONS OF SYNAPTIC INPUT.

Rall, W., Burke, R., Smith, T., Nelson, P. G., & Frank, K. (1967). Dendritic location of synapses and possible mechanisms for the monosynaptic EPSP in motoneurons. *J. Neurophysiol, 30*(5), 884-915.

Rancz, E. A., Franks, K. M., Schwarz, M. K., Pichler, B., Schaefer, A. T., & Margrie, T. W. (2011). Transfection via whole-cell recording in vivo: bridging single-cell physiology, genetics and connectomics. *Nat Neurosci, 14*(4), 527-532. doi:http://www.nature.com/neuro/journal/v14/n4/abs/nn.2765.html - supplementary-information

Rauschecker, J. P., & Tian, B. (2000). Mechanisms and streams for processing of "what" and "where" in auditory cortex. *Proceedings of the National Academy of Sciences, 97*(22), 11800-11806.

Read, H. L., Winer, J. A., & Schreiner, C. E. (2001). Modular organization of intrinsic connections associated with spectral tuning in cat auditory

cortex. *Proceedings of the National Academy of Sciences, 98*(14), 8042-8047.

Recanzone, G. H., Guard, D. C., Phan, M. L., & Su, T.-I. K. (2000). Correlation between the activity of single auditory cortical neurons and sound-localization behavior in the macaque monkey. *Journal of neurophysiology, 83*(5), 2723-2739.

Rees, A., & Møller, A. R. (1983). Responses of neurons in the inferior colliculus of the rat to AM and FM tones. *Hearing research, 10*(3), 301-330.

Rhode, W. S., & Greenberg, S. (1994). Lateral suppression and inhibition in the cochlear nucleus of the cat. *Journal of neurophysiology, 71*(2), 493-514.

Ringach, D. L., Shapley, R. M., & Hawken, M. J. (2002). Orientation selectivity in macaque V1: diversity and laminar dependence. *The Journal of Neuroscience, 22*(13), 5639-5651.

Romanski, L. M., & LeDoux, J. E. (1993). Organization of rodent auditory cortex: anterograde transport of PHA-L from MGv to temporal neocortex. *Cerebral cortex, 3*(6), 499-514.

Rosenblith, W. A., & Stevens, K. N. (1953). On the DL for Frequency. *The Journal of the Acoustical Society of America, 25*(5), 980-985. doi:doi:http://dx.doi.org/10.1121/1.1907230

Rothschild, G., Nelken, I., & Mizrahi, A. (2010). Functional organization and population dynamics in the mouse primary auditory cortex. *Nature neuroscience, 13*(3), 353-360.

Russell, I., Richardson, G., & Cody, A. (1986). Mechanosensitivity of mammalian auditory hair cells in vitro.

Ryugo, D., & Fekete, D. (1982). Morphology of primary axosomatic endings in the anteroventral cochlear nucleus of the cat: a study of the endbulbs of Held. *Journal of Comparative Neurology, 210*(3), 239-257.

Sakata, S., & Harris, K. D. (2009). Laminar structure of spontaneous and sensory-evoked population activity in auditory cortex. *Neuron, 64*(3), 404-418.

Sakmann, B., & Neher, E. (1984). Patch clamp techniques for studying ionic channels in excitable membranes. *Annual review of physiology, 46*(1), 455-472.

Sando, I. (1965). The anatomical interrelationships of the cochlear nerve fibers. *Acta oto-laryngologica, 59*(2-6), 417-436.

Sarid, L., Bruno, R., Sakmann, B., Segev, I., & Feldmeyer, D. (2007). Modeling a layer 4-to-layer 2/3 module of a single column in rat neocortex: interweaving in vitro and in vivo experimental observations. *Proceedings of the National Academy of Sciences, 104*(41), 16353-16358.

Scanziani, M., & Häusser, M. (2009). Electrophysiology in the age of light. *Nature, 461*(7266), 930-939.

Schnupp, J. W., Hall, T. M., Kokelaar, R. F., & Ahmed, B. (2006). Plasticity of temporal pattern codes for vocalization stimuli in primary auditory cortex. *The Journal of Neuroscience, 26*(18), 4785-4795.

Scholl, B., Gao, X., & Wehr, M. (2010). Nonoverlapping sets of synapses drive on responses and off responses in auditory cortex. *Neuron, 65*(3), 412-421.

Schooneveldt, G. P., & Moore, B. C. (1987). Comodulation masking release (CMR): Effects of signal frequency, flanking‐band frequency, masker bandwidth, flanking‐band level, and monotic versus dichotic presentation of the

flanking band. *The Journal of the Acoustical Society of America, 82*(6), 1944-1956.
Schreiner, C. E. (1998). Spatial distribution of responses to simple and complex sounds in the primary auditory cortex. *Audiology and Neurotology, 3*(2-3), 104-122.
Schreiner, C. E., & Cynader, M. S. (1984). Basic functional organization of second auditory cortical field (AII) of the cat. *Journal of neurophysiology, 51*(6), 1284-1305.
Schreiner, C. E., & Sutter, M. L. (1992). Topography of excitatory bandwidth in cat primary auditory cortex: single-neuron versus multiple-neuron recordings. *Journal of neurophysiology, 68*(5), 1487-1502.
Schreiner, C. E., & Winer, J. A. (2007). Auditory cortex mapmaking: principles, projections, and plasticity. *Neuron, 56*(2), 356-365.
Schubert, D., Staiger, J. F., Cho, N., Kötter, R., Zilles, K., & Luhmann, H. J. (2001). Layer-specific intracolumnar and transcolumnar functional connectivity of layer V pyramidal cells in rat barrel cortex. *The Journal of Neuroscience, 21*(10), 3580-3592.
Scott, B. H., Malone, B. J., & Semple, M. N. (2011). Transformation of temporal processing across auditory cortex of awake macaques. *Journal of neurophysiology, 105*(2), 712-730.
Sherman, S., & Guillery, R. (2006). Exploring the thalamus and its role in cortical functioning: Academic Press, New York.
Sherman, S. M. (2007). The thalamus is more than just a relay. *Current opinion in neurobiology, 17*(4), 417-422.
Sivaramakrishnan, S., Sterbing-D'Angelo, S. J., Filipovic, B., D'Angelo, W. R., Oliver, D. L., & Kuwada, S. (2004). GABAA synapses shape neuronal responses to sound intensity in the inferior colliculus. *The Journal of Neuroscience, 24*(21), 5031-5043.
Smith, A. L., Parsons, C. H., Lanyon, R. G., Bizley, J. K., Akerman, C. J., Baker, G. E., . . . King, A. J. (2004). An investigation of the role of auditory cortex in sound localization using muscimol‐releasing Elvax. *European Journal of Neuroscience, 19*(11), 3059-3072.
Smith, P. H., & Rhode, W. S. (1989). Structural and functional properties distinguish two types of multipolar cells in the ventral cochlear nucleus. *Journal of Comparative Neurology, 282*(4), 595-616.
Sollini, J., Morris, A., & Chadderton, P. (2014). *Co-modulation as a means of enhancing signal detection and object formation in mouse primary auditory cortex.* Paper presented at the Proceedings of The Physiological Society.
Sotelo, C. (2003). Viewing the brain through the master hand of Ramon y Cajal. *Nature Reviews Neuroscience, 4*(1), 71-77.
Sousa-Pinto, A. (1973). *Cortical projections of the medial geniculate body in the cat*: Springer.
South, D. A., & Weinberger, N. M. (1995). A comparison of tone-evoked response properties of 'cluster'recordings and their constituent single cells in the auditory cortex. *Brain research, 704*(2), 275-288.
Spoendlin, H. (1972). Innervation densities of the cochlea. *Acta oto-laryngologica, 73*(2-6), 235-248.
Spruston, N. (2008). Pyramidal neurons: dendritic structure and synaptic integration. *Nature Reviews Neuroscience, 9*(3), 206-221.

Stosiek, C., Garaschuk, O., Holthoff, K., & Konnerth, A. (2003). In vivo two-photon calcium imaging of neuronal networks. *Proceedings of the National Academy of Sciences, 100*(12), 7319-7324.

Suga, N. (1989). Principles of auditory information-processing derived from neuroethology. *Journal of Experimental Biology, 146*(1), 277-286.

Suga, N. (2008). Role of corticofugal feedback in hearing. *Journal of Comparative Physiology A, 194*(2), 169-183.

Suga, N., & Ma, X. (2003). Multiparametric corticofugal modulation and plasticity in the auditory system. *Nature Reviews Neuroscience, 4*(10), 783-794.

Sullivan, W., & Konishi, M. (1984). Segregation of stimulus phase and intensity coding in the cochlear nucleus of the barn owl. *The Journal of Neuroscience, 4*(7), 1787-1799.

Sun, Y. J., Kim, Y.-J., Ibrahim, L. A., Tao, H. W., & Zhang, L. I. (2013). Synaptic mechanisms underlying functional dichotomy between intrinsic-bursting and regular-spiking neurons in auditory cortical layer 5. *The Journal of Neuroscience, 33*(12), 5326-5339.

Sutter, M., & Schreiner, C. (1995). Topography of intensity tuning in cat primary auditory cortex: single-neuron versus multiple-neuron recordings. *Journal of neurophysiology, 73*(1), 190-204.

Sutter, M. L. (2000). Shapes and level tolerances of frequency tuning curves in primary auditory cortex: quantitative measures and population codes. *Journal of neurophysiology, 84*(2), 1012-1025.

Sutter, M. L., & Schreiner, C. E. (1991). Physiology and topography of neurons with multipeaked tuning curves in cat primary auditory cortex. *Journal of neurophysiology, 65*(5), 1207-1226.

Szobota, S., Gorostiza, P., Del Bene, F., Wyart, C., Fortin, D. L., Kolstad, K. D., . . . Aaron, H. L. (2007). Remote control of neuronal activity with a light-gated glutamate receptor. *Neuron, 54*(4), 535-545.

Takahashi, N., Kitamura, K., Matsuo, N., Mayford, M., Kano, M., Matsuki, N., & Ikegaya, Y. (2012). Locally synchronized synaptic inputs. *Science, 335*(6066), 353-356.

Takasaka, T., & Smith, C. A. (1971). The structure and innervation of the pigeon's basilar papilla. *Journal of ultrastructure research, 35*(1-2), 20-65.

Tian, B., & Rauschecker, J. (2003). *On-and off-responses in Rhesus monkey auditory cortex.* Paper presented at the Soc Neurosci Abstr.

Tian, L., Hires, S. A., Mao, T., Huber, D., Chiappe, M. E., Chalasani, S. H., . . . Schreiter, E. R. (2009). Imaging neural activity in worms, flies and mice with improved GCaMP calcium indicators. *Nature methods, 6*(12), 875-881.

Tramo, M. J., Shah, G. D., & Braida, L. D. (2002). Functional role of auditory cortex in frequency processing and pitch perception. *Journal of neurophysiology, 87*(1), 122-139.

Ulanovsky, N., Las, L., Farkas, D., & Nelken, I. (2004). Multiple time scales of adaptation in auditory cortex neurons. *The Journal of Neuroscience, 24*(46), 10440-10453.

Ulanovsky, N., Las, L., & Nelken, I. (2003). Processing of low-probability sounds by cortical neurons. *Nature neuroscience, 6*(4), 391-398.

Velenovsky, D. S., Cetas, J. S., Price, R. O., Sinex, D. G., & McMullen, N. T. (2003). Functional subregions in primary auditory cortex defined by

thalamocortical terminal arbors: an electrophysiological and anterograde labeling study. *The Journal of Neuroscience, 23*(1), 308-316.

Vélez-Fort, M., Rousseau, C. V., Niedworok, C. J., Wickersham, I. R., Rancz, E. A., Brown, A. P., . . . Margrie, T. W. (2014). The stimulus selectivity and connectivity of layer six principal cells reveals cortical microcircuits underlying visual processing. *Neuron, 83*(6), 1431-1443.

Verhey, J. L., Dau, T., & Kollmeier, B. (1999). Within-channel cues in comodulation masking release (CMR): Experiments and model predictions using a modulation-filterbank model. *The Journal of the Acoustical Society of America, 106*(5), 2733-2745.

Verhey, J. L., Ernst, S. M., & Yasin, I. (2012). Effects of sequential streaming on auditory masking using psychoacoustics and auditory evoked potentials. *Hearing research, 285*(1), 77-85.

Verhey, J. L., Pressnitzer, D., & Winter, I. M. (2003). The psychophysics and physiology of comodulation masking release. *Experimental brain research, 153*(4), 405-417.

Versnel, H., Mossop, J. E., Mrsic-Flogel, T. D., Ahmed, B., & Moore, D. R. (2002). Optical imaging of intrinsic signals in ferret auditory cortex: responses to narrowband sound stimuli. *Journal of neurophysiology, 88*(3), 1545-1558.

Viaene, A. N., Petrof, I., & Sherman, S. M. (2011a). Synaptic properties of thalamic input to layers 2/3 and 4 of primary somatosensory and auditory cortices. *Journal of neurophysiology, 105*(1), 279-292.

Viaene, A. N., Petrof, I., & Sherman, S. M. (2011b). Synaptic properties of thalamic input to the subgranular layers of primary somatosensory and auditory cortices in the mouse. *The Journal of Neuroscience, 31*(36), 12738-12747.

Volkov, I., & Galazjuk, A. (1991). Formation of spike response to sound tones in cat auditory cortex neurons: interaction of excitatory and inhibitory effects. *Neuroscience, 43*(2), 307-321.

Walker, A. E. (1938). The primate thalamus.

Wallace, M., & Palmer, A. (2008). Laminar differences in the response properties of cells in the primary auditory cortex. *Experimental brain research, 184*(2), 179-191.

Wehr, M., & Zador, A. M. (2005). Synaptic mechanisms of forward suppression in rat auditory cortex. *Neuron, 47*(3), 437-445.

Weible, A. P., Moore, A. K., Liu, C., DeBlander, L., Wu, H., Kentros, C., & Wehr, M. (2014). Perceptual gap detection is mediated by gap termination responses in auditory cortex. *Current Biology, 24*(13), 1447-1455.

Whitfield, I., & Evans, E. (1965). Responses of auditory cortical neurons to stimuli of changing frequency. *Journal of neurophysiology*.

Wilson, M., Cragg, B., Ainsworth, A., & Toyne, M. (1969). Projections from the medial geniculate body to the cerebral cortex in the cat. *Brain research, 13*(3), 462-475.

Wilson, M. A., & McNaughton, B. L. (1993). Dynamics of the hippocampal ensemble code for space. *Science, 261*(5124), 1055-1058.

Winer, J., & Larue, D. (1989). Populations of GABAergic neurons and axons in layer I of rat auditory cortex. *Neuroscience, 33*(3), 499-515.

Winer, J. A. (1984). The human medial geniculate body. *Hearing research, 15*(3), 225-247.

Winer, J. A. (2005). Decoding the auditory corticofugal systems. *Hearing research, 207*(1), 1-9.

Wollberg, Z., & Newman, J. D. (1972). Auditory cortex of squirrel monkey: response patterns of single cells to species-specific vocalizations. *Science, 175*(4018), 212-214.

Xu, N., Fu, Z.-Y., & Chen, Q.-C. (2014). The function of offset neurons in auditory information processing. *Translational Neuroscience, 5*(4), 275-285.

Xu, X., Roby, K. D., & Callaway, E. M. (2010). Immunochemical characterization of inhibitory mouse cortical neurons: three chemically distinct classes of inhibitory cells. *Journal of Comparative Neurology, 518*(3), 389-404.

Yaron, A., Hershenhoren, I., & Nelken, I. (2012). Sensitivity to Complex Statistical Regularities in Rat Auditory Cortex. *Neuron, 76*(3), 603-615. doi:http://dx.doi.org/10.1016/j.neuron.2012.08.025

Ylinen, A., Bragin, A., Nádasdy, Z., Jandó, G., Szabo, I., Sik, A., & Buzsaki, G. (1995). Sharp wave-associated high-frequency oscillation (200 Hz) in the intact hippocampus: network and intracellular mechanisms. *The Journal of Neuroscience, 15*(1), 30-46.

Yu, Y.-C., Bultje, R. S., Wang, X., & Shi, S.-H. (2009). Specific synapses develop preferentially among sister excitatory neurons in the neocortex. *Nature, 458*(7237), 501-504.

Zatorre, R. J., & Penhune, V. B. (2001). Spatial localization after excision of human auditory cortex. *The Journal of Neuroscience, 21*(16), 6321-6328.

Zhai, R. G., & Bellen, H. J. (2004). The architecture of the active zone in the presynaptic nerve terminal. *Physiology, 19*(5), 262-270.

Zilles, K., & Amunts, K. (2010). Centenary of Brodmann's map—conception and fate. *Nature Reviews Neuroscience, 11*(2), 139-145.

A life goal:

- **25 p36 deer**
- **Mishchenko's energy force and a spanish dude**
- **Hardcastle sticking to bob marley**

How far can a dog run into the woods?